MODELING OF DIFFUSION-REACTION-DEFORMATION PHENOMENA IN TWO-PHASE BINARY SOLIDS

Surabhi Joshi

Department of Mechanical Engineering

McGill University

Montréal, Québec

A thesis submitted to McGill University in partial fulfillment of the requirements of the degree of Doctor of Philosophy

For my parents

Table of contents

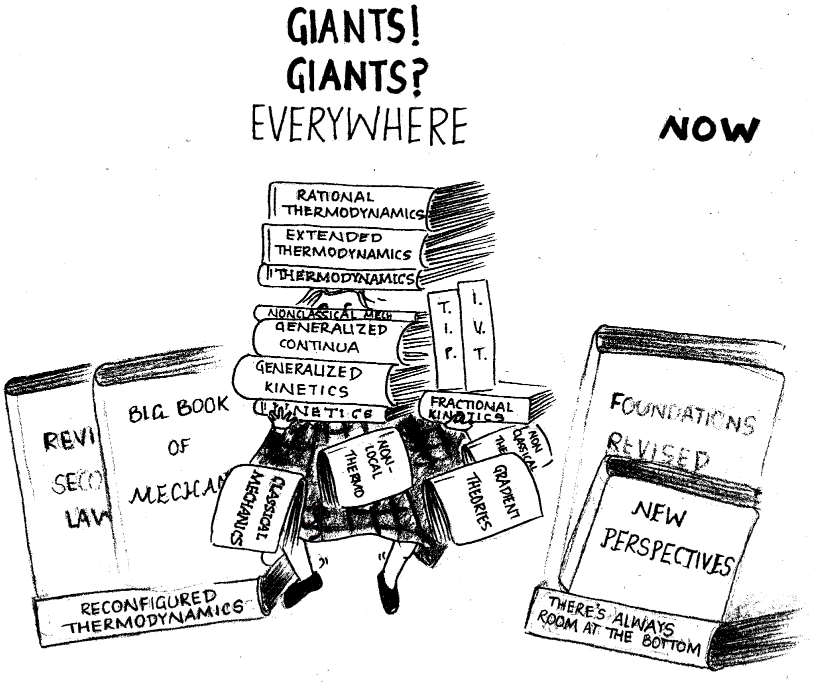

Continuum mechanics & thermodynamics, and kinetics literature - A beginner's view

Acknowledgements

My deepest gratitude to Prof. Siva Nadarajah for stepping in as my supervisor to guide my progress.

Many thanks to McGill's efforts during the pandemic; the expanded electronic resources provided by the libraries during lockdown were invaluable in sustaining my research. I have also benefited greatly from the numerous resources, training programs, and spaces added since my previous time here as a Master's student, including the Doctoral Internship Program (DIP) and Building 21.

I would like to thank Dr. Srikar Vengallatore for introducing me to the publications of F. C. Larché and J. W. Cahn, and providing an opportunity to explore a subject brand new to me. The topic of modeling in general and coupled phenomena in particular has opened my appetite for lifelong research, which is exactly how I imagined a revivifying PhD experience. Nevertheless, the circumstances and challenges of the past few years meant that much of the work and research training has been conducted independently; the form that the thesis took naturally perhaps reflects this self-training.

While I enjoyed the immersive experience in this vast area of research, the Damoclesian sword of a PhD thesis and its requirements meant juggling two modes of working, one with a research advisor's sensibility. This undertaking would not have been possible without my family. My endless gratitude to my father, Bipin, and my partner, Kavish, for their constant support, patience, and unbounded warmth, while I spent countless hours in *A Room of One's Own*.

Many thanks to Anne-Marie Pierre, the department's Graduate Program Coordinator, who kindly answered all my questions over the years and ensured a smooth process.

Finally, I would like to thank the National Sciences and Engineering Research Council of Canada (NSERC), and the McGill Engineering Doctoral Awards (MEDA) program for their financial support.

Abstract

Diffusion-reaction-deformation phenomena are ubiquitous in materials processing and manufacturing, and govern the performance and reliability of several key modern technologies. While diffusion, reaction, and deformation have been studied in their uncoupled form for more than 200 years, modeling their interactions is an active area of research spanning several fields, making it both a classical and a modern topic. Nevertheless, a close survey of the literature reveals several aspects of diffusion-reaction-deformation that remain to be investigated theoretically.

In this thesis, a consolidated theoretical approach is investigated to address the gaps in knowledge with respect to the modeling of diffusion-reaction-deformation. It is shown that the classical growth kinetics of two model systems, namely, a core-shell spherical particle, and a thin-film bilayer can be derived using a combination of Larché-Cahn (L-C) thermostatics and kinetics. Previously, these equations have been derived solely from kinetic considerations using fitting parameters; to extend the models to incorporate the effects of stress, ad hoc models are generally used. To gain a better understanding of the effects of coupling, the thesis uses a thermodynamic-kinetic approach. Subsequently, several diverse yet universal phenomena are predicted, which have been observed experimentally in various material systems, including lithium-ion batteries. These coupled phenomena include enhanced diffusion, reaction block, and hysteresis; reaction block entails the slowing down and eventual arrest of the phase transformation front.

The intrinsic nature of thermodynamic hysteresis, which continues to persist with vanishing kinetics, is deduced and explored using a new graphical analysis based on stability considerations. The palladium-hydrogen system proves to be a suitable candidate to compare these deductions qualitatively. It is noted that thermodynamic hysteresis is ubiquitous in several phase transforming systems including lithium-ion batteries and metal hydrides. The origin of hysteresis in palladium hydrides has been under debate since the 1960s. This material system continues to be studied experimentally; recently, single particle and atomistic experiments have also been undertaken. The hysteresis analyses presented in this thesis complement the observations of these experiments as well as the key results of the Schwarz-Khachaturyan (S-K) thermodynamic theory.

Kinetics of mass transfer are also pertinent in polymeric, biological, and pharmaceutical applications. The mechanics of viscoelasticity is of key interest in such systems. A transient diffusion problem is formulated in the presence of a general semi-permeable phase interface, and a viscoelastic thin film is considered. The interface model is identified with a modified Kedem-Katchalsky (K-K) equation, which is well-known in membrane transport literature. To solve for the composition field and viscoelastic stresses, a protocol is devised using an extended separation of variables technique, and the correspondence principle between elasticity and viscoelasticity.

The exploration of diffusion-reaction-deformation undertaken in this work is summarized with key modeling insights using a chemical kinetics perspective. The phenomenon of stress-enhanced diffusion is revisited in the presence of strong coupling to extend the model and present a reasoned connection between the reaction block phenomenon and the waiting time solution of nonlinear degenerate diffusion.

Résumé

Les phénomènes de diffusion-réaction-déformation sont omniprésents dans le traitement et la fabrication des matériaux, et régissent les performances et la fiabilité de plusieurs technologies modernes clés. Bien que la diffusion, la réaction et la déformation soient étudiées indépendamment depuis plus de 200 ans, la modélisation de leurs interactions est une filière de recherche active couvrant plusieurs domaines, ce qui en fait à la fois un sujet classique et un sujet moderne. Néanmoins, une étude approfondie de la littérature révèle plusieurs aspects du phénomène diffusion-réaction-déformation qui restent à étudier théoriquement.

Dans cette thèse, une approche théorique consolidée est formulée pour combler les lacunes dans la modélisation du phénomène de diffusion-réaction-déformation. Il est démontré que la cinétique de croissance classique de deux systèmes modèles: une particule sphérique noyau-coquille, et un 'bilayer' à couche mince peut être dérivé en utilisant une combinaison de la théorie thermodynamique et cinétique. Précédemment, ces équations étaient dérivées uniquement avec une approche cinétique en utilisant des paramètres d'ajustement; pour inclure les effets du stress, des modèles 'ad hoc' sont généralement utilisés. Ici, une approche thermodynamique-cinétique est utilisée pour étudier les effets du couplage; par la suite, plusieurs phénomènes divers mais universels sont prédits. Ces phénomènes sont aussi observés expérimentalement dans différents systèmes, y compris les batteries lithium-ion. Ces effets du couplage incluent une augmentation de diffusion, un ralentissement de réaction, et l'hystérésis.

La nature intrinsèque de l'hystérésis thermodynamique est étudiée à l'aide d'une nouvelle analyse graphique basée sur des considérations de stabilité. Le système de palladium-hydrogène est un candidat approprié pour comparer ces analyses qualitativement. Il est à noter que l'hystérésis thermodynamique, qui persiste avec la disparition de la cinétique, est omniprésente dans plusieurs systèmes de transformation de phase, y compris les batteries lithium-ion et les hydrures métalliques. L'origine de l'hystérésis dans les hydrures de palladium est en discussion depuis les années 1960. Ce système matériel continue d'être étudié expérimentalement; récemment, des expériences à particule unique et atomistique ont également été entreprises. Les analyses d'hystérésis présentées dans cette thèse sont complémentaires aux observations de ces expériences ainsi que la théorie de Schwarz-Khachaturyan (S-K).

La cinétique du transfert de masse est pertinente dans les systèmes biologiques et pharmaceutiques; la mécanique de la viscoélasticité est d'un intérêt clé dans ces systèmes. Un problème de diffusion transitoire en présence d'une interface de phase semi-perméable générale et de viscoélasticité dans les 'bilayers' à couche mince est formulé. Le modèle d'interface est identifié avec une équation modifiée de Kedem-Katchalsky (K-K), bien connue dans la littérature sur le transport membranaire. Pour résoudre le champ de composition et les contraintes viscoélastiques, une approche impliquant la technique 'extended separation of variables' et le 'elastic-viscoelastic correspondence principle' est conçue.

L'exploration de la diffusion-réaction-déformation entreprise dans cette étude est résumée par des modélisations clés d'une perspective cinétique chimique. Le phénomène de diffusion accentuée par le stress est revisité en présence d'un couplage fort pour étendre le modèle et présenter une connexion entre le phénomène de ralentissement de réaction et la solution de 'waiting time' de diffusion dégénérée non linéaire.

List of figures

List of tables

List of abbreviations and symbols

Abbreviations

D-G	Deal-Grove
DIS	Diffusion-induced stresses
G-B	Ginstling-Brounshtein
IBC	Interfacial boundary condition
IVT	Internal variable theory
K-K	Kedem-Katchalsky
L-C	Larché-Cahn
LAS	Local accompanying state
LIB	Lithium-ion battery
NW	Nanowire
PSS	Pseudo-steady state solution
QSS	Quasi-steady state solution
S-K	Schwarz-Khachaturyan
SED	Stress-enhanced diffusion
SF, S	Stress-free, stressed

TEM	Transmission electron microscopy
TIP	Thermodynamics of irreversible processes
TIV	Thermodynamics of internal variables

Latin symbols

$\tilde{a}$	Ratio of the core's radius to the shell's radius
A, B	Chemical species
a	Radius of the core
a_α	Lattice constant of the α-phase
a_β	Lattice constant of the β-phase
$A_{\mathrm{DG}}, B_{\mathrm{DG}}$	D-G model parameters
A_f	Surface area of the film
b	Radius of the particle
B_α, B_β	Constants
C, C_B	Concentration of B-atoms
C^*	Prescribed surface concentration
C^α	Concentration of B-atoms in the α-phase
C^β	Concentration of B-atoms in the β-phase
C_0^α, C_0^β	Stress-free equilibrium concentrations
C_1, C_2	Orthogonality factors
C_a, C_b	Prescribed concentrations
C_A	Molar density of A-atoms

C_A^α	Molar density of A-atoms in the α-phase
C_A^β	Molar density of A-atoms in the β-phase
C_{eq}	Equilibrium concentration
C_{ijkl}	Elastic stiffness tensor
C_I	Interfacial concentration
C_i	Initial concentration of the drug in the Higuchi model
C_o	Overall concentration of B-atoms in a closed system
C_S	Concentration at the moving boundary
C_s	Solubility of the drug in the Higuchi model
$\hat{C}$	Ratio of equilibrium concentrations
$\boldsymbol{d}$	Net displacement of the interface
D, D'	Diffusivities
De	Deborah number
$\overline{E}$	Biaxial modulus
$\overline{E}^\beta$	Biaxial modulus of the β-phase
$\overline{E}_V$	Laplace transformed biaxial modulus
$\overline{E}_V^\beta$	Laplace transformed biaxial modulus of the β-phase
E	Young's modulus
$\boldsymbol{F}$	Deformation gradient
F	Total energy of the bilayer at constant temperature
$f^\alpha(z), f^\beta(z)$	Quasi-orthogonal eigenfunctions

F_n	Series coefficient
$\mathscr{f}$	Helmholtz energy density
G	Gibbs energy (Chapter 1), Shear modulus (Chapter 7)
H	Enthalpy
$\mathscr{g}$	Gibbs energy density
h	Thickness
h_b	Location of the bending axis
$\boldsymbol{I}$	Identity matrix
$\boldsymbol{J}, J$	Flux of B-atoms
J^*	Applied flux
J_I^α, J_I^β	Interfacial flux on the α- and β- side
J_r	Flux in the radial direction
J_z	Flux in the z-direction
K	Bulk modulus
k	Kinetic parameter
k_1, k_α	Reaction constant for the forward reaction
k_2, k_β	Reaction constant for the forward reaction
K_p	Equilibrium constant
Kn	Knudsen number
L_{char}	Characteristic length scale

$\mathcal{L}$	Laplace transform
$\boldsymbol{M}$	Mobility matrix
M^α, M^β	Mobility of B-atoms in the α- and β-phases
M_t	Cumulative amount of drug released at time t
$\boldsymbol{N}$	Unit normal vector perpendicular to the interface
n	Number of moles
n_A^α, n_A^β	Number of moles of the A-atoms in the α- and β-phases
n_B^α, n_B^β	Number of moles of the B-atoms in the α- and β-phases
$\mathcal{O}$	Asymptotic notation
P	Hydrostatic pressure, Hydrostatic stress in the core (Chapter 5)
p_i	Partial pressure of component i
P_m, Q_m	Model-dependent operators
Q	Extensive property
q^α, q^α	Density of Q in α- and β-phases
Q^I	Interfacial excess quantity corresponding to Q
q_I	Normalized Q^I with respect to the interfacial area
R	Gas constant
r	Radial coordinate
r_b	Radius of curvature of the bilayer
$\mathcal{S}$	Total entropy

$\boldsymbol{\mathcal{S}}^{\alpha}$	Entropy of the α-phase
$\boldsymbol{\mathcal{S}}^{\beta}$	Entropy of the β-phase
$S(t)$	Location of the interface at time t
S_{ijkl}	Elastic compliance tensor
s_{ij}, e_{ij}	Deviatoric components of stress and strain
$S_{PSS}(t)$	Location of the PSS interface
$\mathscr{s}$	Entropy density
T, T_0	Absolute temperatures
t	Time
t_w	Waiting time
$\boldsymbol{u}$	Displacement
$\mathcal{U}$	Total internal energy
$\mathcal{U}^{\alpha}$,$\mathcal{U}^{\beta}$	Internal energy of the α- and β-phases
$u(r)$	Radial displacement
$u(z,t)$	Transformed variable to satisfy the homogeneous boundary conditions
$\mathscr{u}$	Internal energy density
$v(t)$	Transformed variable to satisfy the initial conditions (Chapter 7), Net rate of reaction (Appendix C)
V	Volume
V^{α}, V^{β}	Volumes of the α- and β-phases
$v_1, v_{\alpha\rightarrow\beta}$	Rates of forward reactions

$v_2, v_{\beta\to\alpha}$	Rates of backward reactions
V_0	Characteristic velocity of the moving interface, Permeability of the stationary interface (Chapter 7)
V_A	Volume occupied by the A-atoms
V_A^α, V_A^β	Volume of A-atoms in the α- and β-phases
v_I	Velocity of the interface
$w(z)$	Transformed variable to satisfy the nonhomogeneous boundary conditions (Chapter 7)
x, y, z	Cartesian coordinate
X	Mole fraction
x	Volume fraction of the β-phase
X_A^α, X_A^β	Mole fraction of the A-atoms in the α- and β-phases
X_B^α, X_B^β	Mole fraction of the B-atoms in the α- and β-phases
x_i, x_0	Initial and total thickness of the oxide layer in the D-G model
y	Boundary fixing transformation
$\boldsymbol{X}$	Vector in the undeformed configuration
$\boldsymbol{x}$	Vector in the deformed configuration
$\dot{z}_I$	Velocity of the planar interface at time t
z_I	Thickness of the planar film
z_I^0	Initial thickness of the film
z_o	Thickness of the bilayer

Greek symbols

α	Core and substrate phase
β	Shell and film phase
γ	Activity coefficient of the B-atoms
$\delta\mu$	Deviation in chemical potential from equilibrium
ΔC	Change in concentration
δC	Deviation in concentration from equilibrium
ΔG_T^0	Change in Gibbs energy of the reaction under standard conditions
ΔG_T	Change in Gibbs energy of the reaction
δz	Displacement of the interface along its normal
Δ, Γ	Dimensionless material parameters
δ_{ij}	Kronecker delta function
∇	Gradient operator in the deformed state
∇_0	Gradient operator in the undeformed configuration
$\boldsymbol{\epsilon}$	Small strain tensor
$\boldsymbol{\epsilon}^\alpha, \boldsymbol{\epsilon}^\beta$	Small strain tensors of the α- and β-phases
$\dot{\epsilon}$	Strain rate
ϵ	Total strain of the bilayer
ϵ^0	Uniform strain component
$\epsilon^\alpha, \epsilon^\alpha$	Equibiaxial strains in the bilayer
ϵ_{ij}^c	Component of a stress-free strain

ϵ_{ij}^{e}	Component of elastic strains
ε	Control parameter
$1/\zeta$	Critical thickness characterizing two growth regimes
η	Index to denote the phase, Viscosity (Chapter 7)
$\theta, \varPhi$	Spherical coordinate
κ', ζ'	Coupled parameters in the presence of elastic deformation
κ	Curvature of Gibbs energy density
$\kappa^{\alpha}, \kappa^{\beta}$	Curvatures of Gibbs energy densities in the α- and β-phases
λ, μ	Lamé moduli (Chapter 7)
Λ	Mean free path Dimensionless material parameter (Chapter 3)
λ	Lagrange multiplier
λ_n	n^{th} eigenvalue
λ_{QSS}	Dimensionless parameter
μ^0	Chemical potential under standard conditions
μ_0	Chemical potential under stress-free equilibrium
μ_B, μ	Chemical potential of the B-atoms
μ_I	Chemical potential at the interface
$\mu_I^{\alpha}, \mu_I^{\beta}$	Interfacial chemical potential on the α- and β-sides of the interface
ν	Poisson's ratio

ξ	Extent of reaction
$\boldsymbol{\sigma}$	Cauchy stress tensor
$\boldsymbol{\sigma}^\alpha, \boldsymbol{\sigma}^\beta$	Cauchy stress tensor in the α- and β-phases
$\overline{\sigma}^\beta$	Average elastic stress in the β-phase
$\overline{\sigma}^\beta_V$	Average viscoelastic stress in the β-phase
$\sigma^\alpha, \sigma^\alpha$	Equibiaxial stresses in the bilayer
σ_h	Hydrostatic stress
σ_{ij}	Component of stress
τ	Relaxation time
Φ	Driving force for phase transformation
ϕ	Strain energy density
χ, χ'	Second derivative of Helmholtz energy density with respect to concentration
$\boldsymbol{\omega}$	Infinitesimal rotation tensor
Ω	Partial molar volume of the B-component at zero stress
ω	Density of the grand canonical potential
$\Omega^\alpha, \Omega^\beta$	Ω in the α- and β-phases

Chapter 1

Introduction

1.1. Introduction to diffusion-reaction-deformation phenomena

Diffusion-reaction-deformation phenomena are ubiquitous in materials processing, manufacturing, and solid-state technologies. Diffusion comprises the transport of multiple species (neutral atoms, ions, charges, radicals) through a solid with complex microstructure (containing defects, grain boundaries, porosity). Solid-state reactions encompass phase transformations (including amorphization, crystallization) and the formation of solid solutions, intermetallics, and compounds (silicides, oxides, salts, and amorphous alloys). Mechanical deformation includes the effects of elasticity, plasticity, inelasticity, anelasticity, viscoelasticity, fracture, creep, and fatigue.

Diffusion, reactions, and deformation have been studied in their uncoupled form for more than 200 years, dating back to the work of Fick [1], Gibbs [2], and Hooke [3]. Diffusion through an isotropic solid is described by relating J, the flux of the diffusing chemical component, to the gradient of C, the concentration of the component via Fick's first law: $J = -D\nabla C$, where D is diffusivity. This model is based on the empirical observation that as the sample becomes homogeneous, the flux vanishes, and equilibrium is attained. Reactions are studied in terms of Gibbs energy, $G = H - TS$, which accounts for the contributions of enthalpy, H, and entropy, S, at temperature T; a minimum in the Gibbs energy characterizes the equilibrium under conditions of constant temperature, pressure, and composition. Finally, to describe the deformation in a linearly elastic material, Hooke's law, given by $\sigma = E\epsilon$, relates the stresses, σ, and strains, ϵ, via E, the elastic modulus.

There aren't many studies of the interactions between these three phenomena; most are primarily limited to pairs of phenomena, such as the effect of stress on diffusion, the effect of reaction on stress, and similar binary couplings [4–12]. Nevertheless, diffusion-reaction-deformation phenomena — coupled at multiple spatial and temporal scales — govern the performance and reliability of several key modern technologies. Additional factors, such as the geometry of the system, structural dynamics, and operating temperature further modulate this tertiary coupling. Consequently, modeling these coupled phenomena is of key interest in applications of diffusion, which range from energy storage to drug delivery, where diffusion often sustains the accompanying chemical reactions.

1.2. Illustrative example from energy storage technologies

Energy storage solutions involving lithium-ion batteries (LIBs) and hydrogen storage in metal hydrides are under intense study, where the goal is to maximize and maintain high capacity during device operation [13–16].

This section considers diffusion-reaction-deformation in the context of LIBs. During the charging of these batteries, lithium-ions travel to the anode, through the electrolyte. The interactions between the anode and lithium-ions during charging (lithiation) and discharging (delithiation) generate swelling, phase transformations, and stresses in the electrode.

Phenomena
Diffusion
Solid state reaction
Deformation (anelastic, plastic flow)

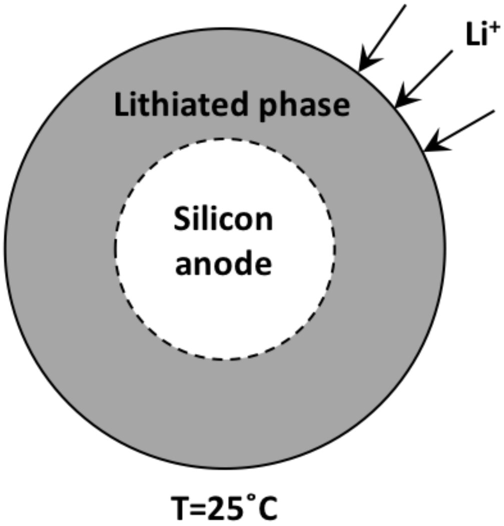

Effects
Swelling
Amorphization
Recrystallization
Stresses
Property changes
Morphology changes
Porosity
Cracks
Fracture
Fatigue
Reduced output voltage

Figure 1.1: Schematic illustration of a silicon anode using a spherical particle as the representative microstructure. During the charging of a LIB, key governing phenomena include transport of lithium ions to the silicon anode and their reaction, which is accompanied by deformation of the anode (left table). The solid-state chemical reaction creates an interface between the original silicon anode and the newly formed lithiated phase (grey), called the phase boundary or reaction interface (dashed circle). This phase boundary propagates inwards as further silicon is consumed by the reaction. These diffusion-reaction-deformation phenomena generate numerous effects that degrade the electrochemical performance of LIBs (right table).

When the anode is made of silicon, it undergoes volumetric changes up to 300% accompanied by solid-state amorphization. This constrained swelling generates large elastic-plastic deformation and stress in the anode, which can lead to cracks, and subsequent fracture. As a result, silicon anodes — which in theory offer high capacity for LIBs than the conventional graphite anodes — cannot sustain multiple charge-discharge cycles and fracture within a few ($\sim$10) cycles. The effects of these coupled diffusion-reaction-deformation phenomena (Fig. 1.1) have been observed by several experiments using ex-situ and in-situ techniques such as transmission electron microscopy (TEM), scanning electron microscopy (SEM), atomic force microscopy (AFM), X-ray diffraction (XRD), nuclear magnetic resonance (NMR), and many others; their combined effects on morphology, crack formation, material properties, and electrochemical performance (output voltage, efficiency of the battery) have also been measured for crystalline and amorphous silicon anodes ([14, 17–22] and the references therein). For example, observing particles of amorphous active materials directly via in-situ optical and atomic force microscopy has revealed isotropic expansion of the particles when lithium is inserted [20]. Subsequently, the kinetics and fracture response of amorphous silicon is favorable compared to crystalline silicon, as revealed by in-situ TEM, which has shown that nanospheres of amorphous silicon can withstand fracture up to a diameter of 870 nm, as opposed to crystalline silicon spheres, which exhibit a critical diameter of 150 nm [21]. Additionally, the atomically sharp (thickness of $\sim$1 nm) crystalline-amorphous phase boundary has been observed via high-resolution TEM [20].

There is ongoing research to develop models of lithium-ion batteries that capture these coupled diffusion-reaction-deformation phenomena as well as predict their effect on electrochemical performance ([14, 16, 23] and the references therein).

These citations do not form an exhaustive list as references pertaining to both experiments and models continue to grow with various topics of emphasis within these broad fields. Of particular interest is the investigation of coupled phenomena in nanoparticles and thin films; using nanostructures as battery electrodes has been shown to lower stresses, improve capacity retention and resilience against mechanical degradation [16, 17]. This trend towards nanostructuring has prompted several modeling attempts to include the effects of surface mechanics, determine the critical particle sizes below which cracks do not nucleate, as well as predict, or at least describe, anomalous behaviors [14, 16, 24]. In several models, the coupling is invoked via effective parameters, and restricted to partial and binary couplings. For example, Bhandakkar and Gao [25] predict the critical conditions for crack nucleation in an isotropic elastic thin strip electrode by applying a cohesive zone model of fracture; however, their model does not consider the full coupling between stress and diffusion. In [24], Haftbaradaran et al. couple internal stresses and activation energy for diffusion via an effective stress-dependent diffusivity, ignoring the phase transformation reaction. Many anomalous phenomena observed in experiments have also motivated fundamental inquiries, which are expounded in the next chapter.

In summary, as modern technologies and devices for energy conversion and storage evolve and use multifunctional materials with complex micro- and nanostructures, several concurrent physical phenomena govern their behavior at various length- and time-scales. For example, batteries, solid oxide fuel cells (SOFCs), polymer electrolyte membrane fuel cells (PEMFC), and processing of microsystems use multilayered thin films, which experience electromagnetic, electrostatic, thermal, piezoelectric, inertial, viscous, and elastic-plastic effects. The multiple couplings between these phenomena cannot be ignored. Thus, efficient and reliable models are required to capture the kinetics of the system under the combined action of the various phenomena.

To model these systems, it is valuable to formulate a multiphysics continuum framework of the coupled phenomena of transport processes, deformation, reaction, and their induced effects. Constructing such a framework is the first step towards developing predictive models for estimating the performance; analyzing the behavior; controlling the solid-state processing and synthesis; and guiding the design of solid state systems.

To this end, we consider two model systems, withholding any context-specific complexity at present. These systems are analyzed subsequently within a continuum framework.

1.3. System geometries and material properties

Two binary systems are investigated. The spherical particle under consideration has a core-shell structure, comprising a spherical core encapsulated in a spherical shell. The bilayer under consideration consists of a thin film attached to a substrate. Both solids are isolated systems.

The constituents of each system, i.e. core and shell, and film and substrate, are binary solid solutions with different phase equilibria. Under isothermal conditions at absolute temperature T_0, the equilibrium phases are denoted β and α for the shell and core respectively in the spherical case, and the film and substrate respectively in the planar case, as shown in Fig. 1.2.

Each phase consists of two chemical species denoted A and B. The number of moles of the atoms is n, and X is the mole fraction of the chemical constituents. Both n and X are denoted with a subscript for the type of atom, and a superscript for the phase. For example, n_A^α represents the number of moles of A-atoms in the α-phase, and X_B^α represents the mole fraction of B-atoms in the α-phase. The mole fraction of the B-atoms is given by

$$\begin{aligned} X_B^\alpha &= \frac{n_B^\alpha}{n_A^\alpha + n_B^\alpha}, \\ X_B^\beta &= \frac{n_B^\beta}{n_A^\beta + n_B^\beta}. \end{aligned} \tag{1.1}$$

The B-atoms are present in dilute amounts compared to A-atoms in both phases; subsequently, Eq. (1.1)a can be simplified as

$$X_B^\alpha \approx \frac{n_B^\alpha}{n_A^\alpha}, \tag{1.2}$$

which, in terms of concentrations, is given by

$$X_B^\alpha = \frac{n_B^\alpha / V_A^\alpha}{n_A^\alpha / V_A^\alpha} = \frac{C_B^\alpha}{C_A}, \tag{1.3}$$

where V_A^α is the volume of A-atoms in the α-phase, C_B^α is the molar concentration (mol/m^3) of the B-atoms in the α-phase and C_A is the molar density (mol/m^3) of the A-atoms. It is assumed that $C_A^\alpha = C_A^\beta = C_A$; the molar volume of the A-atoms remains the same in the two phases.

Similarly, $X_B^\beta = C_B^\beta / C_A$. The composition of the system is characterized using C_B^α and C_B^β, the concentration of the B-atoms in the two phases.

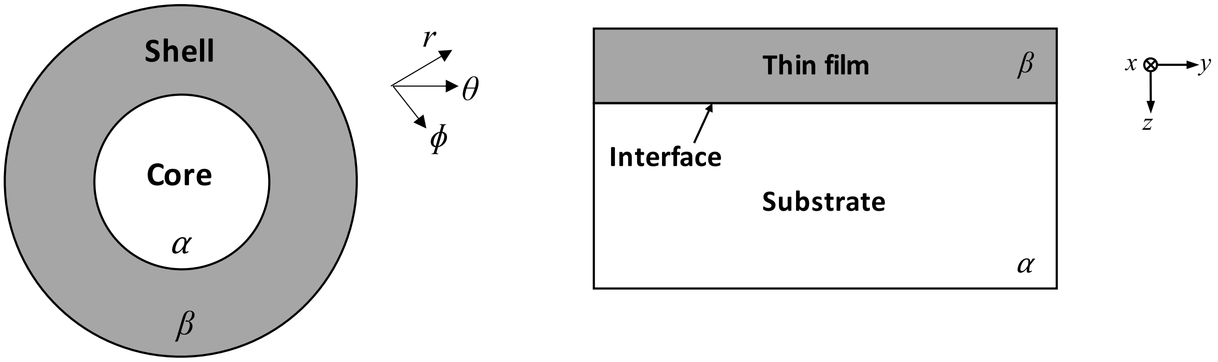

(a) (b)

Figure 1.2: Schematic cross-section of a (a) core-shell particle and a (b) bilayer.

1.3.1 Diffusion-reaction-deformation in binary systems

At T_0, the mobility of A-atoms is assumed to be negligible compared to the B-atoms. Thus, the A-atoms constitute a lattice. The B-atoms diffuse with respect to the A-lattice, which undergoes small strains leading to elastic deformation.

During phase transition, the region occupied by the β-phase grows at the expense of the region occupied by the α-phase via the migration of the α/β interface along its normal. The interface is assumed to be sharp (negligible thickness), and coherent (perfect continuity between the two A-lattices at the interface), as shown in Fig. 1.3 for Cartesian coordinates. The energy of the interface is assumed negligible.

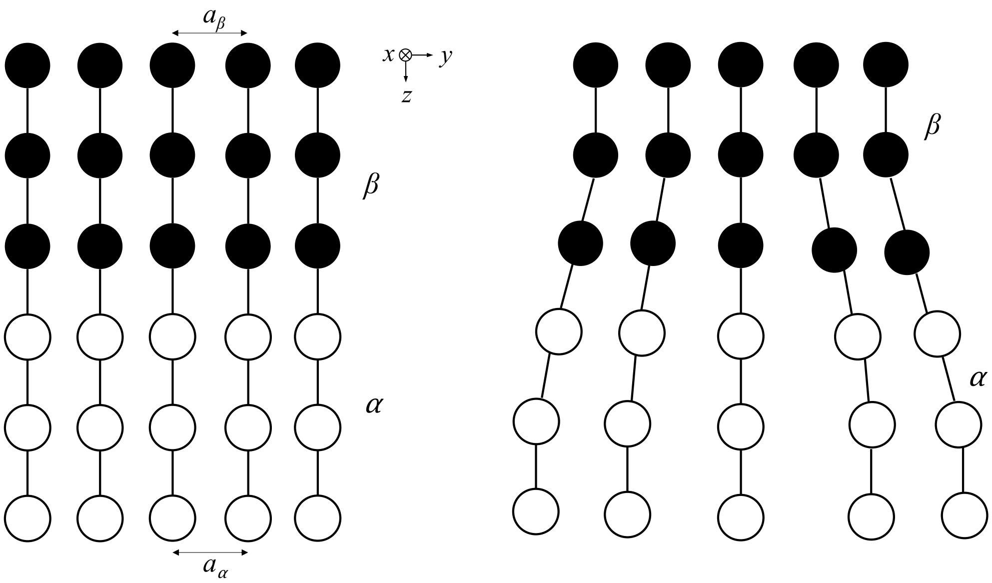

Figure 1.3: Schematic of a coherent interface separating two phases of the same structure that differ in their chemical composition in the (a) undeformed state and (b) elastically strained state [10]. The lattice constant is denoted a.

The thermodynamic description of sharp interfaces assumes that both phases are homogeneous up to the interface, and the interface is homogeneous in each direction that is perpendicular to its normal [26]. To describe variations of an extensive property, Q, for phases that are not homogeneous close to the interface, Gibbs introduced interfacial excess quantities such that $Q = q^\alpha V^\alpha + q^\beta V^\beta + Q^I$, where q is the density of Q, and Q^I is the interfacial excess, which can be normalized by the interface area to obtain the interfacial excess density, q^I, a property of the sharp interface. In this work, the excess fields associated with the interface are ignored.

In the absence of deformation of the A-lattice, the phase change is expressed using the vector $\boldsymbol{N}\delta z$, where $\boldsymbol{N}$ is the unit normal perpendicular to the interface, and δz is the displacement of the interface along the normal.[1] In the presence of deformation of the A-lattice, the elastic

---

[1] It is noted that the variation is δr in the spherical case. The equilibrium conditions and subsequent analyses do not feature this term, which is why we are using δz in the derivation to avoid extraneous notation.

deformation must be accounted for in the phase change, and is given by $(\boldsymbol{I}+\boldsymbol{\epsilon})\cdot\boldsymbol{N}\delta z$ in the deformed state, where $\boldsymbol{\epsilon}$ is the small strain tensor, and $\boldsymbol{I}$ is the identity matrix. The derivation in presented in *Appendix A*.

1.3.2 Objectives

The overarching goal is to predict the key diffusion-reaction-deformation phenomena in binary two-phase solids, particularly in thin-films. This goal entails solving for the concentration field and stress fields in the two phases, and the location and velocity of the α/β interface, taking into account the full diffusion-reaction-deformation coupling. These objectives are achieved by solving the following problems.

The first problem derives the governing equations for the mechanics and thermodynamics of the systems under consideration.

The second problem analyzes two uncoupled models involving diffusion and phase transformation. Deformation is ignored.

The third problem analyzes two fully coupled diffusion-reaction-deformation models for steady state diffusion. The deformation is linear elastic.

The fourth problem analyzes a partially coupled model for unsteady (transient) diffusion. The deformation is viscoelastic. Phase transformation is ignored.

1.4. Organization of the thesis

Chapter 2 presents a survey of the literature, focusing on the growth kinetics as well as the effects induced by elasticity that modify this kinetic behavior. The rigorous thermodynamic framework of Larché and Cahn, which extends the classical Gibbsian thermodynamics to include nonhydrostatic stresses, is selected as the starting point. The equilibrium (thermostatics) equations are derived by applying the Larché-Cahn (L-C) theory to two-phase binary solids.

Chapter 3 presents the moving boundary problems for a core-shell particle and a thin-film bilayer assuming small deviations from equilibrium. The L-C thermodynamic framework is extended to include diffusion and phase growth. The corresponding kinetic equations use thermodynamic driving forces for diffusion and phase transformation, which are identified from the results of *Chapter 2*. The Legendre transformation procedure enables the representation of these driving forces, containing elastically-coupled contributions, in terms of the densities of Gibbs energy and grand canonical energy.

Chapters 4 and 5 apply the moving boundary formulations of *Chapter 3* to investigate the uncoupled (no deformation) and elastically-coupled quasi-steady state models respectively. Subsequently, closed-form approximate analytical solutions are obtained for the concentration field, stress fields, and the location and velocity of the interface. The uncoupled growth kinetics are compared to the classical growth kinetics equations in Chapter 4. The thermodynamic effects predicted by the elastically-coupled analyses are compared to the experimental observations of several material systems in Chapter 5.

Chapter 6 investigates coherent equilibrium in a thin-film bilayer model using a free energy formulation as the starting point. Qualitative graphical analyses are presented to query the stability of the phases in the presence of elastic stresses. The results of these analyses are compared qualitatively to single-particle experiments and the Schwarz-Khachaturyan (S-K) theory in the context of the palladium-hydrogen system.

Chapter 7 undertakes a transient diffusion analysis of the thin-film bilayer using an extended separation of variables technique. Assuming the thin film is viscoelastic, a stress analysis is undertaken using the elastic-viscoelastic correspondence, a continuum mechanics concept. Together, the formulation presents a partially-coupled model for diffusion-induced viscoelastic stresses in the presence of a stationary interface model that is derived from chemical kinetics considerations. The general nature of this interface is demonstrated.

Chapter 8 reflects and extends key diffusion-reaction-deformation modeling insights using a kinetics perspective. The examples considered in this chapter offer further understanding of model formulations and findings of *Chapters 3-5*, and *7*. These sample problems illustrate the salient points of bounds, errors, estimates, and diffusion-reaction relations, which are pertinent to experimental modeling. Subsequently, the results of *Chapter 5* are revisited to draw a conspicuous connection with the framework of nonlinear degenerate diffusion and motivate topics within this realm for future research.

Finally, Chapter 9 presents the main contributions of the thesis, ending with a summary of the key conclusions, implications, and future work.

Chapter 2

Literature Survey

Diffusion is analyzed using classical continuum mechanics and classical discrete mechanics. The former applies when continuum hypothesis holds, i.e. when the Knudsen number, $Kn = \Lambda/L_{char} \ll 1$, where Λ is the mean free path of the diffusing species, and L_{char} is a characteristic length scale of the system.

Fick's first law is a continuum approximation that applies when $Kn < 0.1$ [27]; its literature is reviewed in *Section 2.1.* Subsequently, *Section 2.2* presents the equilibrium conditions for binary two-phase systems, and *Section 2.3* discusses the literature pertinent to growth kinetics and its modeling in the presence of deformation.

2.1. Continuum models for diffusion-reaction-deformation

In 1885, Adolf E. Fick [1] described the diffusive transport of matter in a single-phase material by drawing an analogy between Fourier's law of thermal conduction and diffusion; deformation and reactions were ignored. His phenomenological 1-D continuum model for isotropic diffusion, Fick's first law, assumed a linear relationship between the local flux and the local concentration gradient via a diffusion parameter, called the diffusivity, that is scalar and constant. This purely linear diffusional theory cannot capture all the processes involved in Fig. 1.1, for example, the heterogeneous reactions occurring at the moving interface.

Several physical phenomena in nature are described by a discontinuous first-order solid state transformation where the change of state occurs by a rearrangement of the atoms. These changes may be accompanied by changes in shape, volume, and chemical composition and is actively studied in the field of physical chemistry since Gibbs' seminal work on the equilibrium of heterogeneous substances [2].

To include the effects of such chemical reactions as well as additional considerations (anisotropy, external fields), an effective diffusivity is typically defined that is dependent on concentration, stress, and ionic species. For example, phase transformations can be modeled by introducing a concentration-dependent diffusivity [28]. Such heuristic additions are frequently used to model coupled phenomena. For instance, stress dependence is incorporated phenomenologically in rates of diffusion and rates of reactions. In these models, the diffusion-reaction-deformation coupling is not well-defined; instead, the phenomenological equations are justified by comparing them to experimental data and evaluating the fitting parameters, if any.

Li, in 1966, and Larché and Cahn, in 1973, undertook a systematic study of the interactions between diffusion and stress. Their research was one of the first attempts to develop a consistent theory that includes the combined effects of stress and concentration gradients on thermodynamic equilibrium in stressed solids [29–35]. These solids included one or more mobile components that move freely within an immobile matrix, for example, atoms which occupy interstitial spaces in a solid.

The L-C theory, which has been the basis for several diffusion-reaction-deformation theories since the 1970s, is based on a variational problem: minimization of the free energy of the system subjected to constraints that are incorporated using Lagrange multipliers. Using this foundation, the L-C formulation extended the definition of the chemical potential — the work required to add or remove a mole of the mobile component — to stressed solids [31–35].

The L-C stress-dependent chemical potential describes diffusion in elastic crystalline solids. Since then, the effects of strain energy have been incorporated and it has also been shown that, in general, chemical potential is a tensor [36–38]. The L-C framework has also been extended to solids undergoing finite strains, plastic deformation, chemical reactions, and to solids containing multiple charged species [23, 39–42].

To model reactions involving phase transformations, the phase boundary is described using a sharp (negligible thickness) interface or a diffuse interface (non-zero thickness). The sharp interface approach leads to a free boundary problem which is solved to obtain the stresses and concentration distributions within the particle [23,28,43–45]. Phase field models (PFM) use diffuse interfaces and are generally applied to materials with complex geometries or anisotropy. General PFM formalisms based on Cahn-Hilliard theory that couple diffusion, stress, and elastic-plastic deformation have been developed [46,47]. Models of stress-assisted reactions that use tensors to describe the chemical potential and the kinetics of the reaction have also been developed [38, 45, 48, 49].

Theories that model the full tertiary coupling in diffusion-reaction-deformation phenomena are still evolving. This thesis uses the L-C framework. The original publications present a general formulation involving multiple phases and components, which makes the derivation lengthy and difficult to follow; the next section applies this framework to the two systems of Fig. 1.2.

2.2. Equilibrium thermostatics

> "Where shall I begin, please your
> Majesty?" he asked.
> "Begin at the beginning"
>
> *Alice in Wonderland*
> *Lewis Carroll*

Gibbs stated the criterion of equilibrium in systems using energy and entropy. The varying values of these two functions characterize the effects generated by the system as it passes from one state to another [2]. The condition for equilibrium can be expressed in two ways:

1. At equilibrium, the total internal energy of an isentropic system (constant entropy) is minimized, which is given by

$$\text{Min}\,\mathcal{U} \text{ at constant } \mathcal{S}, \tag{2.1}$$

   where $\mathcal{U}$ is the total internal energy, and $\mathcal{S}$ is the total entropy of the system.

2. At equilibrium, the total entropy of an isolated system (constant internal energy) is maximized, which is given by

$$\text{Max}\,\mathcal{S} \text{ at constant } \mathcal{U} \tag{2.2}$$

The above conditions for equilibrium are equivalent; the second condition is the second law of thermodynamics. Depending on the system under consideration, the system may be subjected to additional constraints related to the total number of moles, interface, etc.

In 1878, Gibbs applied this thermodynamic treatment to solids in his classic treatise on thermodynamics, *Equilibrium of heterogeneous substances* [2]. Solid state diffusion was prohibited as it was not known at the time. Thus, for solids, Gibbs did not define chemical potentials, which are prescribed for the chemical species that can undergo internal rearrangements. Since then, several frameworks have been developed for treating solid-solid equilibrium [29, 31–33, 35, 50–53]. The starting point for all of them is the first and second law of thermodynamics. The problems in *Chapters 4* and *5* will be solved by applying and extending the framework by Larché and Cahn [32].

2.2.1 Thermochemical equilibrium of a stressed two-phase solid

The equations for thermal, mechanical, chemical, and interfacial equilibrium can be derived using a variational formulation approach based on the postulates of equilibrium thermostatics.

Specifically, we will minimize the total internal energy of the isentropic system, subjected to the internal constraints of the system, including constant total entropy. This condition is written mathematically as

$$\delta \mathcal{U} = 0, \tag{2.3}$$

where Eq. (2.3) is subjected to the constraints, and infinitesimals of higher orders of $\mathcal{U}$ are neglected. Furthermore, as the internal energy is an extensive quantity, it is additive over its constituent phases. Thus, the total internal energy of the systems in Fig. 1.2 is given by

$$\mathcal{U} = \mathcal{U}^{\alpha} + \mathcal{U}^{\beta}, \tag{2.4}$$

where $\mathcal{U}^{\alpha}$ and $\mathcal{U}^{\beta}$ represent the internal energy of the α-phase and β-phase respectively.

Internal constraints

The internal constraints of the system are related to the total entropy, total number of moles of B-atoms, and the interface.

The total entropy of an isentropic system is constant. It is assumed that the total entropy is additive over its two phases. Thus, the first variation of entropy is expressed as

$$\delta \mathcal{S} = \delta \mathcal{S}^{\alpha} + \delta \mathcal{S}^{\beta} = 0, \tag{2.5}$$

where $\mathcal{S}^{\alpha}$ and $\mathcal{S}^{\beta}$ represent the entropy of the two phases.

The total number of moles of the B-component is conserved:

$$\delta n_B = \delta n_B^{\alpha} + \delta n_B^{\beta} = 0. \tag{2.6}$$

To express the interface constraint, consider the net displacement of the interface, denoted as $\delta \boldsymbol{d}$, which entails the deformation of the A-lattice and the local phase change caused by an infinitesimal change in location of the interface. The overall displacement of the interface is given by

$$\delta \boldsymbol{d} = \delta \boldsymbol{u} + (\boldsymbol{I} + \boldsymbol{\epsilon}) \cdot \boldsymbol{N} \delta z, \tag{2.7}$$

where $\delta \boldsymbol{u}$ is the elastic displacement of the A-matrix and the term, $(\boldsymbol{I} + \boldsymbol{\epsilon}) \cdot \boldsymbol{N} \delta z$ represents the displacement due to phase change, presented in *Section 1.3.1*.

Variational procedure for deriving equations of equilibrium

The total internal energy of the system is minimized, as per Eq. (2.3). The constraints given by Eqs. (2.5) and (2.6) are incorporated using Lagrange multipliers. The interface constraint will be incorporated explicitly within the subsequent equations.

Thus, the first variation of the total internal energy of the system, subjected to its internal constraints, is given by

$$\delta \mathcal{U} - T \delta \mathcal{S} - \mu_B \delta n_B = 0, \tag{2.8}$$

where T and μ_B are Lagrange multipliers corresponding to the entropy constraint, and conservation of the B-atoms respectively.[2]

The internal energy and entropy are expressed as volume integrals in terms of their densities; the internal energy density is denoted $\mathpzc{u}$ and the entropy density is denoted $\mathpzc{s}$. For example, the entropy is given by

$$\mathcal{S} = \int_{V^\alpha} \mathpzc{s}\, dV + \int_{V^\beta} \mathpzc{s}\, dV, \tag{2.9}$$

where V^α and V^β are the volumes of the α-phase and β-phase respectively. Similarly, the number of moles of the B-atoms are expressed as volume integrals in terms of C_B.

Variation of each quantity generates volume integrals and surface integrals. The surface terms appear because of the movement of the interface. For example, the first variation of each integrand in Eq. (2.9) is given by

$$\delta(\mathpzc{s}\, dV) = \delta\mathpzc{s}\, dV + \mathpzc{s}\,\delta(dV), \tag{2.10}$$

where the changes in the volume element can be represented as $\delta(dV) = \delta(z dS) = \delta z dS$, where dS is a surface element.

Thus, the first variation of the entropy is given by

$$\delta\mathcal{S} = \int_{V^\alpha} \delta\mathpzc{s}\, dV + \int_{V^\beta} \delta\mathpzc{s}\, dV + \int_{\Sigma} \mathpzc{s}^\alpha \delta z^\alpha dS + \int_{\Sigma} \mathpzc{s}^\beta \delta z^\beta dS, \tag{2.11}$$

where Σ denotes the interface boundary. The last two terms denote the variation in entropy because of phase changes in the α-phase and β-phase respectively. The superscripts on the variables in the surface integrals indicate the appropriate side of the interface.

---

[2] In our model systems, we assume the B-atoms occupy interstitial sites; subsequently the two phases are interstitial solid solutions. In binary substitutional solid solutions, both A- and B-atoms occupy substitutional sites; Eq. (2.8) will then include another term: $-\mu_A \delta n_A$. This scenario also requires a network constraint, namely, the conservation of the total number of atomic sites.

Expanded forms of $\delta\mathcal{U}$, $\delta\mathcal{S}$, and δn_B have similar forms to Eq. (2.11); these are substituted in the variation equation, Eq. (2.8). The volume integrals of $\delta\mathcal{U}$ contain $\delta\mathscr{u}$, which is further expanded as the internal energy density is a function of the strain, entropy density, and concentration, $\mathscr{u} = \mathscr{u}(\boldsymbol{\epsilon}, \mathscr{s}, C_B)$. The variation of $\mathscr{u}$ is given by

$$\delta\mathscr{u} = \frac{\partial\mathscr{u}}{\partial\boldsymbol{\epsilon}} : \delta\boldsymbol{\epsilon} + \frac{\partial\mathscr{u}}{\partial\mathscr{s}}\delta\mathscr{s} + \frac{\partial\mathscr{u}}{\partial C_B}\delta C_B, \tag{2.12}$$

where : denotes the inner product in the space of second order tensors. This operation is a double contraction containing two repeated indices; it is analogous to the dot product in vector spaces. Using the definition of :, the first term of Eq. (2.12) is given by

$$\boldsymbol{\sigma} : \delta\boldsymbol{\epsilon} = \mathrm{tr}(\boldsymbol{\sigma}^T\delta\boldsymbol{\epsilon}) = \sigma_{ij}\delta\epsilon_{ij}, \tag{2.13}$$

where $\partial\mathscr{u}/\partial\boldsymbol{\epsilon}$ is identified as the Cauchy stress tensor, which is denoted by $\boldsymbol{\sigma}$.

To simplify Eq. (2.13), consider the product identity for a tensor field $\boldsymbol{T}$, and a vector field $\boldsymbol{a}$ given by[3]

$$\mathrm{div}(\boldsymbol{T}^{\boldsymbol{T}}\boldsymbol{a}) = \boldsymbol{T} : \mathrm{grad}\boldsymbol{a} + \boldsymbol{a}\cdot\mathrm{div}\boldsymbol{T}, \tag{2.14}$$

where div and grad denote the divergence ($\nabla\cdot$) and gradient (∇) operators respectively. Using the classical divergence theorem,[4] we obtain

$$\int_V \mathrm{div}(\boldsymbol{T}^{\boldsymbol{T}}\boldsymbol{a})\,dV = \int_\Sigma (\boldsymbol{T}^{\boldsymbol{T}}\boldsymbol{a})\cdot\boldsymbol{N}\,dS, \tag{2.15}$$

where $\boldsymbol{T}^{\boldsymbol{T}}\boldsymbol{a}$ represents a vector field. Thus, using Eqs. (2.14)-(2.15), we obtain

$$\int_V \boldsymbol{T} : \mathrm{grad}\boldsymbol{a}\,dV = \int_\Sigma (\boldsymbol{T}^{\boldsymbol{T}}\boldsymbol{a})\cdot\boldsymbol{N}\,dS - \int_V \boldsymbol{a}\cdot\mathrm{div}\boldsymbol{T}\,dV. \tag{2.16}$$

---

[3] Equation (3.20) in [6].

[4] Equation (4.1) in [6].

Using $\boldsymbol{a} = \delta\boldsymbol{u}$ implies grad$\boldsymbol{a} = \delta\boldsymbol{\epsilon}$ as $\boldsymbol{\epsilon} = \text{grad}\boldsymbol{u}$ and the operators grad and δ commute. The tensor field is set as $\boldsymbol{T} \equiv \partial\mathscr{u}/\partial\boldsymbol{\epsilon}$. Substituting these definitions in Eq. (2.16) leads to the following equation:

$$\int_V \boldsymbol{\sigma} : \delta\boldsymbol{\epsilon}\, dV = -\int_V (\nabla \cdot \boldsymbol{\sigma}) \cdot \delta\boldsymbol{u}\, dV + \int_\Sigma \boldsymbol{N} \cdot (\boldsymbol{\sigma}^T \cdot \delta\boldsymbol{u})\, dS, \tag{2.17}$$

where the divergence is expressed in terms of the nabla operator $(\nabla\cdot)$.

Thus, the variation equation is transformed into a sum of three integrals: a volume integral in the α-phase, IntV_α, a volume integral in the β-phase, IntV_β, and a surface integral, Int$S$; hence, Eq. (2.8) can be expressed as

$$\text{Int}V_\alpha + \text{Int}V_\beta + \text{Int}S = 0. \tag{2.18}$$

The volume integral in the α-phase is given by

$$\text{Int}V_\alpha = \int_{V^\alpha} \Big[\Big(\frac{\partial\mathscr{u}}{\partial\mathscr{s}} - T\Big)\delta\mathscr{s} - \nabla \cdot \boldsymbol{\sigma} \cdot \delta\boldsymbol{u} + \Big(\frac{\partial\mathscr{u}}{\partial C_B} - \mu_B\Big)\delta C_B\Big] dV, \tag{2.19}$$

where the inner product of Eq. (2.12) was transformed using Eq. (2.17). The volume integral for β-phase has the same form as Eq. (2.19). The surface integral is given by

$$\text{Int}S = \int_\Sigma \Big[\omega^\alpha \delta z^\alpha + \omega^\beta \delta z^\beta + \boldsymbol{N}^{\boldsymbol{\alpha}} \cdot \boldsymbol{\sigma}^{\alpha T} \cdot \delta\boldsymbol{u}^\alpha + \boldsymbol{N}^{\boldsymbol{\beta}} \cdot \boldsymbol{\sigma}^{\beta T} \cdot \delta\boldsymbol{u}^\beta\Big] dS, \tag{2.20}$$

where ω is given by

$$\omega \equiv \mathscr{u} - T\mathscr{s} - \mu_B C_B. \tag{2.21}$$

This ω free energy density can be interpreted as the density of the grand canonical potential. The superscript denotes the side of the interface. For example, $\omega^\alpha = \mathscr{u}^\alpha - T\mathscr{s}^\alpha - \mu C_B^\alpha$, and its superscript implies ω is calculated on the α-side of the interface.

The variations in Eq. (2.20) are not independent of each other. To express Int$S$ in terms of two independent variations, for example, $\delta \boldsymbol{u}^\beta$ and δz^α, we use the following conditions which characterize the coherent interface:

$$\begin{aligned} \delta \boldsymbol{d}^\alpha &= \delta \boldsymbol{d}^\beta, \\ \boldsymbol{N^\beta} &= -\boldsymbol{N^\alpha}, \\ \delta z^\alpha \boldsymbol{N^\alpha} &= \delta z^\beta \boldsymbol{N^\beta}, \end{aligned} \tag{2.22}$$

where Eq. (2.22)a expresses the fact that there is no gap nor any sliding between the two phases. Equation (2.22)c is also a consequence of the coherent constraint, as the β-phase grows at the expense of the α-phase and vice versa. These equations along with Eq. (2.7) imply the following relations:

$$\begin{aligned} \delta \boldsymbol{u}^\alpha &= \delta \boldsymbol{u}^\beta + (\boldsymbol{\epsilon}^\beta - \boldsymbol{\epsilon}^\alpha) \cdot \boldsymbol{N}^\alpha \delta z^\alpha, \\ \delta z^\alpha &= -\delta z^\beta. \end{aligned} \tag{2.23}$$

Thus, Eq. (2.20) is transformed and given by

$$\mathrm{Int}S = \int_\Sigma \Big[(\omega^\alpha - \omega^\beta + \boldsymbol{N^\alpha} \cdot \boldsymbol{\sigma}^{\alpha T} \cdot (\boldsymbol{\epsilon}^\beta - \boldsymbol{\epsilon}^\alpha) \cdot \boldsymbol{N^\alpha}) \delta z^\alpha + (\boldsymbol{N^\alpha} \cdot \boldsymbol{\sigma}^{\alpha T} + \boldsymbol{N^\beta} \cdot \boldsymbol{\sigma}^{\beta T}) \cdot \delta \boldsymbol{u}^\beta \Big] dS. \tag{2.24}$$

Substituting Eq. (2.19) for the volume integrals, and Eq. (2.24) for the surface integral, in Eq. (2.18), we obtain

$$\begin{aligned} &\int_{V^\alpha} \Big[\Big(\frac{\partial \mathscr{u}}{\partial \mathscr{s}} - T \Big) \delta \mathscr{s} - \nabla \cdot \frac{\partial \mathscr{u}}{\partial \boldsymbol{\epsilon}} \cdot \delta \boldsymbol{u} + \Big(\frac{\partial \mathscr{u}}{\partial C_B} - \mu_B \Big) \delta C_B \Big] dV + \\ &\int_{V^\beta} \Big[\Big(\frac{\partial \mathscr{u}}{\partial \mathscr{s}} - T \Big) \delta \mathscr{s} - \nabla \cdot \frac{\partial \mathscr{u}}{\partial \boldsymbol{\epsilon}} \cdot \delta \boldsymbol{u} + \Big(\frac{\partial \mathscr{u}}{\partial C_B} - \mu_B \Big) \delta C_B \Big] dV + \\ \int_\Sigma \Big[(\omega^\alpha - \omega^\beta &+ (\boldsymbol{\epsilon}^\beta - \boldsymbol{\epsilon}^\alpha) \cdot \boldsymbol{\sigma}^\alpha) \delta z^\alpha + (\boldsymbol{N^\alpha} \cdot \boldsymbol{\sigma}^{\alpha T} + \boldsymbol{N^\beta} \cdot \boldsymbol{\sigma}^{\beta T}) \cdot \delta \boldsymbol{u}^\beta \Big] dS = 0. \end{aligned} \tag{2.25}$$

This equation contains variations of the independent variables in each integral.[5]

---

[5] Spherical systems use r instead of z in Eq. (2.25)c.

Equilibrium conditions

For Eq. (2.25) to hold, each of the three integrals must be 0. Thus, the interior of the α-phase satisfies $\text{Int}V_\alpha = 0$, the interior of the β-phase satisfies $\text{Int}V_\beta = 0$, and the interface satisfies $\text{Int}S = 0$. For arbitrary variations of the independent variables, the corresponding coefficients must vanish; the subsequent equations provide the conditions for equilibrium.

First, $\text{Int}V_\alpha = 0$ is considered. The coefficient of $\delta\mathscr{s}$ set to 0 is given by

$$T = \frac{\partial \mathscr{u}}{\partial \mathscr{s}} \quad \text{(thermal equilibrium)}, \tag{2.26}$$

where T is identified as temperature, and is constant as it is a Lagrange multiplier. Equation (2.26) represents the condition for thermal equilibrium.

The coefficient of $\delta\boldsymbol{u}$ set to 0 is given by

$$\nabla \cdot \left(\frac{\partial \mathscr{u}}{\partial \boldsymbol{\epsilon}}\right) = \nabla \cdot \boldsymbol{\sigma} = 0 \quad \text{(mechanical equilibrium)}, \tag{2.27}$$

and represents the condition for mechanical equilibrium.

The coefficient of δC_B set to 0 is given by

$$\mu_B = \mu_{eq} = \frac{\partial \mathscr{u}}{\partial C_B} \quad \text{(chemical equilibrium)}, \tag{2.28}$$

where μ_B is identified as the equilibrium chemical potential of the B-species, μ_{eq}, and is constant as it is a Lagrange multiplier. Equation (2.28) represents the condition for chemical equilibrium.[6]

The same procedure is followed for $\text{Int}V_\beta = 0$. Thus, Eqs. (2.26)-(2.28) describe the internal equilibrium of the α-phase and β-phase. Furthermore, the temperature, and the chemical potential of the B-component are uniform across the two phases.

---

[6] In binary substitutional solid solutions, chemical equilibrium corresponds to a constant *diffusion potential*, which is identified with the Lagrange multiplier difference, given by $\mu_B - \mu_A$ [35].

For Int$S = 0$, setting the coefficients of $\delta \boldsymbol{u}^\beta$ and δz^α to 0 provides the conditions for equilibrium along the coherent interface:

$$\left.\begin{aligned} \boldsymbol{N^\alpha} \cdot \boldsymbol{\sigma}^{\alpha T} + \boldsymbol{N^\beta} \cdot \boldsymbol{\sigma}^{\beta T} = 0, \\ \omega^\beta - \omega^\alpha - (\boldsymbol{\epsilon}^\beta - \boldsymbol{\epsilon}^\alpha) \cdot \boldsymbol{\sigma}^\alpha = 0. \end{aligned}\right. \quad \text{(coherent interfacial equilibrium)} \tag{2.29}$$

Equation (2.29)a describes the mechanical equilibrium at the interface and reflects the continuity of the normal tractions across the interface, which can also be expressed in the component form as

$$\sigma_{ij}^\alpha N_j^\alpha = -\sigma_{ij}^\beta N_j^\beta. \tag{2.30}$$

Thus, the stress is balanced along the coherent interface. Equation (2.29)b represents the condition for phase stability and specifies the jump in the grand canonical free energy across the interface.

In summary, the volume of each phase exhibits thermal, mechanical, and chemical equilibrium, collectively known as internal or bulk equilibrium. The α/β interface entails mechanical equilibrium and interfacial equilibrium. Together, these conditions describe the thermochemical equilibrium of a stressed system, which is also known as thermomechanical equilibrium.

2.3. Kinetics

Kinetics of chemical processes drive the applications of materials by instigating changes in their composition, shape, size, and microstructures. Describing the progress of these changes in time and space as well as their rates is the realm of chemical kinetics; in the solid state, structural constraints must also be accounted for [4, 54].

Fick's law describes the nonequilibrium process of diffusion in terms of the gradient of concentration. However, the state variable corresponding to chemical equilibrium was found to be the chemical potential of B-atoms, as shown by Eq. (2.28). Modified Fick's law describes diffusion in terms of the gradient of the chemical potential, and is used in *Chapter 3*.

The models of Fig. 1.2 are phase-transforming systems. The interfacial chemical reaction consumes the diffusing species locally, thereby affecting the local concentration. Subsequently, this kinetic process occurs in a narrow region of space, and the interface is idealized to a sharp moving front which marks a discontinuous change in the concentration and material properties. These moving boundaries characterize the growth kinetics of such phase-transforming systems, and are typically described using empirical models.

2.3.1 Classical models of growth kinetics

Classical rate models in the literature include the Ginstling-Brounshtein (G-B) model for diffusive reaction in spherical particles [55], Deal-Grove (D-G) model for planar silicon oxidation [56], and the Higuchi equation for rate of drug release from ointment films, which is of key interest within the pharmaceutical sciences [57].

The G-B equation (1950) is a well known 'shrinking core model' in chemical engineering literature [55]. Shrinking core models describe the rate of retreat of the surface of a partially reacted spherical solid particle. The rate-controlling step is the diffusion of reactants through a product layer to an interface at which an instantaneous reaction takes place; the product layer directly replaces the space filled by the initial reactant particle with no change in volume. Such models are also known as *Shell and Core models* or *Unreacted Core models*, and have contributions from both diffusion and geometric controls [58]. For the spherical system in Fig. 1.2, the G-B kinetic equation is given by

$$\boxed{3 - 2\xi - 3(1-\xi)^{2/3} = \frac{kt}{b^2},} \tag{2.31}$$

where $\xi = 1 - \left(\frac{a}{b}\right)^3$, which is a fractional degree of reaction or extent of reaction, a and b are the inner and outer radii respectively, and k is a rate constant that depends on the diffusivity [58].

The D-G equation (1965) is a well-known linear-parabolic model from silicon oxidation literature and is given by Eq. (11) of [56]:

$$\boxed{x_0^2 + A_{\mathrm{DG}} x_0 = B_{\mathrm{DG}} t + x_i^2 + A_{\mathrm{DG}} x_i,} \tag{2.32}$$

where x_0 is the total oxide thickness and x_i is the initial layer of oxide; A_{DG} and B_{DG} are parameters that depend on the effective diffusivity of the mobile oxidant species, rate constants associated with the outer surface and interface, and equilibrium concentration of the oxidant in the oxide.

The Higuchi equation is well known in pharmaceutical literature for quantifying the release of solid drugs suspended in thin films [57]. This equation demonstrates a square root of time type release kinetics, which is given by [59]

$$\frac{M_t}{A_f} = \sqrt{2C_i D C_s t}, \tag{2.33}$$

where M_t denotes the cumulative amount of drug that is released at time t from the film, A_f denotes the surface area of the film, C_i is the initial concentration of the drug, and C_s denotes the solubility of the drug.

2.3.2 Effects of diffusion-reaction-deformation

The effects of diffusion-reaction-deformation have been observed experimentally thanks to an astounding progress in in-situ techniques. Internal stresses have been observed to slow down and inhibit phase transformation reactions in silicon structures, thereby affecting the growth kinetics; some studies attribute this stalling to stress-reaction coupling, while others postulate that it is governed by stress-diffusion coupling [60–69].

In niobium hydrogen thin films, Wagner et al. [70] observed that plastic deformation was suppressed below a critical film thickness, and the elastic stress state altered the chemical potential of hydrogen, phase stability, and critical temperature. Such manifestations of coupling affect the system's utility. Thus, fundamental understanding of diffusion-reaction-deformation is required to advance system miniaturization, which can make devices less susceptible to mechanical damage. Several single particle studies [71–74] have investigated the absorption and desorption of hydrogen in individual palladium nanoparticles with nanometer to atomic scale spatial resolution and millisecond time resolution. It has been observed that single-crystalline nanocubes do not exhibit thermodynamic phase coexistence [71], nanocrystals over a substantial size and shape range exhibit distinct and wide hysteresis between absorption and desorption [74], and in general, phase coexistence occurs above a critical size and is accompanied by defects [72, 73].

Hysteresis, a dissipative phenomena that lowers the efficiency of any device operating under cyclic conditions, is observed in both lithium-ion batteries and metal hydrides, and continues to persist with vanishing kinetics; in electrochemical systems, the subsequent residual voltage is called a zero-current offset [20, 71, 74–76]. Schwarz and Khachaturyan attribute the ubiquitous hysteresis in palladium hydrides to an intrinsic thermodynamic phenomena that maintains the coherency of the interface, and is accompanied by an elastic strain energy that generates a nucleation energy barrier [77–80]. Freidin and Eremeyev developed a model to explain the phenomena of hysteresis in stress-induced phase transformations [81]. They also considered the effects of energy barriers due to nucleation and metastability; the latter leads to hysteresis even in quasi-equilibrium. In phase-transforming electrodes of lithium-ion batteries, Dreyer et al. attributed the inherent thermodynamic hysteresis to the sequential charging and discharging of particles in an electrode comprising multiple particles and predicted the existence of multiple equilibria [75, 82]. Subsequently, zero-current hysteresis was predicted even for a single particle via the pinning of the phase front by heterogeneities [83]. These references do not form an exhaustive list; for example, the interpretation of hysteresis in metal hydrides has a long history during which the underlying cause remained an open question [84–87].

2.3.3 Modeling of diffusion-reaction-deformation phenomena

Kinetic models are most useful to technology. However, many coupled kinetic models are developed using an ad hoc approach for a specific problem at hand, namely, by modifying or extending classical models of diffusion and phase growth to improve their fit with experimental observations of a given material system.

The classical models of growth kinetics in *Section 2.3.1* do not include the effects of deformation and the subsequent coupled effects. They are derived using Fick's law of diffusion, which implies an instantaneous response of the flux to a change in the driving force. To include the effects of deformation in the stress-free (SF) classical rate models, the constant material and kinetic parameters are often replaced with their effective values varying with concentration, stresses, temperature, as well as time when considering viscoelastic and stress relaxation effects. For example, in the D-G silicon oxidation model, stress-dependent effective diffusivities and reaction rate constants are used; the nature of these equations is based on intuition, using the concept of activation volumes and fitting parameters [60,61,88–93]. The D-G model is also used as the basis for studying the experimental data of other material systems, including hydrides and silicides [94–97], where modifications and extensions are incorporated to fit the data. This theoretical approach is commonly adopted by coupled models; while these models may describe the experimental observations, they do not have any predictive capabilities. In the next chapter, we formulate uncoupled and elastically-coupled models using a thermodynamic-kinetic approach to model the phase growth as well as predict the effects of elasticity on diffusion and reaction.

Chapter 3

Moving boundary problems

This chapter formulates the kinetic models that are used subsequently in the uncoupled and elastically-coupled analyses for the two geometries.

3.1. Kinetic processes

When the system is driven away from equilibrium, thermal, mechanical, chemical, and interfacial processes kick in to drive the system to equilibrium. The rates of the physical processes are generally described using the theory of irreversible thermodynamics. In this work, the simplest descriptions are used to model the kinetics of the irreversible processes, assuming small deviations of the system from its equilibrium state.

3.2. Local equilibrium

The quasi-steady state analysis requires the assumption of local equilibrium. In addition, it assumes that thermal and mechanical equilibria are rapidly established compared to the time required to establish compositional and phase equilibria.

3.3. Coupling

The coupling between the diffusion-reaction-deformation phenomena can be explicitly seen in the chemical potential and the grand canonical free energy.

Differences in the chemical potential of the B-species drive the diffusion of B-atoms. From Eq. (2.28), the chemical potential of the B-atoms is given by

$$\mu_B = \frac{\partial \mathscr{u}(\boldsymbol{\epsilon}, \mathscr{s}, C_B)}{\partial C_B}, \tag{3.1}$$

where the internal energy density depends on the composition and strain, and hence, reaction and deformation respectively.

Equation (2.29)b represents phase change, and can be expressed using Eq. (2.21) as

$$[\![\omega]\!] - [\![\boldsymbol{\epsilon}]\!] \cdot \boldsymbol{\sigma}^{\alpha} = [\![\mathscr{u}]\!] - T[\![\mathscr{s}]\!] - \mu_B[\![C_B]\!] - [\![\boldsymbol{\epsilon}]\!] \cdot \boldsymbol{\sigma}^{\alpha} = 0, \tag{3.2}$$

where $[\![\,]\!]$ denotes the jump across the interface, for example, $[\![\omega]\!] = \omega^{\beta} - \omega^{\alpha}$.

When $[\![\omega]\!] - [\![\boldsymbol{\epsilon}]\!] \cdot \boldsymbol{\sigma}^{\alpha} \neq 0$, it drives the interface motion, with ω coupling phase transformation to deformation, reaction, and diffusion, via the internal energy density, the chemical potential, and composition.

3.4. Diffusion

When a phase is not in chemical equilibrium, its chemical potential is not a constant. Instead, there is a gradient in the potential, which is assumed to generate and drive diffusion fluxes.

To describe the diffusive transport of the B-atoms, an empirical relationship is identified for the local diffusion flux and the local diffusion force using the principles of irreversible thermodynamics, specifically, the rate of local production of entropy. The driving force is interpreted as the negative gradient of the chemical potential. This phenomenological model for diffusion is expressed as [4, 7]

$$\begin{aligned} \boldsymbol{J_B^\eta} &= -C_B^\eta \boldsymbol{M_B^\eta} \cdot \nabla \mu_B^\eta, \\ \frac{\partial C_B^\eta}{\partial t} &= -\nabla \cdot \boldsymbol{J_B^\eta}, \end{aligned} \qquad \eta = \alpha, \beta \tag{3.3}$$

where $\boldsymbol{J_B^\eta}$, $\boldsymbol{M_B^\eta}$, $\nabla \mu_B^\eta$ respectively describe the flux, mobility, and the gradient of the chemical potential of the B-atoms in the phase under consideration, and t is time. The flux is measured with respect to the A-lattice, which provides a reference frame. The mobility is a function of concentration and stress at a given temperature.[7] Equation (3.3)b represents the conservation of the B-atoms in the differential form. Equation (3.3)a is called Modified Fick's force-flux (empirical) law [4].

We assume both systems exhibit isotropic mobility. Furthermore, as only the B-atoms are mobile, we drop the subscript B for the subsequent sections.

For the spherical system, one-dimensional diffusion is assumed to occur along the r direction, i.e. only the r-component of flux is non-zero. Thus, the equations for the flux and the conservation of B-atoms are given by

$$\begin{aligned} J^\eta &= -M^\eta C^\eta \frac{\partial \mu^\eta}{\partial r}, \\ \frac{\partial C^\eta}{\partial t} &= -\nabla_r J_r, \\ &= -\frac{\partial J^\eta}{\partial r} - \frac{2}{r} J_r, \end{aligned} \qquad \eta = \alpha, \beta \tag{3.4}$$

where $\nabla_r = \frac{\partial}{\partial r} + \frac{2}{r}$, and is the only contributing term.[8]

---

[7] For ideal dilute solutions undergoing small deviations from equilibrium, M^η is related to the diffusivity of the B-atoms in the phase under consideration, D^η, and is given by $M^\eta = D^\eta/RT$, where R is the gas constant; the derivation is shown in *Appendix B.*

[8] Divergence of a vector field (in spherical coordinates), $\boldsymbol{F}(r, \phi, \theta)$, is given by $\nabla \cdot \boldsymbol{F} = \frac{\partial F_r}{\partial r} + \frac{2}{r} F_r + \frac{1}{r} \frac{\partial F_\phi}{\partial \phi} + \frac{\cot \phi}{r} F_\phi + \frac{1}{r \sin \phi} \frac{\partial F_\theta}{\partial \theta}$, where $\boldsymbol{F} = F_r(r, \theta, \phi) \hat{\boldsymbol{r}} + F_\theta(r, \theta, \phi) \hat{\boldsymbol{\theta}} + F_\phi(r, \theta, \phi) \hat{\boldsymbol{\phi}}$ [98].

For the planar system, one-dimensional diffusion is assumed to occur along the z direction. Thus, the diffusion equations are given by

$$\begin{aligned} J^\eta &= -M^\eta C^\eta \frac{\partial \mu^\eta}{\partial z}, \\ \frac{\partial C^\eta}{\partial t} &= -\frac{\partial J^\eta}{\partial z}. \end{aligned} \qquad \eta = \alpha, \beta \tag{3.5}$$

3.5. Phase transformation

When the two phases are not in equilibrium, there is a driving force, denoted by Φ, that generates and drives the motion of the interface until it reaches equilibrium. To describe this driving force, Eq. (3.2) is modified and expressed as

$$\Phi = \llbracket \omega \rrbracket - \llbracket \boldsymbol{\epsilon} \rrbracket \cdot \boldsymbol{\sigma}^\alpha = \llbracket \mathscr{u} \rrbracket - T \llbracket \mathscr{s} \rrbracket - \mu \llbracket C \rrbracket - \llbracket \boldsymbol{\epsilon} \rrbracket \cdot \boldsymbol{\sigma}^\alpha. \tag{3.6}$$

3.5.1 Velocity of the interface

Models of interface motion usually express the normal velocity of the interface as a function of Φ. When the system is close to equilibrium, the velocity of the interface is assumed to be linearly proportional to the driving force, and characterizes the kinetics of the interface [23]. We use the following kinetic model:

$$v_I = -\frac{V_0}{C_A R T} \Phi, \tag{3.7}$$

where V_0 is a characteristic velocity and v_I is the velocity of the interface; the model is derived in *Appendix C*.

3.5.2 Mass balance at the interface

The mass balance at the interface is given by

$$\begin{aligned} v_I &= -\frac{\llbracket J_r \rrbracket}{\llbracket C \rrbracket} \qquad \text{(spherical)}, \\ v_I &= \frac{\llbracket J_z \rrbracket}{\llbracket C \rrbracket} \qquad \text{(planar)}, \end{aligned} \tag{3.8}$$

where the speed of the interface is related to the flux of the B-atoms crossing the boundary.

3.5.3 Chemical equilibrium at the interface

The interface is assumed to be at local chemical equilibrium. Consequently, at the phase boundary, the chemical potentials of the two phases are equal:

$$\mu_I^{\alpha} = \mu_I^{\beta} \equiv \mu_I, \tag{3.9}$$

where μ_I^{η} is the chemical potential at the interface on the η-side of the interface.

3.6. Local entropy production

It is noted that the phenomenological diffusion and reaction models satisfy the thermodynamic restriction of local entropy imbalance, or the Clausius-Duhem inequality because $-J \cdot \nabla\mu > 0$ and $-v_I \cdot \Phi > 0$.

3.7. Legendre transformation for small strains

The general relationships for the chemical potential and grand canonical potential density are determined formally from the first two laws of thermodynamics, which yield

$$d\mathscr{u} = T d\mathscr{s} + \sigma_{ij} d\epsilon_{ij} + \mu dC. \tag{3.10}$$

The above equation follows directly from Eq. (2.12) once equilibrium has been assumed and the constraints on the variation of the B-atoms have been accounted for [99]. The independent variables are $\mathscr{s}$, ϵ_{ij}, and C.

To obtain a change in variable, we define a new function, $\mathscr{g}$, Gibbs energy density for nonhydrostatic stresses.[9] For small strains, $\mathscr{g}$ is given by

$$\mathscr{g} = \mathscr{u} - T\mathscr{s} - \boldsymbol{\sigma} : \boldsymbol{\epsilon}. \tag{3.11}$$

Gibbs energy density is a state function whose value depends on the current thermodynamic state and is independent of the path taken to reach this state. The total differential of Gibbs energy density is given by

$$\begin{aligned} d\mathscr{g} &= d\mathscr{u} - Td\mathscr{s} - \mathscr{s}dT - \sigma_{ij}d\epsilon_{ij} - \epsilon_{ij}d\sigma_{ij}, \\ &= Td\mathscr{s} + \sigma_{ij}d\epsilon_{ij} + \mu dC - Td\mathscr{s} - \mathscr{s}dT - \sigma_{ij}d\epsilon_{ij} - \epsilon_{ij}d\sigma_{ij}, \\ &= -\mathscr{s}dT + \mu dC - \epsilon_{ij}d\sigma_{ij}, \end{aligned} \tag{3.12}$$

where Eq. (3.10) was used. Thus, $\mathscr{g}$ can be considered a function of T, σ_{ij}, and C. Since $\mathscr{g}$ is a state function of these variables, d$\mathscr{g}$ is an exact differential, and is given by

$$d\mathscr{g} = (\frac{\partial \mathscr{g}}{\partial T})dT + (\frac{\partial \mathscr{g}}{\partial C})dC + (\frac{\partial \mathscr{g}}{\partial \sigma_{ij}})d\sigma_{ij}. \tag{3.13}$$

Comparing Eqs. (3.12) and (3.13), we obtain

$$\begin{aligned} \frac{\partial \mathscr{g}}{\partial T} &= -s, \\ \frac{\partial \mathscr{g}}{\partial C} &= \mu, \\ \frac{\partial \mathscr{g}}{\partial \sigma_{ij}} &= -\epsilon_{ij}. \end{aligned} \tag{3.14}$$

---

[9] The Gibbs energy density used here is analogous to the classical Gibbs energy; the latter is an appropriate function to use under conditions of constant temperature, composition, and hydrostatic pressure.

For an exact differential, the order of differentiation can be exchanged. Thus, we obtain

$$\frac{\partial}{\partial C}\Big(\frac{\partial \mathscr{G}}{\partial \sigma_{ij}}\Big) = \frac{\partial}{\partial \sigma_{ij}}\Big(\frac{\partial \mathscr{G}}{\partial C}\Big). \tag{3.15}$$

Substituting Eqs. (3.14)b and (3.14)c in Eq. (3.15) gives the following Maxwell's relation:

$$-\Big(\frac{\partial \epsilon_{ij}}{\partial C}\Big)\Big|_{T,\sigma_{ij}} = \Big(\frac{\partial \mu}{\partial \sigma_{ij}}\Big)\Big|_{T,C,\sigma_{kl\neq ij}}. \tag{3.16}$$

Equation (3.16) requires a constitutive law connecting the stress and the strain. As the temperature is assumed constant, stresses are induced when the material is deformed or a compositional change occurs, and are given by

$$\sigma_{ij} = C_{ijkl}\Big(\epsilon_{kl} - \epsilon^c_{kl}\Big), \tag{3.17}$$

where ϵ^c_{ij} is a stress-free strain, and C_{ijkl} is the elastic stiffness tensor. Solving Eq. (3.17) for strain leads to

$$\epsilon_{ij} = \epsilon^c_{ij} + S_{ijkl}\sigma_{kl}, \tag{3.18}$$

where S_{ijkl} is the elastic compliance tensor. Equation (3.18) can also be interpreted as an additive decomposition of the total strain, $\epsilon_{ij} = \epsilon^c_{ij} + \epsilon^e_{ij}$, where ϵ^e_{ij} is the elastic strain, which is related to stress using Hooke's law.

Integrating Eq. (3.16) from zero stress to σ_{ij} gives $\mu(\sigma, C)$, the stress-dependent chemical potential:

$$\mu(C,\sigma) = \mu(C,0) - \Big(\frac{\partial \epsilon^c_{ij}}{\partial C}\sigma_{ij} + \frac{\partial S_{ijkl}}{\partial C}\sigma_{ij}\sigma_{kl}\Big), \tag{3.19}$$

where $\mu(C,0)$ is the stress-free chemical potential, given by Eq. (3.14)b in terms of Gibbs energy density. Assuming the material properties are constants, the chemical potential for the stressed system is given by

$$
\begin{aligned}
\mu(C,\sigma) &= \mu(C,0) - \frac{\partial \epsilon^c_{ij}}{\partial C}\sigma_{ij}, \\
&= \frac{\partial \mathscr{G}}{\partial C}\Big|_{(C,0)} - \frac{\partial \epsilon^c_{ij}}{\partial C}\sigma_{ij}.
\end{aligned}
\tag{3.20}
$$

At uniform composition and temperature, the total differential of the Gibbs energy density, Eq. (3.13), simplifies to

$$
d\mathscr{G} = -\epsilon^e_{ij} d\sigma_{ij}, \tag{3.21}
$$

where the only contribution to strain is the elastic strain. Integrating from zero stress to σ_{ij}, we obtain $\mathscr{G}$ for a linearly elastic solid, which is given by

$$
\mathscr{G}(T, C, \boldsymbol{\sigma}) = \mathscr{G}(T, C, 0) - \phi, \tag{3.22}
$$

where the strain energy of the solid, $\phi = \sigma_{ij}\epsilon^e_{ij}/2$, and the Gibbs energy density at zero stress, $\mathscr{G}(T, C, 0) = \omega + \mu C$, using Eqs. (2.21) and (3.11).

Equation (3.22) is simplified to

$$
\mathscr{G}(T, C, \boldsymbol{\sigma}) = \omega + \mu C - \phi. \tag{3.23}
$$

Thus, the jump in the grand canonical potential density can be written as

$$
[\![\omega]\!] = [\![\mathscr{G}]\!] - \mu_I [\![C]\!] + [\![\phi]\!], \tag{3.24}
$$

where μ_I is the chemical potential at the interface.

The driving force for phase boundary migration is expressed using Eqs. (3.6) and (3.24):

$$
\Phi = [\![\mathscr{G}]\!] - \mu_I [\![C]\!] + [\![\phi]\!] - [\![\epsilon_{ij}]\!]\sigma^\alpha_{ij}, \tag{3.25}
$$

where the last contribution represents the interface work term.

Equations (3.20) and (3.25) are the transformed equations corresponding to Eqs. (3.1) and (3.2) respectively; they assume small strains, and exhibit the diffusion-reaction-deformation coupling.

3.8. Research methodology and model summary

To study the systems shown in Fig. 1.2, we use concepts from *Equilibrium Thermostatics* and *Kinetics*. The former included a variational formulation based on the laws of equilibrium thermostatics to obtain the equations for thermal, chemical, mechanical, and interfacial equilibrium in the two phases as well as at the interface. In this chapter, the chemical and phase equilibrium assumptions were relaxed to introduce kinetics into the problem. The framework is summarized in Table 3.1.

Thermodynamics	- first and second laws - equations for thermal, mechanical equilibrium	Laws
Interface	- coherent - other possibilities: incoherent, semicoherent	Choice
Kinetics	- close to equilibrium - local chemical equilibrium at the interface - local entropy production	Assumptions

Table 3.1: Framework summary

The quantities to be computed include the composition of the two phases away from the interface (C^α and C^β), the interfacial compositions in the two phases (C_I^α and C_I^β), and the stresses ($\boldsymbol{\sigma}^\alpha$ and $\boldsymbol{\sigma}^\beta$) and strains ($\boldsymbol{\epsilon}^\alpha$ and $\boldsymbol{\epsilon}^\beta$) in the two phases. Furthermore, as the phase boundary moves with time, location of the interface, a and z_I, and velocity of the moving interface, v_I, are not known in advance and must be determined as part of the solution. This characteristic of computing part of the domain, makes the problem at hand a *moving* *boundary problem.* When the boundary is stationary, the problem is known as a *free boundary problem* [100].

Moving boundary problems are often called Stefan problems, after Josef Stefan who formulated the problem in the context of heat conduction. A Stefan condition is required to describe the conservation of mass at the interface; this mass balance equation is given by Eq. (3.8); it is a nonlinear equation as the interfacial concentrations and the velocity of the interface are unknown. The kinetic equations also exhibit nonlinearities, as seen in Eqs. (3.4) and (3.5).

To study the behavior of the two systems, we undertake two analyses for each system: a stress-free (SF) uncoupled analysis and an elastically coupled analysis. The starting point for each problem is the SF system at equilibrium.

3.9. Stress-free system at equilibrium

Initially, the α and β phases are assumed to be at equilibrium with concentrations C_{eq}^{α} and C_{eq}^{β} respectively, as shown in Fig. 3.1(a,b). Such a SF equilibrium state is also known as thermochemical equilibrium.

Chemical equilibrium implies $\mu^{\alpha} = \mu^{\beta} = \mu_{eq}$, which includes chemical equilibrium at the interface: $\mu_I^{\alpha} = \mu_I^{\beta} = \mu_{eq}$, where μ_{eq} corresponds to Eq. (2.28) of the framework. Subsequently, there is no diffusion, and the B-atoms do not move. Interfacial equilibrium implies the driving force for the phase transformation reaction is zero, i.e., $\Phi = 0$; subsequently, the velocity of the interface is 0 and the interface does not move.

From Eq. (3.25), chemical and interfacial equilibria in a SF system imply

$$[\![\mathscr{G}]\!] - \mu_{eq}[\![C]\!] = 0, \tag{3.26}$$

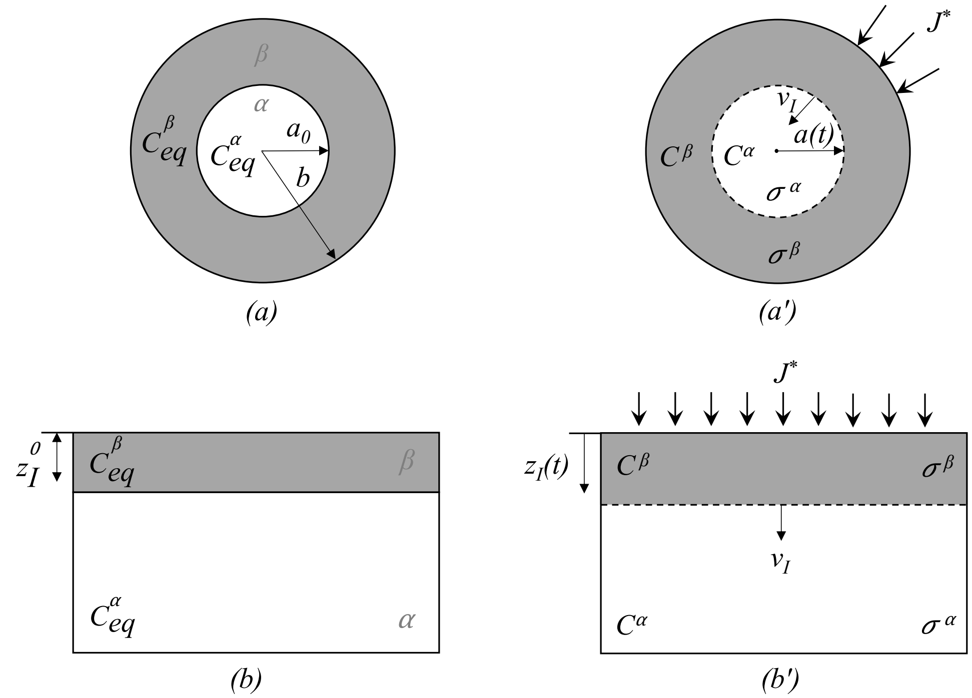

Figure 3.1: Schematic cross-section of a spherical core-shell particle and a planar bilayer at T_0. At equilibrium, the concentration is C_{eq} and the interfaces are at (a) $r = a_0$ and (b) $z = z_I^0$. The prescribed flux, J^*, drives the systems away from equilibrium. The kinetics of the systems include diffusion and phase transformation, accompanied by stresses, σ. The position and velocity of the interface are denoted respectively as (a′) $a(t)$, $v_I = -\frac{da}{dt}$; (b′) $z_I(t)$, $v_I = \frac{dz_I}{dt}$.

where the terms related to deformation were ignored. Expanding this equation, we obtain

$$\mathscr{g}(C_{eq}^{\beta}) - \mathscr{g}(C_{eq}^{\alpha}) - \mu_{eq}(C_{eq}^{\beta} - C_{eq}^{\alpha}) = 0, \tag{3.27}$$

which expresses the equilibrium condition using a *common tangent construction*, which is shown graphically in Fig. 3.2.

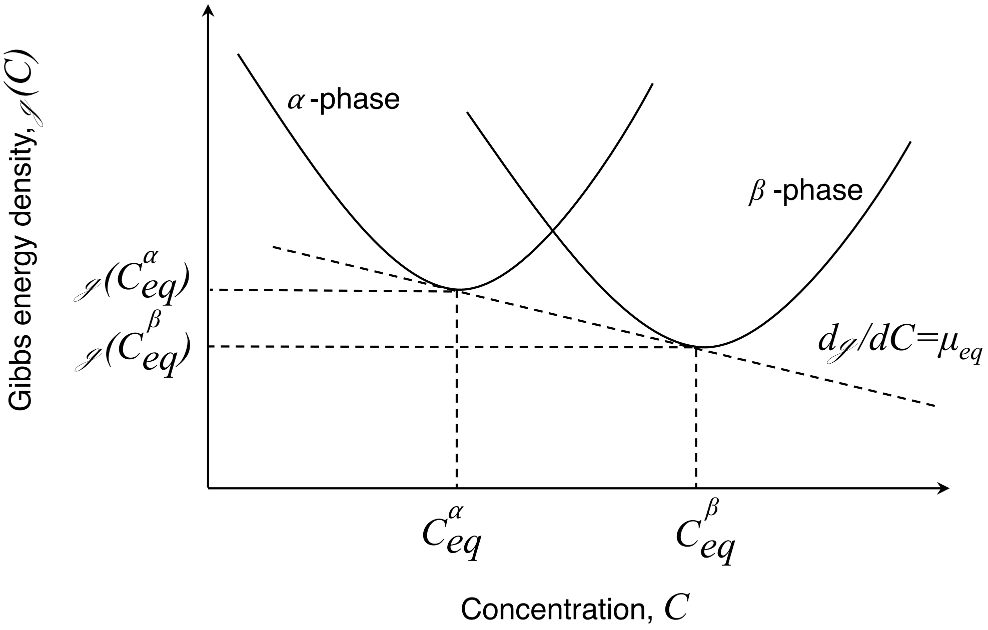

Figure 3.2: Schematic of the variation in Gibbs energy density with respect to composition in the absence of stress. The equilibrium compositions exhibit a common tangent.

3.10. System undergoing diffusion and phase transformation

At time, $t = 0$, a flux, J^*, is applied to the spherical system at $r = b$ and to the planar system at $z = 0$, as shown in Fig. 3.1(a',b'). The transport of the B-atoms induces diffusion and reaction, which modify the stress and concentration distributions, and move the α/β interface. To analyze these effects on the two systems, the following assumptions are used:

(A1) The two phases undergo small deviations from equilibrium. The concentrations of the B-atoms in the two phases are given by

$$\begin{aligned} C^{\alpha} &= C_{eq}^{\alpha} + \delta C^{\alpha}, \\ C^{\beta} &= C_{eq}^{\beta} + \delta C^{\beta}, \end{aligned} \tag{3.28}$$

where it is assumed that the concentration change, $\delta C \ll C_{eq}$; consequently, terms containing higher orders of δC will be ignored. Furthermore, we are able to write linearized Taylor expressions for the chemical potential, and Gibbs energy density, which are given by

$$\begin{aligned} \mu^\alpha &= \mu_{eq} + \delta\mu^\alpha, \\ \mu^\beta &= \mu_{eq} + \delta\mu^\beta, \end{aligned} \tag{3.29}$$

$$\begin{aligned} \mathscr{g}^\alpha =& \mathscr{g}(C^\alpha_{eq}) + \mu_{eq}\delta C^\alpha, \\ \mathscr{g}^\beta =& \mathscr{g}(C^\beta_{eq}) + \mu_{eq}\delta C^\beta, \end{aligned} \tag{3.30}$$

where $\delta\mu$ is the change in the chemical potential; in the absence of stress, it is simplified to

$$\begin{aligned} \delta\mu^\alpha &= \kappa^\alpha \delta C^\alpha, \\ \delta\mu^\beta &= \kappa^\beta \delta C^\beta, \end{aligned} \quad \text{(uncoupled)} \tag{3.31}$$

where κ^α and κ^β denote the curvatures of $\mathscr{g}$: $\kappa^\alpha = \left.\dfrac{d^2\mathscr{g}^\alpha}{dC^2}\right|_{C^\alpha_{eq}}$ and $\kappa^\beta = \left.\dfrac{d^2\mathscr{g}^\beta}{dC^2}\right|_{C^\beta_{eq}}$.

(A2) The interface is at chemical equilibrium as per Eq. (3.9), which can be simplified using Eq. (3.29) to

$$\delta\mu^\alpha_I = \delta\mu^\beta_I, \tag{3.32}$$

where $\delta\mu^\alpha_I$ and $\delta\mu^\beta_I$ are the chemical potential deviations just adjacent to the phase boundary in the α- and β-phases respectively.

(A3) The system is undergoing steady state diffusion, i.e. $\dfrac{\partial C^\eta}{\partial t} = 0$ as per Eq. (3.3)b.

(A4) The two phases have constant material properties. Furthermore, the material properties are the same in both phases.

(A4) (planar case) We assume the two phases of the planar system exhibit an equibiaxial state of stresses and strains:

$$\begin{aligned} \sigma^{\alpha}_{xx} &= \sigma^{\alpha}_{yy} = \sigma^{\alpha}, \\ \sigma^{\beta}_{xx} &= \sigma^{\beta}_{yy} = \sigma^{\beta}, \\ \sigma^{\alpha}_{zz} &= \sigma^{\beta}_{zz} = 0, \\ \epsilon_{xx} &= \epsilon_{yy} = \epsilon, \end{aligned} \tag{3.33}$$

where ϵ is the total strain of the bilayer.

3.10.1 Mechanical equilibrium

The kinetics under consideration assume mechanical equilibrium, as highlighted in *Section 3.2*. Therefore, the elastic stresses must satisfy the mechanical equilibrium conditions in the bulk and at the interface, which are given by Eqs. (2.27) and (2.29)a respectively. For the spherical system, these two conditions simplify to

$$\begin{gathered} \nabla \cdot \boldsymbol{\sigma} = \frac{\partial \sigma_{rr}}{\partial r} + \frac{2}{r}\Big(\sigma_{rr} - \sigma_{\theta\theta}\Big) = 0 \quad \text{(in the bulk)}, \\ \boldsymbol{N^{\alpha}} \cdot \boldsymbol{\sigma}^{\alpha T} + \boldsymbol{N^{\beta}} \cdot \boldsymbol{\sigma}^{\beta T} = \sigma^{\alpha}_{rr} - \sigma^{\beta}_{rr} = 0 \quad \text{(at the interface)}. \end{gathered} \tag{3.34}$$

In the planar case, the condition for mechanical equilibrium at the interface is satisfied trivially for the assumed equibiaxial stresses and strains because the interfacial stresses, σ^{η}_{I} $(\eta = \alpha, \beta)$ are not functions of z and $\sigma_{zz} = 0$. We will revisit the bulk mechanical equilibrium condition in *Chapter 5*.

3.10.2 Interface conditions

The general expression for the driving force for the migration of the phase boundary or interface is given by Eq. (3.25), where $[\![\mathscr{G}]\!] - \mu_I [\![C]\!]$ can be further simplified using Eqs.

(3.28) to (3.30) as follows:

$$\begin{aligned}
[\![\mathscr{g}]\!] - \mu_I[\![C]\!] =& \mathscr{g}(C^{\beta}_{eq}) + \mu_{eq}\delta C^{\beta}_{I} - (\mathscr{g}(C^{\alpha}_{eq}) + \mu_{eq}\delta C^{\alpha}_{I}) - \mu_I(C^{\beta}_{eq} + \delta C^{\beta}_{I} - C^{\alpha}_{eq} - \delta C^{\alpha}_{I}),\\
=& \mathscr{g}(C^{\beta}_{eq}) - \mathscr{g}(C^{\alpha}_{eq}) + \mu_{eq}(\delta C^{\beta}_{I} - \delta C^{\alpha}_{I}) - \mu_I(C^{\beta}_{eq} - C^{\alpha}_{eq}) - \mu_I(\delta C^{\beta}_{I} - \delta C^{\alpha}_{I}),\\
=& \mathscr{g}(C^{\beta}_{eq}) - \mathscr{g}(C^{\alpha}_{eq}) + \mu_{eq}(\delta C^{\beta}_{I} - \delta C^{\alpha}_{I}) - (\mu_{eq} + \delta\mu^{\beta}_{I})(C^{\beta}_{eq} - C^{\alpha}_{eq})\\
& - (\mu_{eq} + \delta\mu^{\beta}_{I})(\delta C^{\beta}_{I} - \delta C^{\alpha}_{I}).
\end{aligned} \tag{3.35}$$

Equation (3.35) is further simplified using the common tangent condition at equilibrium, Eq. (3.27), and ignoring the terms containing $(\delta C)^2$:

$$\begin{aligned}
[\![\mathscr{g}]\!] - \mu_I[\![C]\!] &= -\delta\mu^{\beta}_{I}(C^{\beta}_{eq} - C^{\alpha}_{eq}) \qquad \text{(coupled)},\\
&= -\kappa^{\beta}\delta C^{\beta}_{I}(C^{\beta}_{eq} - C^{\alpha}_{eq}) \qquad \text{(uncoupled)},
\end{aligned} \tag{3.36}$$

where Eq. (3.31) is used for the uncoupled case. Thus, Eq. (3.25) is expanded and written as

$$\Phi = -\delta\mu^{\beta}_{I}(C^{\beta}_{eq} - C^{\alpha}_{eq}) + [\![\phi]\!] - [\![\epsilon_{ij}]\!]\sigma^{\alpha}_{ij}. \tag{3.37}$$

Equation 3.37 shows that the driving force for the interface motion entails three key interfacial terms involving the stressed chemical potential, strain energy, and interface work.

The interface kinetics and mass balance condition, Eqs. (3.7) and (3.8), involve the velocity of the interface, v_I, which is given by

$$\begin{aligned}
v_I &= -\frac{da}{dt} \qquad \text{(spherical)},\\
v_I &= \frac{dz_I}{dt} \qquad \text{(planar)}.
\end{aligned} \tag{3.38}$$

The jumps in the fluxes and concentrations are given by [23]

$$\begin{aligned}
[\![J_r]\!] &= \lim_{\varepsilon\to 0}\big(J_r(a+\varepsilon) - J_r(a-\varepsilon)\big), \\
& \qquad\qquad\qquad\qquad\qquad\qquad \text{(spherical)} \\
[\![C]\!] &= \lim_{\varepsilon\to 0}\big(C(a+\varepsilon) - C(a-\varepsilon)\big), \\
[\![J_z]\!] &= \lim_{\varepsilon\to 0}\big(J_z(z_I-\varepsilon) - J_z(z_I+\varepsilon)\big), \\
& \qquad\qquad\qquad\qquad\qquad\qquad \text{(planar)} \\
[\![C]\!] &= \lim_{\varepsilon\to 0}\big(C(z_I-\varepsilon) - C(z_I+\varepsilon)\big).
\end{aligned} \tag{3.39}$$

Fig. 3.1 shows that $a+\varepsilon$ and $z_I-\varepsilon$ refer to the β-side of the interface; $a-\varepsilon$ and $z_I+\varepsilon$ refer to the α-side of the interface. For small deviations from equilibrium, the jump in the concentration for both systems is given by

$$[\![C]\!] = C^{\beta}_{eq} + \delta C^{\beta}_{I} - (C^{\alpha}_{eq} + \delta C^{\alpha}_{I}) = C^{\beta}_{eq} - C^{\alpha}_{eq} + \delta C^{\beta}_{I} - \delta C^{\alpha}_{I}, \tag{3.40}$$

where δC^{α}_{I} and δC^{β}_{I} are the concentration deviations just adjacent to the phase boundary in the α- and β-phases respectively. The jump in flux, $[\![J]\!] = J^{\beta}_{I} - J^{\alpha}_{I}$, is simplified using Eq. (3.5)a:

$$\begin{aligned}
[\![J_z]\!] &= \lim_{\epsilon\to 0}\Big\{ - M^{\beta}C^{\beta}_{I}\frac{\partial \mu^{\beta}}{\partial z}\Big|_{z_I-\epsilon} + M^{\alpha}C^{\alpha}_{I}\frac{\partial \mu^{\alpha}}{\partial z}\Big|_{z_I+\epsilon}\Big\}, \\
&= \lim_{\epsilon\to 0}\Big\{ - M^{\beta}C^{\beta}_{I}\frac{\partial \delta\mu^{\beta}_{I}}{\partial z}\Big|_{z_I-\epsilon} + M^{\alpha}C^{\alpha}_{I}\frac{\partial \delta\mu^{\alpha}_{I}}{\partial z}\Big|_{z_I+\epsilon}\Big\}, && \text{(coupled)} \\
&= \lim_{\epsilon\to 0}\Big\{ - M^{\beta}(C^{\beta}_{eq} + \delta C^{\beta}_{I})\kappa^{\beta}\frac{\partial \delta C^{\beta}}{\partial z}\Big|_{z_I-\epsilon} + M^{\alpha}(C^{\alpha}_{eq} + \delta C^{\alpha}_{I})\kappa^{\alpha}\frac{\partial \delta C^{\alpha}}{\partial z}\Big|_{z_I+\epsilon}\Big\} && \text{(uncoupled)} \\
[\![J_r]\!] &= \lim_{\epsilon\to 0}\Big\{ - M^{\beta}C^{\beta}_{I}\frac{\partial \mu^{\beta}}{\partial r}\Big|_{a+\epsilon} + M^{\alpha}C^{\alpha}_{I}\frac{\partial \mu^{\alpha}}{\partial r}\Big|_{a-\epsilon}\Big\}, && \text{(coupled)} \\
&= \lim_{\epsilon\to 0}\Big\{ - M^{\beta}(C^{\beta}_{eq} + \delta C^{\beta}_{I})\kappa^{\beta}\frac{\partial \delta C^{\beta}}{\partial r}\Big|_{a+\epsilon} + M^{\alpha}(C^{\alpha}_{eq} + \delta C^{\alpha}_{I})\kappa^{\alpha}\frac{\partial \delta C^{\alpha}}{\partial r}\Big|_{a-\epsilon}\Big\}, && \text{(uncoupled)}
\end{aligned} \tag{3.41}$$

where Eqs. (3.28), (3.29), and (3.31) were used.

3.10.3 Boundary conditions

The flux is specified:

$$
\begin{aligned}
-M^\beta C^\beta \frac{\partial \mu^\beta}{\partial r}\Big|_{r=b} &= J^* \quad \text{(spherical)},\\
-M^\beta C^\beta \frac{\partial (\delta\mu^\beta)}{\partial r}\Big|_{r=b} &= J^* \quad (\textit{coupled}),\\
-M^\beta C^\beta \kappa^\beta \frac{\partial (\delta C^\beta)}{\partial r}\Big|_{r=b} &= J^* \quad (\textit{uncoupled}),
\end{aligned}
\tag{3.42}
$$

$$
\begin{aligned}
-M^\beta C^\beta \frac{\partial \mu^\beta}{\partial z}\Big|_{z=0} &= J^* \quad \text{(planar)},\\
-M^\beta C^\beta \frac{\partial (\delta\mu^\beta)}{\partial z}\Big|_{z=0} &= J^* \quad (\textit{coupled}),\\
-M^\beta C^\beta \kappa^\beta \frac{\partial (\delta C^\beta)}{\partial z}\Big|_{z=0} &= J^* \quad (\textit{uncoupled}),
\end{aligned}
$$

where Eqs. (3.29) and (3.31) were used to simplify.

The flux boundary condition is further simplified using $\Big(1 + \frac{\delta C^\beta}{C^\beta_{eq}}\Big)^{-1} \approx 1 - \frac{\delta C^\beta}{C^\beta_{eq}}$. For example, consider the flux boundary condition for the planar case:

$$
\begin{aligned}
\Big[(C^\beta_{eq} + \delta C^\beta)\frac{\partial(\delta\mu^\beta)}{\partial z}\Big]_{z=0} &= -\frac{J^*}{M^\beta},\\
\Big[\big(1 + \frac{\delta C^\beta}{C^\beta_{eq}}\big)\frac{\partial(\delta\mu^\beta)}{\partial z}\Big]_{z=0} &= -\frac{J^*}{M^\beta C^\beta_{eq}},\\
\frac{\partial(\delta\mu^\beta)}{\partial z}\Big|_{z=0} &= -\frac{J^*}{M^\beta C^\beta_{eq}\big(1 + \frac{\delta C^\beta}{C^\beta_{eq}}\Big|_{z=0}\big)},\\
\frac{\partial(\delta\mu^\beta)}{\partial z}\Big|_{z=0} &= -\frac{J^*}{M^\beta C^\beta_{eq}}\big(1 - \frac{\delta C^\beta}{C^\beta_{eq}}\Big|_{z=0}\big).
\end{aligned}
\tag{3.43}
$$

The same procedure is used for the boundary condition in the spherical case. Thus, the final set of flux boundary conditions are given by

$$\begin{aligned} \left(\frac{\partial(\delta\mu^\beta)}{\partial r} + \zeta\kappa^\beta\delta C^\beta\right)\Big|_{r=b} &= \zeta\kappa^\beta C_{eq}^\beta \qquad \text{(spherical coupled)}, \\ \left(\frac{d(\delta C^\beta)}{dr} + \zeta\delta C^\beta\right)\Big|_{r=b} &= \zeta C_{eq}^\beta \qquad \text{(spherical uncoupled)}, \\ \left(\frac{\partial(\delta\mu^\beta)}{\partial z} - \zeta\kappa^\beta\delta C^\beta\right)\Big|_{z=0} &= -\zeta\kappa^\beta C_{eq}^\beta \quad \text{(planar coupled)}, \\ \left(\frac{d(\delta C^\beta)}{dz} - \zeta\delta C^\beta\right)\Big|_{z=0} &= -\zeta C_{eq}^\beta \qquad \text{(planar uncoupled)}, \end{aligned} \tag{3.44}$$

where $\zeta = \dfrac{J^*}{M^\beta\kappa^\beta(C_{eq}^\beta)^2}$; in uncoupled analyses, the flux boundary condition is a Robin condition because it involves δC and its derivative.

The second boundary condition specifies the concentration at the interface, which is given by

$$\left.\begin{aligned} C^\eta\Big|_{r=a} &= C_{eq}^\beta + \delta C_I^\eta \quad \text{(spherical)}, \\ C^\eta\Big|_{z=z_I} &= C_{eq}^\eta + \delta C_I^\eta \qquad \text{(planar)}. \end{aligned}\right. \quad \eta = \alpha, \beta \tag{3.45}$$

Chapter 4

Uncoupled quasi-steady state analyses of diffusive phase growth

This chapter considers uncoupled diffusion and phase transformation in the binary systems, and ignores deformation. The diffusion equations are solved to obtain the concentration deviation in the phases. The interfacial equations are used to solve the concentration deviation at the interface as well as the location and velocity of the interface.

In the absence of stress, Eq. (3.29) simplifies to

$$\begin{aligned} \mu^\alpha &= \mu_{eq} + \kappa^\alpha \delta C^\alpha, \\ \mu^\beta &= \mu_{eq} + \kappa^\beta \delta C^\beta. \end{aligned} \tag{4.1}$$

The chemical equilibrium condition at the interface, Eq. (3.32), simplifies to

$$\kappa^\alpha \delta C_I^\alpha = \kappa^\beta \delta C_I^\beta. \tag{4.2}$$

In the absence of deformation, the driving force for the phase transformation reaction, Eq. (3.37), simplifies to

$$\Phi = -\kappa^\beta \delta C_I^\beta (C_{eq}^\beta - C_{eq}^\alpha), \tag{4.3}$$

where Eq. (3.36)b is used. Substituting Eq. (4.3) in Eq. (3.7) gives the velocity of the interface:

$$v_I = \frac{V_0}{C_A RT}\kappa^\beta \delta C_I^\beta (C_{eq}^\beta - C_{eq}^\alpha). \tag{4.4}$$

4.1. Spherical core-shell particle

4.1.1 Concentration deviations

The steady state diffusion in the α-phase is described by

$$\frac{\partial J_r^\alpha}{\partial r} + \frac{2}{r} J_r^\alpha = 0, \tag{4.5}$$

where Eq. (3.4)b is used with $\dfrac{\partial C^\beta}{\partial t} = 0$. It can be seen that J_r^α must vanish for the above equality to hold because $r = 0$ is part of the core domain, $0 \leq r \leq a$. Near equilibrium, $J_r^\alpha = 0$ simplifies to $\dfrac{d\delta C^\alpha}{dr} = 0$, using Eqs. (3.4)a and (3.29)a. Thus, δC^α is constant. Using the boundary condition, Eq. (3.45)a, the α-phase solution is given by

$$\delta C^\alpha = \delta C_I^\alpha, \tag{4.6}$$

where δC_I^α is to be determined. Thus, at steady state, the core exhibits uniform concentration; the deviation in concentration of the core is equal to its interfacial value.

The steady state diffusion in the β-phase near equilibrium is described by

$$\begin{aligned} \frac{\partial J_r^\beta}{\partial r} + \frac{2}{r} J_r^\beta &= 0, \\ \frac{1}{r^2}\frac{d}{dr}\left(r^2 \frac{d\delta C^\beta}{dr}\right) &= 0, \\ \frac{d}{dr}\left(r^2 \frac{d\delta C^\beta}{dr}\right) &= 0, \end{aligned} \tag{4.7}$$

where Eqs. (3.4)a and (3.29)b are used to simplify. Integrating twice with respect to r:

$$\delta C^{\beta}(r) = -\frac{A_s}{r} + B_s. \tag{4.8}$$

At $r = a$, $\delta C^{\beta} = \delta C_I^{\beta}$ as per Eq. (3.45)a, and we obtain

$$B_s = \delta C_I^{\beta} + \frac{A_s}{a}. \tag{4.9}$$

Thus, the deviation in concentration in the shell is given by

$$\delta C^{\beta}(r) = A_s\Big(\frac{1}{a} - \frac{1}{r}\Big) + \delta C_I^{\beta}, \tag{4.10}$$

where A_s and δC_I^{β} are unknown. Using the flux BC, Eq. (3.44), we obtain

$$A_s = \frac{\zeta(C_{eq}^{\beta} - \delta C_I^{\beta})}{\Big\{\frac{1}{b^2} + \zeta\Big(\frac{1}{a} - \frac{1}{b}\Big)\Big\}} \approx \frac{\zeta C_{eq}^{\beta}}{\Big\{\frac{1}{b^2} + \zeta\Big(\frac{1}{a} - \frac{1}{b}\Big)\Big\}}. \tag{4.11}$$

Thus, the concentration field in the shell is given by

$$\delta C^{\beta}(r) = \delta C_I^{\beta} + \frac{\zeta C_{eq}^{\beta}}{\Big\{\frac{1}{b^2} + \zeta\Big(\frac{1}{a} - \frac{1}{b}\Big)\Big\}}\Big(\frac{1}{a} - \frac{1}{r}\Big), \tag{4.12}$$

where only a is a function of time.

4.1.2 Interfacial concentration deviations

For the quasi-steady state analysis, δC_I^{α} is independent of r; subsequently, the derivative in the second term of Eq. (3.41) is zero. Substituting Eq. (4.12) in Eq. (3.41) (uncoupled), and setting the velocity of the interface from the mass balance condition equal to the velocity of the interface from the phase kinetics equation, we obtain

$$\begin{aligned}\delta C_I^\beta &= \frac{M^\beta RT(C_{eq}^\beta)^2 C_A}{(C_{eq}^\beta - C_{eq}^\alpha)^2 V_0} \frac{\zeta}{a^2\left\{\frac{1}{b^2} + \zeta\left(\frac{1}{a} - \frac{1}{b}\right)\right\}}, \\ &= \frac{J^* RTC_A}{\kappa^\beta V_0 (C_{eq}^\beta - C_{eq}^\alpha)^2} \frac{1}{a^2\left\{\frac{1}{b^2} + \zeta\left(\frac{1}{a} - \frac{1}{b}\right)\right\}},\end{aligned} \tag{4.13}$$

where $(\delta C_I^\beta)^2$ terms were ignored, and the definition of ζ was used to simplify.

The interfacial concentration change in the core is given by Eq. (4.2):

$$\delta C_I^\alpha = \frac{\kappa^\beta}{\kappa^\alpha} \delta C_I^\beta. \tag{4.14}$$

4.1.3 Interface kinetics

Using Eq. (4.13)b in Eq. (4.4), we obtain

$$\frac{da}{dt} = -\frac{J^*}{\left(C_{eq}^\beta - C_{eq}^\alpha\right)} \frac{b^2}{a^2\left\{1 + \zeta b\left(\frac{b}{a} - 1\right)\right\}}, \tag{4.15}$$

which alternately, can also be derived using the mass balance condition at the interface. Integrating the equation from $t = 0$ to t gives the location of the interface:

$$(1 - \zeta b)\frac{(a^3 - a_0^3)}{3} + \zeta b^2 \frac{(a^2 - a_0^2)}{2} = -\frac{J^* b^2}{(C_{eq}^\beta - C_{eq}^\alpha)} t, \tag{4.16}$$

where a_0 is the position of the interface at $t = 0$.

4.2. Planar bilayer

4.2.1 Concentration deviations

For uncoupled steady-state diffusion and small deviations from equilibrium, the diffusion Eq. (3.5) for the β-phase simplifies to

$$\frac{\partial^2 \delta C^\beta}{\partial z^2} = 0, \tag{4.17}$$

which results in a linear variation of the concentration field with respect to z:

$$\delta C^\beta(z) = A_p z + B_p. \tag{4.18}$$

Using the BCs, Eqs. (3.44) and (3.45), we obtain

$$\begin{aligned} A_p &= -\frac{\zeta C_{eq}^\beta - \delta C_I^\beta)}{1+\zeta z_I} \approx -\frac{\zeta C_{eq}^\beta}{1+\zeta z_I}, \\ B_p &= \delta C_I^\beta + \frac{\zeta (C_{eq}^\beta - \delta C_I^\beta) z_I}{1+\zeta z_I} = \delta C_I^\beta + \frac{\zeta C_{eq}^\beta z_I}{1+\zeta z_I}, \end{aligned} \tag{4.19}$$

which results in the following quasi-steady state solution:

$$\begin{aligned} \delta C^\beta(z) &= \delta C_I^\beta + \frac{\zeta C_{eq}^\beta}{1+\zeta z_I}(z_I - z), \\ \delta C^\alpha(z) &= \delta C_I^\alpha = \frac{\kappa^\beta}{\kappa^\alpha}\delta C_I^\beta, \end{aligned} \tag{4.20}$$

where only z_I is a function of time.

4.2.2 Interfacial concentration deviations

For the quasi-steady state analysis, δC_I^α is independent of z; subsequently, the derivative in the second term of Eq. (3.41) is zero and $[\![J]\!]$ simplifies to

$$[\![J]\!] = -M^\beta (C_{eq}^\beta + \delta C_I^\beta)\kappa^\beta \lim_{\epsilon\to 0} \frac{\partial \delta C^\beta}{\partial z}\Big|_{z_I - \epsilon}. \tag{4.21}$$

Substituting Eqs. (3.40) and (4.21) in Eq. (3.41), we obtain

$$-M^{\beta}(C_{eq}^{\beta}+\delta C_I^{\beta})\kappa^{\beta}\lim_{\epsilon\to 0}\frac{\partial \delta C^{\beta}}{\partial z}\Big|_{z_I-\epsilon}=(C_{eq}^{\alpha}-C_{eq}^{\beta}+\delta C_I^{\alpha}-\delta C_I^{\beta})\frac{dz_I}{dt}. \tag{4.22}$$

Using the steady state solution of Eq. (4.20), and Eq. (4.4) into Eq. (4.22), and ignoring higher orders of δC_I^{β}, we can solve for δC_I^{β}, which is given by

$$\begin{aligned}\delta C_I^{\beta} &= \frac{M^{\beta}RT(C_{eq}^{\beta})^2 C_A}{(C_{eq}^{\beta}-C_{eq}^{\alpha})^2 V_0}\frac{\zeta}{\Big(1+\zeta z_I\Big)},\\ &= \frac{J^{*}RTC_A}{\kappa^{\beta}V_0(C_{eq}^{\beta}-C_{eq}^{\alpha})^2}\frac{1}{\Big(1+\zeta z_I\Big)},\end{aligned} \tag{4.23}$$

where the definition of ζ was used to simplify.

4.2.3 Interface kinetics

Substituting Eq. (4.23) in Eq. (4.4) provides the velocity of the interface:

$$\frac{dz_I}{dt}=\frac{J^{*}}{\Big(C_{eq}^{\beta}-C_{eq}^{\alpha}\Big)\Big(1+\zeta z_I\Big)}. \tag{4.24}$$

Integrating the equation from $t=0$ to t gives the location of the interface:

$$\boxed{z_I+\frac{\zeta}{2}z_I^2=z_I^0+\frac{\zeta}{2}(z_I^0)^2+\frac{J^{*}t}{\Big(C_{eq}^{\beta}-C_{eq}^{\alpha}\Big)},} \tag{4.25}$$

where z_I^0 is the position of the interface at $t=0$.

4.3. Discussion

By ignoring deformation, we are assuming the two phases are rigid and incompressible.

4.3.1 Planar limit

Let us consider the solution when a and b approach infinity with $b-a$ and $\frac{b}{a}$ maintaining finite values, which corresponds to a planar limit. To check if we recover the planar solution, we consider Eqs. (4.12), (4.13), and (4.15) with these limits.

By comparing the geometric and planar pictures, we notice the following limits:

$$\begin{aligned} & b-a \rightarrow z_I, \\ & \lim_{a\rightarrow\infty} \frac{b}{a} \rightarrow \lim_{a\rightarrow\infty} \frac{z_I+a}{a} \rightarrow 1, \\ & r-a \rightarrow z_I - z. \end{aligned} \tag{4.26}$$

Thus, the geometric terms appearing in Eqs. (4.12), (4.13), and (4.15) are simplified to

$$\begin{aligned} \frac{\left(\frac{1}{a}-\frac{1}{r}\right)}{\left\{\frac{1}{b^2}+\zeta\left(\frac{1}{a}-\frac{1}{b}\right)\right\}} &= \frac{r-a}{\frac{r}{b}\left\{\frac{a}{b}+\zeta(b-a)\right\}} \rightarrow \frac{z_I-z}{(1+\zeta z_I)}, \\ a^2\left\{\frac{1}{b^2}+\zeta\left(\frac{1}{a}-\frac{1}{b}\right)\right\} &= \frac{a^2}{b^2}+\zeta\frac{a(b-a)}{b} \rightarrow 1+\zeta z_I, \\ \zeta b\left(\frac{b}{a}-1\right) &= \zeta\frac{b}{a}(b-a) \rightarrow \zeta z_I, \end{aligned} \tag{4.27}$$

which correspond to the planar terms in Eqs. (4.20), (4.23), and (4.24).

4.3.2 Limit analysis of the spherical solution

Consider the kinetic regime given by $\zeta b\left(\frac{b}{a}-1\right) \ll 1$. This limit can also be written as $\zeta\left(b-a\right) \ll \frac{a}{b}$.

The velocity corresponding to this limit is given by

$$\frac{da}{dt} = -\frac{J^*}{\left(C_{eq}^{\beta}-C_{eq}^{\alpha}\right)}\frac{b^2}{a^2}. \tag{4.28}$$

The location of the interface corresponding to this limit is given by

$$\frac{a^3 - a_0^3}{3} = -\frac{J^* b^2}{(C_{eq}^{\beta} - C_{eq}^{\alpha})} t, \tag{4.29}$$

where only the cubic terms appear.

Next, we consider the kinetic regime given by $\zeta b\Big(\frac{b}{a} - 1\Big) \gg 1$. The velocity corresponding to this limit is given by

$$\frac{da}{dt} = -\frac{J^*}{\Big(C_{eq}^{\beta} - C_{eq}^{\alpha}\Big)} \frac{b}{\zeta a(b-a)}. \tag{4.30}$$

The location of the interface corresponding to this limit is given by

$$-\frac{(a^3 - a_0^3)}{3} + b\frac{(a^2 - a_0^2)}{2} = -\frac{J^* b}{\zeta(C_{eq}^{\beta} - C_{eq}^{\alpha})} t, \tag{4.31}$$

where both cubic and parabolic terms appear.

4.3.3 Stress-free diffusive phase growth

The closed-form equations describing the uncoupled growth kinetics for the two geometries represent the diffusive phase growth in the absence of stress. These kinetic equations include thermodynamic-kinetic parameters instead of fitting parameters and compare well to the classical (SF) kinetic models.

To compare the derived growth kinetics to the well-known G-B model for spherical particles, a_0 is set to b as the G-B model does not consider an initial thickness; Eq. (4.31) can be expressed as

$$\boxed{3 - 2\xi - 3(1-\xi)^{2/3} = 6M^{\beta}\kappa^{\beta} \frac{(C_{eq}^{\beta})^2}{(C_{eq}^{\beta} - C_{eq}^{\alpha}) b^2} t,} \tag{4.32}$$

where ξ is the extent of reaction, introduced in *Chapter 2*. It is iterated that for ideal dilute solutions, the mobility of the B-atoms is related to their diffusivity via $M = D/RT$ in Eq. (4.32).

Equations (4.32) and (4.25) compare qualitatively to the G-B and D-G models respectively, given by Eqs. (2.31) and (2.32).

4.3.4 Validity of the steady-state assumption

The solutions are quasi-steady state (QSS) approximations because they were derived in the presence of a moving interface by assuming steady state diffusion.

Consider the dimensionless parameter, λ_{QSS}, which is given by [23]

$$\begin{aligned} \lambda_{QSS} &= \frac{B\text{-atoms in the bulk}}{B\text{-atoms at the interface}} \\ &= \frac{\dfrac{\partial \delta C^{\beta}}{\partial t} \cdot \text{volume of film}}{[C] \cdot \text{surface area of the interface} \cdot v_I}. \end{aligned} \tag{4.33}$$

For example, for the planar system, using Eq. (4.20) for $z = 0$, where the maximum deviation in concentration occurs, λ_{QSS} is derived and is given by

$$\lambda_{QSS} = \frac{\left(C_{eq}^{\beta} - \dfrac{J_B RT C_A}{\kappa^{\beta} V_0 (C_{eq}^{\beta} - C_{eq}^{\alpha})^2}\right) \dfrac{\zeta z_I}{(1 + \zeta z_I)^2}}{(C_{eq}^{\beta} - C_{eq}^{\alpha})}. \tag{4.34}$$

The quasi-steady state assumption (i.e. $\dfrac{\partial \delta C^{\beta}}{\partial t} \approx 0$) is valid when $\lambda_{QSS} \ll 1$.

Further discussion related to the growth kinetics results is presented together with the elastically-coupled discussion in the next chapter.

Chapter 5

Elastically-coupled quasi-steady state analyses of diffusive phase growth

This chapter formulates and solves the steady-state problem of elastically-coupled diffusive phase growth for both spherical and planar geometries.

It is assumed that the spherical deformation is axisymmetric; subsequently, $\theta = \phi$, and the displacement in each phase, u^{η}, is a function of r only. The planar system is assumed to be in an equibiaxial state of stress and strain.

5.1. Strain contributions

For small strains, the total strain of each system can be written as

$$\epsilon_{ij} = \epsilon_{ij}^{c} + \epsilon_{ij}^{e}, \tag{5.1}$$

where ϵ^{e} denotes elastic strains, and ϵ^{c} denotes diffusion-induced strains.

Furthermore, the total strains are related to the displacement $u(r)$ of the axisymmetric spherical problem:

$$\begin{aligned} \epsilon_{rr} &= \frac{du}{dr}, \\ \epsilon_{\theta\theta} &= \frac{u}{r}. \end{aligned} \quad \text{(spherical)} \tag{5.2}$$

5.1.1 Diffusion-induced strains

Diffusion-induced strains are stress-free strains that arise because changes in chemical composition lead to chemical expansion which produces a change in lattice dimensions, and hence volume. To model these strains, we assume the solutions generate isotropic volumetric (or dilatational) strains; subsequently, we can assume the solid solutions obey Vegard's law which states that the diffusion-induced strains vary linearly with concentration, which is expressed as [31]

$$\begin{gathered} \boldsymbol{\epsilon}^c = \frac{\Omega}{3}\delta C \boldsymbol{I}, \\ \text{or} \\ \epsilon^c_{ij} = \frac{\Omega}{3}\delta C \delta_{ij}, \end{gathered} \tag{5.3}$$

where Ω is the partial molar volume of the B-component at zero stress. We assume Ω has the same value in both phases.

5.1.2 Elastic strains

For an isotropic, linearly elastic material, the elastic strains are given by

$$\epsilon^e_{ij} = \frac{1}{E}\Big[(1+\nu)\sigma_{ij} - \nu\sigma_{kk}\delta_{ij}\Big], \tag{5.4}$$

where ν is Poisson's ratio. The stresses are generated because of composition changes; consequently, they are often known as diffusion-induced stresses (DISs) in the literature.

For the spherical system, the constitutive equation is derived in *Appendix D* and given by Eq. (27):

$$\begin{bmatrix} \sigma_{rr} \\ \sigma_{\theta\theta} \end{bmatrix} = \frac{E}{(1+\nu)(1-2\nu)} \begin{bmatrix} 1-\nu & 2\nu \\ \nu & 1 \end{bmatrix} \begin{bmatrix} \epsilon^e_{rr} \\ \epsilon^e_{\theta\theta} \end{bmatrix}. \tag{5.5}$$

For an equibiaxial state of stress and strain, the stress-strain relationship, Eq. (5.4) simplifies to

$$\begin{aligned} \sigma^\eta &= \frac{E^\eta}{1-\nu^\eta}\epsilon^{e\eta}, \\ &= \overline{E}^\eta(\epsilon - \epsilon^{c\eta}), \end{aligned} \qquad \eta = \alpha, \beta \tag{5.6}$$

where $\overline{E} = \dfrac{E}{1-\nu}$, and is called the biaxial modulus.

In summary, we have two binary systems where the mobile interstitial B-atoms diffuse and generate stress-free strains, $\epsilon^{c\eta}_{ij}$. The A-lattice resists this volume expansion and undergoes elastic strains, $\epsilon^{e\eta}_{ij}$, generating elastic stresses, σ^η_{ij}, in each phase. The nature of the elastic stresses and strains is governed by the system geometries.

5.2. Core-shell particle

Introducing deformation into the analysis leads to five new unknowns in each phase: σ_{rr}, $\sigma_{\theta\theta}$, ϵ^e_{rr}, $\epsilon^e_{\theta\theta}$, and $u(r)$. This requires five equations which are given by the two equations of (5.2) combined with Eq. (5.1), the two equations of (5.5), and (3.34)a. All unknowns depend on r and δC. Furthermore, we have the following conditions at the outer surface and at the interface:

$$\begin{aligned} \sigma_{rr}\big|_{r=b} &= 0 && \text{(traction-free surface)}, \\ u^{\alpha}(r)\big|_{r=a} &= u^{\beta}(r)\big|_{r=a} && \text{(displacement continuity at the interface)}, \\ \sigma^{\alpha}_{rr}\big|_{r=a} &= \sigma^{\beta}_{rr}\big|_{r=a} && \text{(mechanical equilibrium at the interface)} \\ \delta\mu^{\alpha}_{I} &= \delta\mu^{\beta}_{I} && \text{(chemical equilibrium at the interface)}, \end{aligned} \tag{5.7}$$

where Eq. (5.7)c is a consequence of Eq. (2.29)a.

Following Bower et al. [23], the method of solution to obtain the concentration deviation in the shell entails solving the steady state diffusion equation, applying the flux boundary condition, and incorporating the shell mechanics by eliminating the displacement.

5.2.1 Core thermodynamics and mechanics

Under quasi-steady state conditions, the core is in a hydrostatic state of stress because the concentration change in the core is independent of the radial coordinate, r, and only depends on the interfacial position, a, because $\delta C^{\alpha} = \delta C^{\alpha}_{I}$. Subsequently, the DIS is independent of the radial coordinate as well. Thus, σ^{α} is not a function of r; hence $\sigma^{\alpha}_{rr} = \sigma^{\alpha}_{\theta\theta} = \sigma^{\alpha}_{\phi\phi} = P$, where P is the hydrostatic stress in the core. Using Eq. (5.5), the elastic strains are given by

$$\epsilon^{e\alpha}_{rr} = \epsilon^{e\alpha}_{\theta\theta} = \frac{(1-2\nu)}{E}P. \tag{5.8}$$

Using Eqs. (5.2) and (5.8), we obtain

$$\frac{du^{\alpha}}{dr} = \frac{u^{\alpha}}{r}. \tag{5.9}$$

Integrating with respect to r gives the displacement in the core:

$$u^{\alpha}(r) = u_{P}r, \tag{5.10}$$

where u_P is a constant of integration and determined using Eqs. (5.10), (5.1), and (5.2):

$$\begin{aligned} u_P &= \frac{u^\alpha}{r} = \epsilon^\alpha_{\theta\theta} + \epsilon^\alpha_{\theta\theta}, \\ u_P &= \frac{(1-2\nu)}{E}P + \frac{\Omega}{3}\delta C_I^\alpha, \end{aligned} \tag{5.11}$$

where Eqs. (5.3) and (5.8) were used to simplify. Thus, the displacement in the core is given by

$$u^\alpha(r) = \Big\{\frac{(1-2\nu)}{E}P + \frac{\Omega}{3}\delta C_I^\alpha\Big\} r. \tag{5.12}$$

The chemical potential change in the core is given by

$$\delta\mu^\alpha = \kappa^\alpha \delta C^\alpha - \frac{\Omega}{3}P. \tag{5.13}$$

The unknowns in Eqs. (5.12) and (5.13) include P and δC_I^α, which will be determined using the conditions at the interface.

5.2.2 Shell thermodynamics and mechanics

First, the steady state diffusion in the β-phase is considered, which is described by Eq. (3.4) with $\dfrac{\partial C^\beta}{\partial t} = 0$. For small deviations from equilibrium, we obtain

$$\frac{\partial}{\partial r}\Big\{(C^\beta_{eq} + \delta C^\beta)\frac{\partial \delta\mu^\beta}{\partial r}\Big\} + \frac{2}{r}(C^\beta_{eq} + \delta C^\beta)\frac{\partial \delta\mu^\beta}{\partial r} = 0, \tag{5.14}$$

which is simplified to

$$\frac{\partial^2 \delta\mu^\beta}{\partial r^2} + \frac{2}{r}\frac{\partial \delta\mu^\beta}{\partial r} = 0,$$

$$\frac{1}{r^2}\left\{\frac{\partial}{\partial r}\left(r^2 \frac{\partial \delta\mu^\beta}{\partial r}\right)\right\} = 0, \tag{5.15}$$

$$\frac{\partial}{\partial r}\left(r^2 \frac{\partial \delta\mu^\beta}{\partial r}\right) = 0,$$

where $r \neq 0$ because it is not part of the β-phase domain. Integrating twice with respect to r, we obtain

$$\delta\mu^\beta = -\frac{c_1}{r} + c_2, \tag{5.16}$$

where c_1 and c_2 are constants of integration. Using Eq. (5.16) in the flux equation (3.44), we obtain

$$\frac{c_1}{b^2} + \frac{J^*}{MC_{eq}^2}\delta C^\beta\Big|_{r=b} = \frac{J^*}{MC_{eq}}. \tag{5.17}$$

Second, the shell mechanics is considered. To obtain an expression in terms of the concentration change only, the displacement is eliminated, and the subsequent mechanics terms are used in the chemical potential expression. To undertake this procedure, we begin with the total radial and hoop strains. Using Eqs. (5.1)-(5.4), the total hoop strain is given by

$$\begin{aligned}\frac{u^\beta}{r} &= \epsilon^{e\beta}_{\theta\theta} + \epsilon^{c\beta}_{\theta\theta},\\ &= \frac{\sigma^\beta_{\theta\theta}}{E} - \frac{\nu}{E}(\sigma^\beta_{rr} + \sigma^\beta_{\phi\phi}) + \frac{\Omega}{3}\delta C^\beta,\\ &= \frac{\sigma^\beta_{\theta\theta}}{E} - \frac{\nu}{E}(\sigma^\beta_{rr} + \sigma^\beta_{\theta\theta} + \frac{\Omega}{3}\delta C^\beta),\\ &= -\frac{\nu}{E}\sigma^\beta_{rr} + \frac{(1-\nu)}{E}\sigma^\beta_{\theta\theta} + \frac{\Omega}{3}\delta C^\beta.\end{aligned} \tag{5.18}$$

Thus, the displacement experienced by the shell is given by

$$u^\beta = -\frac{\nu}{E} r\sigma^\beta_{rr} + \frac{(1-\nu)}{E} r\sigma^\beta_{\theta\theta} + \frac{\Omega}{3} r\delta C^\beta, \tag{5.19}$$

which can be differentiated with respect to r to obtain

$$\frac{du^\beta}{dr} = -\frac{\nu}{E}\Big\{r\frac{\partial\sigma^\beta_{rr}}{\partial r} + \sigma^\beta_{rr}\Big\} + \frac{(1-\nu)}{E}\Big\{r\frac{\partial\sigma^\beta_{\theta\theta}}{\partial r} + \sigma^\beta_{\theta\theta}\Big\} + \frac{\Omega}{3}\Big\{r\frac{d\delta C^\beta}{dr} + \delta C^\beta\Big\}. \tag{5.20}$$

Using Eqs. (5.1)-(5.4), the total radial strain is given by

$$\begin{aligned}\frac{du^\beta}{dr} &= \epsilon^{e\beta}_{rr} + \epsilon^{c\beta}_{rr},\\ &= \frac{\sigma^\beta_{rr}}{E} - \frac{\nu}{E}(\sigma^\beta_{\theta\theta} + \sigma^\beta_{\phi\phi}) + \frac{\Omega}{3}\delta C^\beta,\\ &= \frac{\sigma^\beta_{rr}}{E} - \frac{\nu}{E}(\sigma^\beta_{\theta\theta} + \sigma^\beta_{\theta\theta}) + \frac{\Omega}{3}\delta C^\beta.\end{aligned} \tag{5.21}$$

Equating the two expressions for $\frac{du}{dr}$, Eqs. (5.20) and (5.21), we obtain

$$\frac{(1+\nu)}{E}(\sigma^\beta_{rr} - \sigma^\beta_{\theta\theta}) = \frac{\Omega}{3}\Big(r\frac{d\delta C^\beta}{dr}\Big) - \frac{\nu}{E}\Big(r\frac{\partial\sigma^\beta_{rr}}{\partial r}\Big) + \frac{(1-\nu))}{E}\Big(r\frac{\partial\sigma^\beta_{\theta\theta}}{\partial r}\Big). \tag{5.22}$$

Substituting the derivative of radial stress from the mechanical equilibrium condition, Eq. (3.34), in Eq. (5.22), we obtain the partial derivative of the hoop strain in the shell:

$$\frac{\partial\sigma^\beta_{\theta\theta}}{\partial r} = \frac{\sigma^\beta_{rr} - \sigma^\beta_{\theta\theta}}{r} - \frac{\Omega\overline{E}}{3}\frac{d\delta C^\beta}{dr}. \tag{5.23}$$

The chemical potential change is given by

$$\delta\mu^{\beta} = \kappa^{\beta}\delta C^{\beta} - \frac{\Omega}{3}(\sigma_{rr}^{\beta} + 2\sigma_{\theta\theta}^{\beta}). \tag{5.24}$$

Taking the derivative of Eq. (5.24) with respect to r, and substituting Eqs. (3.34) and (5.23), we obtain

$$\begin{aligned}\frac{\partial\delta\mu^{\beta}}{\partial r} &= \kappa^{\beta}\frac{d\delta C^{\beta}}{dr} - \frac{\Omega}{3}\Big(\frac{\partial\sigma_{rr}^{\beta}}{\partial r} + 2\frac{\partial\sigma_{\theta\theta}^{\beta}}{\partial r}),\\ &= \kappa'^{\beta}\frac{d\delta C^{\beta}}{dr},\end{aligned} \tag{5.25}$$

where

$$\kappa'^{\beta} = \kappa^{\beta} + \frac{2}{9}\overline{E}\Omega^{2}. \tag{5.26}$$

Using Eqs. (5.16) and (5.25), we obtain an expression in terms of the concentration change only, which is given by

$$\frac{d\delta C^{\beta}}{dr} = \frac{c_1}{\kappa'^{\beta}r^{2}}. \tag{5.27}$$

Integrating and using the BCs, Eqs. (3.44) and (3.45), we obtain

$$\delta C^{\beta}(r) = \delta C_{I}^{\beta} + \frac{c_1}{\kappa'^{\beta}}\Big(\frac{1}{a} - \frac{1}{r}\Big), \tag{5.28}$$

where $\dfrac{c_1}{\kappa'^{\beta}} = \dfrac{\zeta' C_{eq}^{\beta}}{\Big\{\zeta'\Big(\dfrac{1}{a} - \dfrac{1}{b}\Big) + \dfrac{1}{b^{2}}\Big\}}$.

Thus, the concentration field in the shell is given by

$$\delta C^{\beta}(r) = \delta C_{I}^{\beta} + \frac{\zeta' C_{eq}^{\beta}}{\Big\{\zeta'\Big(\dfrac{1}{a} - \dfrac{1}{b}\Big) + \dfrac{1}{b^{2}}\Big\}}\Big(\frac{1}{a} - \frac{1}{r}\Big), \tag{5.29}$$

where δC_I^β will be determined from the interfacial conditions.

5.2.3 Stress field

Equation (5.29) is now used in the mechanics equations, Eqs. (5.18) and (5.21). The subsequent set of two equations can be solved for the two stresses, which are expressed in terms of displacement and concentration change, and given by

$$\begin{aligned} \sigma_{rr}^\beta &= \frac{E}{(1+\nu)(1-2\nu)}\Big\{2\nu\frac{u^\beta}{r} + (1-\nu)\frac{du^\beta}{dr} - \frac{\Omega}{3}(1+\nu)\delta C^\beta\Big\}, \\ \sigma_{\theta\theta}^\beta &= \frac{E}{(1+\nu)(1-2\nu)}\Big\{\frac{u^\beta}{r} + \nu\frac{du^\beta}{dr} - \frac{\Omega}{3}(1+\nu)\delta C^\beta\Big\}. \end{aligned} \tag{5.30}$$

Substituting the stresses given by Eq. (5.30) in the mechanical equilibrium condition, Eq. (3.34), we obtain a second-order ordinary differential equation (ODE) for the displacement, $u^\beta(r)$:

$$\begin{aligned} \frac{d^2u^\beta}{dr^2} + \frac{2}{r}\frac{du^\beta}{dr} - 2\frac{u^\beta}{r^2} &= \frac{\Omega}{3}\frac{(1+\nu)}{(1-\nu)}\frac{d\delta C^\beta}{dr}, \\ \frac{d^2u^\beta}{dr^2} + 2\frac{d}{dr}\Big(\frac{u^\beta}{r}\Big) &= \frac{\Omega}{3}\frac{(1+\nu)}{(1-\nu)}\frac{\mu_1}{\kappa'^\beta}r^2. \end{aligned} \tag{5.31}$$

Integrating with respect to r, we obtain

$$\frac{du^\beta}{dr} + \frac{2u^\beta}{r} = -\frac{\Omega}{3}\frac{(1+\nu)}{(1-\nu)}\frac{\frac{\mu_1}{\kappa'^\beta}}{r} + u_1, \tag{5.32}$$

where u_1 is constant. The ODE is now first order; the integrating factor is r^2. Solving this equation provides an expression for the displacement:

$$u^\beta(r) = -\frac{\Omega}{6}\frac{(1+\nu)}{(1-\nu)}\frac{\mu_1}{\kappa'^\beta} + u_1\frac{r}{3} + \frac{u_2}{r^2}, \tag{5.33}$$

where the two unknowns, u_1 and u_2, are solved using the first two conditions of Eq. (5.7). For the first boundary condition, we substitute Eq. (5.33) in Eq. (5.30)a and set the radial stress to zero at $r = b$, which simplifies to

$$\begin{aligned}(1+\nu)\frac{u_1}{3} - 2(1-2\nu)\frac{u_2}{b^3} + 2\nu\frac{u_0}{b} - \frac{\Omega}{3}(1+\nu)\delta C_I^{\beta} - \frac{\Omega}{3}(1+\nu)\frac{c_1}{\kappa'}\Big(\frac{1}{a} - \frac{1}{b}\Big) = 0,\\ u_1 = 6\frac{(1-2\nu)}{(1+\nu)}\frac{u_2}{b^3} + \Omega\delta C_I^{\beta} + \frac{\Omega}{a}\frac{c_1}{\kappa'} - \frac{\Omega}{b}\frac{c_1}{\kappa'}\frac{(1-2\nu)}{(1-\nu)}.\end{aligned} \tag{5.34}$$

To obtain a second expression in terms of u_1 and u_2, we use Eq. (5.7)b, where the two displacements corresponding to the two phases are given by Eqs. (5.12) and (5.33); the substitutions lead to

$$\Big\{\frac{(1-2\nu)}{E}P + \frac{\Omega}{3}\delta C_I^{\alpha}\Big\}a = u_0 + \frac{u_1}{3}a + \frac{u_2}{a^2}. \tag{5.35}$$

Solving Eqs. (5.34) and (5.35) for u_1 and u_2, we obtain

$$\begin{aligned}\frac{u_1}{3} = \frac{1}{\Big(1+\nu+2(1-2\nu)\tilde{a}^3\Big)}\Big[&\frac{2(1-2\nu)^2}{(1-\nu)}\frac{P}{\overline{E}}\tilde{a}^3 - \frac{u_0}{a}\Big\{2-2\nu+2(1-2\nu)\tilde{a}^3 - 2(1-2\nu)\tilde{a}\Big\}\\ &+ 2(1-2\nu)\frac{\Omega}{3}\delta C_I^{\alpha}\tilde{a}^3 + (1+\nu)\frac{\Omega}{3}\delta C_I^{\beta}\Big],\end{aligned} \tag{5.36}$$

$$\begin{aligned}u_2 = \frac{a^3}{\Big(1+\nu+2(1-2\nu)\tilde{a}^3\Big)}\Big[&\frac{(1+\nu)(1-2\nu)}{(1-\nu)}\frac{P}{\overline{E}} + \frac{u_0}{a}\Big\{1-3\nu-2(1-2\nu)\tilde{a}\Big\}\\ &+ (1+\nu)\frac{\Omega}{3}\Big(\delta C_I^{\alpha} - \delta C_I^{\beta}\Big)\Big],\end{aligned} \tag{5.37}$$

where $\tilde{a} = \frac{a}{b}$, $u_0 = -\frac{\Omega}{6}\frac{(1+\nu)}{(1-\nu)}\frac{\mu_1}{\kappa'^{\beta}}$ and $\frac{c_1}{\kappa'^{\beta}}$ is known from *Section 5.2.2.*

Next, we solve for P using Eq. (5.7)c, which is given by

$$P = \frac{E}{(1+\nu)(1-2\nu)}\Big[-\frac{\Omega}{3}(1+\nu)\delta C_I^{\beta} + 2\nu\frac{u_0}{a} + (1+\nu)\frac{u_1}{3} - 2(1-2\nu)\frac{u_2}{a^3}\Big]. \tag{5.38}$$

Substituting u_1 from Eq. (5.34) into Eq. (5.38), we obtain

$$\frac{3(1-\nu)}{a^3}u_2 = \frac{\Omega}{3}(1+\nu)(\delta C_I^{\alpha} - \delta C_I^{\beta}) - \frac{u_0}{a}(1-\nu). \tag{5.39}$$

Extracting u_2 from Eq. (5.39) and setting it equal to Eq. (5.37) provides an expression for P and consequently the stress state of the core:

$$\sigma^{\alpha}_{rr} = \sigma^{\alpha}_{\theta\theta} = P = \frac{\overline{E}\Omega}{9}\Big[\frac{\zeta' C^{\beta}_{eq}}{\Big\{\zeta'\Big(\frac{1}{a}-\frac{1}{b}\Big)+\frac{1}{b^2}\Big\}\tilde{a}b}(\tilde{a}-1)^2(\tilde{a}+2) - 2(1-\tilde{a}^3)(\delta C^{\alpha}_{I} - \delta C^{\beta}_{I})\Big]. \tag{5.40}$$

Equation (5.30) requires the concentration change and displacement of the shell, given by Eqs. (5.29) and (5.33) respectively; the latter equation also requires Eqs. (5.36), (5.37), and (5.40). By making these substitutions, we obtain the stress state of the shell:

$$\begin{aligned}
\sigma^{\beta}_{rr} &= \overline{E}\Big[\frac{2}{9}\Omega(1-\tilde{r}^3)\frac{\tilde{a}^3}{\tilde{r}^3}(\delta C^{\beta}_{I} - \delta C^{\alpha}_{I}) - \frac{\Omega}{9b}\frac{\zeta' C^{\beta}_{eq}}{\Big\{\zeta'\Big(\frac{1}{a}-\frac{1}{b}\Big)+\frac{1}{b^2}\Big\}}\frac{(1-\tilde{r})}{\tilde{r}^3}(\tilde{a}^2+\tilde{a}^2\tilde{r}+\tilde{a}^2\tilde{r}^2-3\tilde{r}^2)\Big],\\
\sigma^{\beta}_{\theta\theta} &= \overline{E}\Big[\frac{\Omega}{9}(1+2\tilde{r}^3)\frac{\tilde{a}^3}{\tilde{r}^3}(\delta C^{\alpha}_{I} - \delta C^{\beta}_{I}) + \frac{\Omega}{6b}\frac{\zeta' C^{\beta}_{eq}}{\Big\{\zeta'\Big(\frac{1}{a}-\frac{1}{b}\Big)+\frac{1}{b^2}\Big\}}\frac{(\tilde{a}^2-6\tilde{r}^3+2\tilde{a}^2\tilde{r}^3+3\tilde{r}^2)}{3\tilde{r}^3}\Big],
\end{aligned} \tag{5.41}$$

where the only unknowns are the interfacial concentrations and the location of the interface.

5.2.4 Interfacial concentrations

The last leg of the steady state analysis entails the computation of the thermodynamic and kinetic characteristics pertinent to the interface, namely the location and velocity of the interface and the interfacial concentrations.

First, we consider the condition of chemical equilibrium at the interface given by Eq. (5.7)d; using Eqs. (5.13) and (5.24), we obtain

$$\begin{aligned}
\kappa^{\alpha}\delta C^{\alpha}_{I} - \Omega P &= \kappa^{\beta}\delta C^{\beta}_{I} - \frac{\Omega}{3}(\sigma^{\beta}_{rr} + 2\sigma^{\beta}_{\theta\theta}\Big|_{r=a}),\\
\kappa^{\alpha}\delta C^{\alpha}_{I} - \Omega P &= \kappa^{\beta}\delta C^{\beta}_{I} - \frac{\Omega}{3}(P + 2\sigma^{\beta}_{\theta\theta}\Big|_{r=a}),\\
\kappa^{\alpha}\delta C^{\alpha}_{I} &= \kappa^{\beta}\delta C^{\beta}_{I} + \frac{2\Omega}{3}(P - \sigma^{\beta}_{\theta\theta}\Big|_{r=a}),
\end{aligned} \tag{5.42}$$

where Eq. (5.7)c is used to simplify. We can simplify this equation further using the hoop shell stress at the interface from Eq. (5.41)b which leads to

$$\kappa^\alpha \delta C_I^\alpha = \kappa^\beta \delta C_I^\beta - \frac{2\overline{E}\Omega^2}{27}(3+4\tilde{a}^3)(\delta C_I^\alpha - \delta C_I^\beta). \tag{5.43}$$

Simplifying the above equation gives the first equation for the unknown interface concentrations:

$$\begin{aligned} \delta C_I^\alpha &= \frac{\Big(\kappa^\beta + \dfrac{2\overline{E}\Omega^2}{27}(3+4\tilde{a}^3)\Big)}{\Big(\kappa^\alpha + \dfrac{2\overline{E}\Omega^2}{27}(3+4\tilde{a}^3)\Big)} \delta C_I^\beta \quad && \kappa^\alpha \neq \kappa^\beta, \\ \delta C_I^\alpha &= \delta C_I^\beta && \kappa^\alpha = \kappa^\beta. \end{aligned} \tag{5.44}$$

To obtain a second equation involving the interfacial concentrations, we consider the phase kinetics. We have two expressions for the velocity of the interface: the mass conservation Eq. (3.8), and the phase kinetics Eq. (3.7). Equating v_I of both equations, we obtain

$$v_I = -\frac{V_0}{C_A RT}\Phi = -\frac{[\![J]\!]}{[\![C]\!]}. \tag{5.45}$$

Using Eqs. (3.40) and (3.41) for the flux and concentration jump terms, we obtain an expression for the driving force:

$$\Phi = -\frac{J^* C_A RT b^2}{V_0 a^2 \Big\{1 + \zeta' b\big(\frac{b}{a} - 1\big)\Big\}(C_{eq}^\beta - C_{eq}^\alpha)}. \tag{5.46}$$

Equation (3.37) is another expression for the driving force; it requires computation of the interfacial strain energy of each phase and the interface work term for the spherical system.

The strain energy of the core is given by

$$\begin{aligned}\phi^{\alpha} &= \frac{1}{2}\sigma^{\alpha}_{rr}\epsilon^{\alpha}_{\theta\theta} + \sigma^{\alpha}_{\theta\theta}\epsilon^{\alpha}_{\theta\theta}, \\ &= \frac{3}{2}\frac{(1-2\nu)}{E}P^2,\end{aligned} \tag{5.47}$$

where Eq. (5.8) is used to simplify. The strain energy of the shell is given by

$$\phi^{\beta} = \frac{1}{2}\sigma^{\beta}_{rr}\epsilon^{\beta}_{\theta\theta} + \sigma^{\beta}_{\theta\theta}\epsilon^{\beta}_{\theta\theta}. \tag{5.48}$$

The jump in the strain energy at the interface is given by $[\![\phi]\!] = \phi^{\beta}\big|_{r=a} - \phi^{\alpha} = 0$. The interface work term is given by

$$[\![\epsilon]\!] \cdot \sigma^{\alpha} = (\epsilon^{\beta}_{rr} - \epsilon^{\alpha}_{rr})\Big|_{r=a} P, \tag{5.49}$$

where ϵ_{rr} of each phase is related to the corresponding displacement via Eq. (5.2). Using the expressions for the displacements, given by Eqs. (5.12) and (5.33), in Eq. (5.2) for each phase, we obtain

$$[\![\epsilon]\!] \cdot \sigma^{\alpha} = \frac{\overline{E}\Omega^2(1+\nu)}{27(1-\nu)} \frac{\zeta' C^{\beta}_{eq}}{\left\{\zeta'\left(\frac{1}{a} - \frac{1}{b}\right) + \frac{1}{b^2}\right\}} \frac{(\tilde{a}-1)^2(\tilde{a}+2)}{a}(\delta C^{\alpha}_{I} - \delta C^{\beta}_{I}), \tag{5.50}$$

where Eqs. (5.36) and (5.37) were used; this step completes the expression for the driving force, given by Eq. (3.37) for the spherical case. Thus, for the two unknown interfacial concentrations, we now have two expressions, given by Eqs. (3.37) (with (5.46)) and (5.44), which can be solved for the interfacial concentrations.

The interfacial concentration solution is presented for the special case when the curvature of the Gibbs energy density, κ, is the same in the two phases. The first equation for interfacial concentrations corresponds to Eq. (5.44)b, which implies the interface work term does not contribute, as per Eq. (5.50). Subsequently, using Eqs. (5.74) and (5.46), we obtain

$$\begin{aligned} -\delta\mu_I^\beta (C_{eq}^\beta - C_{eq}^\alpha) &= -\frac{J^* C_A RT b^2}{V_0 a^2 \Big\{1 + \zeta b\big(\frac{b}{a} - 1\big)\Big\}(C_{eq}^\beta - C_{eq}^\alpha)}, \\ \delta\mu_I^\beta &= \frac{J^* C_A RT b^2}{V_0 a^2 \Big\{1 + \zeta b\big(\frac{b}{a} - 1\big)\Big\}(C_{eq}^\beta - C_{eq}^\alpha)^2}. \end{aligned} \tag{5.51}$$

Using Eq. (5.24) on the left-hand side of the above equation, we obtain

$$\kappa^\beta \delta C_I^\beta - \frac{\Omega}{3}\Big(\sigma_{rr}^\beta + 2\sigma_{\theta\theta}^\beta\Big)\Big|_{r=a} = \frac{J^* C_A RT b^2}{V_0 a^2 \Big\{1 + \zeta b\big(\frac{b}{a} - 1\big)\Big\}(C_{eq}^\beta - C_{eq}^\alpha)^2}, \tag{5.52}$$

which can be further simplified using the solutions for the shell stresses, which leads to

$$\kappa^\beta \delta C_I^\beta - \overline{E}\frac{\Omega^2}{9}\Bigg[\frac{\zeta' C_{eq}^\beta b^2}{\Big\{1 + \zeta b\big(\frac{b}{a} - 1\big)\Big\}} \frac{(\tilde{a} - 1)^2(\tilde{a} + 2)}{\tilde{a} b}\Bigg] = \frac{J^* C_A RT b^2}{V_0 a^2 \Big\{1 + \zeta b\big(\frac{b}{a} - 1\big)\Big\}(C_{eq}^\beta - C_{eq}^\alpha)^2}. \tag{5.53}$$

Thus, the solution to the interfacial concentrations when $\kappa^\alpha = \kappa^\beta = \kappa$ is given by

$$\delta C_I^\alpha = \delta C_I^\beta = \frac{J^* b^2}{\kappa a \Big\{1 + \zeta b\big(\frac{b}{a} - 1\big)\Big\}}\Bigg[\frac{C_A RT}{V_0 a (C_{eq}^\beta - C_{eq}^\alpha)^2} + \frac{\overline{E}\Omega^2}{9}\frac{(\tilde{a} - 1)^2(\tilde{a} + 2)}{M^\beta \kappa C_{eq}^\beta}\Bigg]. \tag{5.54}$$

5.2.5 Interface kinetics

Using the mass conservation Eq. (3.8), the velocity of the interface can be calculated:

$$\frac{da}{dt} = -\frac{J^*}{\Big(C_{eq}^\beta - C_{eq}^\alpha\Big)} \frac{b^2}{a^2 \Big\{1 + \zeta' b\big(\frac{b}{a} - 1\big)\Big\}}. \tag{5.55}$$

Integrating the equation from $t = 0$ to t gives the location of the interface:

$$\boxed{(1 - \zeta' b)\frac{(a^3 - a_0^3)}{3} + \zeta' b^2 \frac{(a^2 - a_0^2)}{2} = -\frac{J^* b^2}{(C_{eq}^\beta - C_{eq}^\alpha)} t.} \tag{5.56}$$

5.3. Planar thin-film bilayer

To investigate the stresses in the planar system, consider the substrate or the α-phase, as shown in Fig. 5.1. The B-atoms are inserted via an applied flux to create a thin layer of the β-phase. In general, the stresses and strains in the two phases are non-zero, and bend the bilayer.

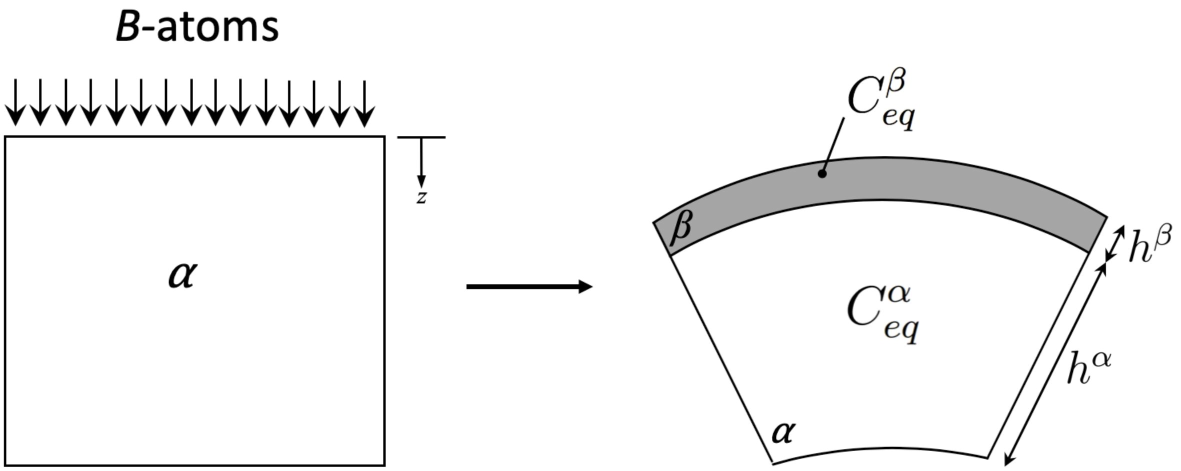

Figure 5.1: Schematic of the fabrication of the bilayer. The applied flux introduces B-atoms leading to diffusion of B-atoms, chemical reaction which forms the β-phase, and elastic deformation of the two phases. The applied flux is then stopped. As the kinetics (diffusion and reaction) subside, the two stressed phases exhibit uniform equilibrium concentrations; h^{α} and h^{β} denote the thicknesses of the substrate and film respectively.

5.3.1 Bilayer deformation

The total strain of the bilayer is expressed using laminate theory [101]:

$$\epsilon = \epsilon^0 + \frac{z - h_b}{r}, \tag{5.57}$$

where the three unknowns are the uniform strain, ϵ^0, the location of the bending axis, h_b, and the radius of curvature of the bilayer, r_b. The bilayer is freestanding and unconstrained.

The linear relationship between the strain and the thickness coordinate is a consequence of the Kirchhoff hypothesis, i.e. the deformation is entirely because of bending and in-plane stretching; transverse shear and transverse normal effects are ignored.[10]

Subsequently, the effects of the resultant forces because of the uniform strain and bending components are zero, and the total bending moment with respect to the bending axis is also zero. Following the procedure by Hseuh [102] to apply these three conditions, the solution is given by

$$\begin{aligned}
\epsilon^0 &= \frac{\frac{\Omega}{3}(\overline{E}^\alpha h^\alpha \delta C^\alpha + \overline{E}^\beta h^\beta \delta C^\beta)}{\overline{E}^\alpha h^\alpha + \overline{E}^\beta h^\beta}, \\
h_b &= \frac{\overline{E}^\beta (h^\beta)^2 - \overline{E}^\alpha (h^\alpha)^2}{2(\overline{E}^\alpha h^\alpha + \overline{E}^\beta h^\beta)}, \\
\frac{1}{r_b} &= \frac{6\overline{E}^\alpha \overline{E}^\beta h^\alpha h^\beta (h^\alpha + h^\beta)\frac{\Omega}{3}(\delta C^\beta - \delta C^\alpha)}{(\overline{E}^\alpha)^2 (h^\alpha)^4 + (\overline{E}^\beta)^2 (h^\beta)^4 + 2\overline{E}^\alpha \overline{E}^\beta h^\alpha h^\beta (2(h^\alpha)^2 + 2(h^\beta)^2 + 3h^\alpha h^\beta)},
\end{aligned} \tag{5.58}$$

where δC is constant for the bilayer in Fig. 5.1. Using Eqs. (5.1) and (5.6), the stress distribution in the bilayer simplifies to

$$\begin{aligned}
\sigma^\alpha &= \overline{E}^\alpha \Big[\frac{\overline{E}^\beta h^\beta \frac{\Omega}{3}(\delta C^\beta - \delta C^\alpha)}{\overline{E}^\alpha h^\alpha + \overline{E}^\beta h^\beta} + \frac{z - h_b}{r} \Big], \\
\sigma^\beta &= \overline{E}^\beta \Big[\frac{\overline{E}^\alpha h^\alpha \frac{\Omega}{3}(\delta C^\alpha - \delta C^\beta)}{\overline{E}^\alpha h^\alpha + \overline{E}^\beta h^\beta} + \frac{z - h_b}{r} \Big].
\end{aligned} \tag{5.59}$$

5.3.2 Thin film simplification

In the limit of a thin film on a substrate, we can forgo the consideration of the stress distribution through the thickness. Instead, we consider the *average* stress through the film

---

[10] It is also noted that the total strain, Eq. (5.57), satisfies the compatibilty condition for this system [103], which is given by $\frac{d^2\epsilon}{dz^2} = 0$.

thickness, which is given by

$$\begin{aligned} \overline{\sigma}^{\beta} &= \frac{1}{h^{\beta}} \int_0^{h^{\beta}} \sigma^{\beta} dz, \\ &= \frac{\overline{E}^{\alpha}\overline{E}^{\beta} h^{\alpha} \frac{\Omega}{3} (\overline{E}^{\alpha}(h^{\alpha})^3 + \overline{E}^{\beta}(h^{\beta})^3)(\delta C^{\alpha} - \delta C^{\beta})}{(\overline{E}^{\alpha})^2 (h^{\alpha})^4 + (\overline{E}^{\beta})^2 (h^{\beta})^4 + 2\overline{E}^{\alpha}\overline{E}^{\beta} h^{\alpha} h^{\beta} (2(h^{\alpha})^2 + 2(h^{\beta})^2 + 3h^{\alpha}h^{\beta})}. \end{aligned} \tag{5.60}$$

When $h^{\beta} \ll h^{\alpha}$, Eqs. (5.58), (5.59)a, and (5.60) simplify to

$$\begin{aligned} h_b &\approx \frac{h^{\alpha}}{2}, \\ \frac{1}{r} &\approx 0, \\ \sigma^{\alpha} &\approx 0, \\ \overline{\sigma}^{\beta} &= \overline{E}^{\beta} \frac{\Omega}{3} \big(\delta C^{\alpha} - \delta C^{\beta}\big). \end{aligned} \tag{5.61}$$

Therefore, for $h^{\beta} \ll h^{\alpha}$, we can assume the substrate is stress-free, the curvature of the interface is negligible, and the stress in the thin film is given by its average stress; this completes the description of the deformation of the binary bilayer at equilibrium, and is depicted in Fig. 5.1b.

5.3.3 Diffusion and elasticity formulation

Before undertaking the coupled analysis, we revisit the framework results which entail deformation and recast them in terms of the average stresses. To do so, we consider the hydrostatic stress, σ_h, for the thin film, which is given by

$$\begin{aligned} \sigma_h^{\beta} &= \frac{\sigma_{xx}^{\beta} + \sigma_{yy}^{\beta} + \sigma_{zz}^{\beta}}{3}, \\ &= \frac{\sigma_{xx}^{\beta} + \sigma_{yy}^{\beta}}{3}, \\ &\approx \frac{\overline{\sigma}^{\beta} + \overline{\sigma}^{\beta}}{3}, \\ &= \frac{2}{3} \overline{\sigma}^{\beta}. \end{aligned} \tag{5.62}$$

Appendix E shows that the mechanical equilibrium condition can be written in terms of the hydrostatic stress and concentration as [104]

$$\nabla \cdot (\sigma_h + \Gamma C) = 0, \tag{5.63}$$

where $\Gamma = \frac{2}{9}\overline{E}\Omega^\beta$. For our system, Eq. (5.63) simplifies to

$$\frac{\partial^2}{\partial z^2}(\sigma_h + \Gamma C) = 0. \tag{5.64}$$

Equation (5.63) entails Laplacians of the hydrostatic stress and the concentration of the mobile B-atoms and displays their proportionality. In the absence of concentration effects, the equation simplifies to a well-known harmonic equation of linear elasticity [105].

Diffusion is driven by gradients in the chemical potential, which is stress-dependent for the β-phase; Eq. (3.20) is simplified using Eqs. (5.3) and (5.62) to

$$\begin{aligned} \mu^\beta(C,\sigma) &= \mu^\beta(C,0) - \frac{\Omega^\beta}{3}\delta_{ij}\sigma^\beta_{ij}, \\ &= \mu^\beta(C,0) - \frac{\Omega^\beta}{3}\sigma^\beta_{kk}, \\ &= \mu^\beta(C,0) - \Omega^\beta\sigma^\beta_h, \\ &= \mu^\beta(C,0) - \frac{2}{3}\Omega^\beta\overline{\sigma}^\beta. \end{aligned} \tag{5.65}$$

Equations (3.5)a and (5.65) show that the diffusive flux has two components: the first corresponds to the stress-free chemical potential gradient, and the second contribution is from the gradient in hydrostatic stress.

The driving force for the phase transformation reaction, Eq. (3.25), under the assumed state of deformation is simplified to

$$\begin{aligned}\Phi &= [\![\mathscr{g}]\!] - \mu_I[\![C]\!] + \phi^\beta, \\ &= [\![\mathscr{g}]\!] - \mu_I[\![C]\!] + \frac{1}{2\overline{E}^\beta}(\sigma^\beta_{xx})^2 + \frac{1}{2\overline{E}^\beta}(\sigma^\beta_{yy})^2, \\ &= [\![\mathscr{g}]\!] - \mu_I[\![C]\!] + \frac{(\overline{\sigma}^\beta)^2}{\overline{E}^\beta}.\end{aligned} \tag{5.66}$$

Thus, the stress modifies the kinetics of diffusion and reaction via the chemical potential and the reaction driving force, as shown by Eqs. (5.65) and (5.66).

Mechanical equilibrium is trivially satisfied by the stress-free substrate, and it is satisfied by the hydrostatic stress in the film as shown by Eqs. (5.64), (5.62), and (5.61).

The Gibbs energy density of the film is now a function of concentration and stress. In general, the common tangent construction need not apply.

5.3.4 Solution

It is assumed that the substrate remains stress-free and the interface remains planar during the kinetic processes. Therefore, the problem is to solve for the new concentrations of the phases, C^α and C^β, the velocity and location of the interface, v_I and z_I respectively, and the thin-film stress, σ^β.

Similar to the uncoupled case, we assume the system undergoes small deviations from equilibrium. We undertake a quasi-steady state analysis, i.e. the bilayer is undergoing steady state diffusion and only the interface moves with time; subsequently, the concentration deviation in the film is only a function of z.

We assume the thin-film stress has the same nature as the equilibrium case, and thereby, exhibits the following relationship to the concentration deviation:

$$\overline{\sigma}^{\beta} \approx \overline{E}^{\beta} \frac{\Omega}{3} \big(\delta C^{\alpha} - \delta C^{\beta}(z)\big), \tag{5.67}$$

where $\delta C^{\alpha} = \delta C^{\alpha}_{I}$, which is constant for a given z_I.

For small deviations from equilibrium, the chemical potential of B-atoms in the β-phase can be written as

$$\mu^{\beta} \approx \mu^{\beta}_{eq} + \delta\mu^{\beta}, \tag{5.68}$$

where $\delta\mu^{\beta}$ is obtained using Eq. (3.20):

$$\begin{aligned} \delta\mu^{\beta} &= \frac{\partial \mu^{\beta}(C^{\beta},0)}{\partial C^{\beta}}\bigg|_{eq} \delta C^{\beta} - \frac{2}{9}\Omega \frac{\partial \overline{\sigma}^{\beta}}{\partial C}\bigg|_{eq} \delta C^{\beta} \\ &= \frac{\partial^2 \mathscr{g}(C^{\beta},0)}{\partial C^{\beta 2}}\bigg|_{eq} \delta C^{\beta} + \frac{2}{9}\overline{E}^{\beta}\Omega^2 \delta C^{\beta}, \\ &= (\kappa^{\beta} + \frac{2}{9}\overline{E}^{\beta}\Omega^2)\delta C^{\beta}, \\ &= \kappa'^{\beta} \delta C^{\beta}, \end{aligned} \tag{5.69}$$

where κ' was introduced in Eq. (5.26).

Thus, the chemical potential of the stressed thin film undergoing small deviations from equilibrium is given by

$$\mu^{\beta} \approx \mu^{\beta}_{eq} + \kappa'^{\beta} \delta C^{\beta}. \tag{5.70}$$

Terms containing second order deviations, $(\delta C)^2$, are ignored, subsequently, the driving force for the phase transformation reaction is simplified and given by $\Phi = [\![\mathscr{g}]\!] - \mu_I [\![C]\!]$.

We find that the equations to be solved are exactly the same as the uncoupled case if the curvature, κ^β, is replaced with the new curvature κ'^β. Therefore, the results of the elastically-coupled analysis are given by

$$\begin{aligned} C^\alpha &= C^\alpha_{eq} + \delta C^\alpha, \\ C^\beta &= C^\beta_{eq} + \delta C^\beta, \end{aligned}$$

$$\begin{aligned} \delta C^\alpha(z) &= \delta C^\alpha_I = \frac{\kappa'^\beta}{\kappa^\alpha}\delta C^\beta_I, \\ \delta C^\beta(z) &= \delta C^\beta_I + \frac{\zeta' C^\beta_{eq}}{1+\zeta' z_I}(z - z_I), \\ \delta C^\beta_I &= \frac{J^* RT C_A}{\kappa'^\beta V_0 \Big(1+\zeta' z_I\Big)(C^\beta_{eq} - C^\alpha_{eq})^2}, \end{aligned} \tag{5.71}$$

$$\frac{dz_I}{dt} = \frac{J^*}{\Big(C^\beta_{eq} - C^\alpha_{eq}\Big)\Big(1+\zeta' z_I\Big)},$$

where $\zeta' = \dfrac{J^* RT}{D^\beta \kappa'^\beta (C^\beta_{eq})^2}$. Integrating the final equation from $t = 0$ to t gives the location of the interface:

$$\boxed{z_I + \frac{\zeta'}{2} z_I^2 = z_I^0 + \frac{\zeta'}{2}(z_I^0)^2 + \frac{J^* t}{\Big(C^\beta_{eq} - C^\alpha_{eq}\Big)}.} \tag{5.72}$$

5.4. Discussion

5.4.1 Stress-enhanced diffusion

The driving force for diffusion in the β-phase, i.e. the gradient of the chemical potential is found to be $\partial\delta\mu/\partial x = \kappa' d\delta C/dx$, where x=r, z for the spherical and planar systems respectively. Thus, diffusion in both systems is governed by $\kappa' = \kappa^\beta + \dfrac{2}{9}\overline{E}^\beta\Omega^2$, which can be interpreted as an increased curvature of the Gibbs energy density for a stressed system. Subsequently, the effect of stress on diffusion can be interpreted as stress-enhanced diffusion (SED).

This effect is illustrated by considering an ideal dilute solution model: $\mu^\beta(C,0) = \mu_0^\beta + RT\ln\left(\frac{C^\beta}{C_A}\right)$, where μ_0 is the chemical potential of B-atoms under standard conditions (generally, 1 atm pressure and system temperature). The gradient of the chemical potential simplifies to $\frac{\partial\mu^\beta}{\partial z} = \left(\frac{RT}{C^\beta} + \frac{2}{9}\overline{E}^\beta\Omega^2\right)\frac{\partial C^\beta}{\partial z}$. Using the mobility of ideal solutions, $M = D/RT$, the flux is given by

$$
\begin{aligned}
J^\beta &= -\frac{D^\beta C^\beta}{RT}\Big(\frac{RT}{C^\beta} + \frac{2}{9}\overline{E}^\beta\Omega^2\Big)\frac{\partial C^\beta}{\partial z}, \\
&= -D^\beta\Big(1 + \frac{2}{9}\frac{\overline{E}^\beta\Omega^2}{RT}C^\beta\Big)\frac{\partial C^\beta}{\partial z}, \\
&= -D^\beta_{\text{eff}}\frac{\partial C^\beta}{\partial z},
\end{aligned}
\tag{5.73}
$$

where the effective diffusivity is given by $D^\beta_{\text{eff}} = D^\beta\Big(1+\frac{2}{9}\frac{\overline{E}^\beta\Omega^2}{RT}C^\beta\Big)$. Equation (5.73) resembles Fick's law of diffusion with a stress-dependent diffusivity, and entails the contribution of the local volume expansion (arising from the local change of composition) to diffusion; D^β_{eff} reduces to D^β in the absence of stress.

The DIS literature, particularly with respect to LIBs, extensively uses stress-enhanced diffusivities as well as the general L-C stress-dependent chemical potential; consequently, the L-C publications are largely cited for their coupled chemical potential result and SED [63, 106–110].

5.4.2 Coupled reaction driving force

The driving force for the phase transformation reaction in the presence of deformation is given by [35, 99]

$$\begin{aligned}\Phi &= [\![\mathscr{g}]\!] - \mu_I [\![C]\!] + [\![\phi]\!] - [\![\epsilon_{ij}]\!]\sigma^{\alpha}_{ij}, \\ &= -\delta\mu^{\beta}_{I}(C^{\beta}_{eq} - C^{\alpha}_{eq}) + [\![\phi]\!] - [\![\epsilon_{ij}]\!]\sigma^{\alpha}_{ij}.\end{aligned} \tag{5.74}$$

The chemical potential change for the spherical system is given by

$$\begin{aligned}\delta\mu^{\alpha} &= -\frac{\overline{E}\Omega^2}{27}\Big[\frac{\zeta' C^{\beta}_{eq}}{\Big\{\zeta'\Big(\dfrac{1}{a} - \dfrac{1}{b}\Big) + \dfrac{1}{b^2}\Big\}\tilde{a}b}(\tilde{a}-1)^2(\tilde{a}+2) - 2(1-\tilde{a}^3)(\delta C^{\alpha}_{I} - \delta C^{\beta}_{I})\Big], \\ \delta\mu^{\beta} &= \delta C^{\beta}_{I}\Big\{\kappa^{\beta} + \frac{2\overline{E}\Omega^2}{9}\frac{(\kappa^{\alpha} - \kappa^{\beta})}{(\kappa^{\alpha} + \dfrac{2\overline{E}\Omega^2}{27}(3+4\tilde{a}^3))}\tilde{a}^3\Big\} \\ &\quad + \frac{\zeta' C^{\beta}_{eq}}{\Big\{\zeta'\Big(\dfrac{1}{a} - \dfrac{1}{b}\Big) + \dfrac{1}{b^2}\Big\}}\Big[\kappa^{\beta}\Big(\frac{1}{a} - \frac{1}{r}\Big) + \frac{\overline{E}\Omega^2}{9r}\big(3\tilde{r} - 2 - \tilde{a}^2\tilde{r}\big)\Big].\end{aligned} \tag{5.75}$$

The chemical potential change for the planar case is given by Eq. (5.69).

5.4.3 Growth kinetics

The equations for the growth kinetics of both geometries match the uncoupled solution, but for the κ'^{β} term instead of κ^{β}, and consequently the ζ' term instead of ζ.

For each phase, the variables for stress, and deviations in chemical potential and concentration can be cast into their dimensionless forms:

$$
\begin{aligned}
\tilde{\sigma}_{ij} &= \frac{\sigma_{ij}}{\overline{E}}, \\
\delta\tilde{\mu} &= \Big(\frac{C_{eq}^{\beta} - C_{eq}^{\alpha}}{\mathscr{g}(C_{eq}^{\alpha}) - \mathscr{g}(C_{eq}^{\beta})}\Big)\delta\mu, \\
\delta\tilde{C} &= \frac{\delta C}{(C_{eq}^{\beta} - C_{eq}^{\alpha})},
\end{aligned}
\tag{5.76}
$$

where, following Bower et al. [23], the dimensionless material parameters are given by

$$
\begin{aligned}
\Delta &= \frac{J^{*}(C_{eq}^{\beta} - C_{eq}^{\alpha})b}{M^{\beta}C_{eq}^{\beta}(\mathscr{g}(C_{eq}^{\alpha}) - \mathscr{g}(C_{eq}^{\beta}))}, \\
\Theta &= \frac{J^{*}}{V_0(C_{eq}^{\beta} - C_{eq}^{\alpha})}\frac{C_A RT}{(\mathscr{g}(C_{eq}^{\alpha}) - \mathscr{g}(C_{eq}^{\beta}))}, \\
\Lambda &= \frac{\overline{E}\tilde{\Omega}^{2}}{3(\mathscr{g}(C_{eq}^{\alpha}) - \mathscr{g}(C_{eq}^{\beta}))}, \\
\tilde{\Omega} &= \Omega(C_{eq}^{\beta} - C_{eq}^{\alpha}), \\
\Gamma &= \frac{\kappa(C_{eq}^{\beta} - C_{eq}^{\alpha})^{2}}{(\mathscr{g}(C_{eq}^{\alpha}) - \mathscr{g}(C_{eq}^{\beta}))},
\end{aligned}
\tag{5.77}
$$

The rate of insertion of B-atoms to the rate of diffusion in the bulk is given by Δ; the rate of insertion of B-atoms to the rate of phase boundary movement is given by Θ. The solubility of B-atoms in each phase is quantified by Γ.

For the spherical system, $\tilde{r} = \dfrac{r}{b}$, and $\tilde{a} = \dfrac{a}{b}$; the latter notation was introduced in *Section 5.2.3*. Subsequently, the location of the interface, Eq. (5.56), is cast into its dimensionless form:

$$
\Big(1 - \frac{3\Delta(1 - K_D)}{(3\Gamma + 2\Lambda)}\Big)\frac{(\tilde{a}^{3} - \tilde{a}_0^{3})}{3} + \frac{3\Delta(1 - K_D)}{(3\Gamma + 2\Lambda)}\frac{(\tilde{a}^{2} - \tilde{a}_0^{2})}{2} = -\tilde{t},
\tag{5.78}
$$

where $K_D = C_{eq}^{\alpha}/C_{eq}^{\beta}$ and $\tilde{t} = t/(b(C_{eq}^{\beta} - C_{eq}^{\alpha})/J^{*})$. This equation can be visualized graphically to analyze the effects of elasticity and chemical thermodynamics; for example, in Fig. 5.2,

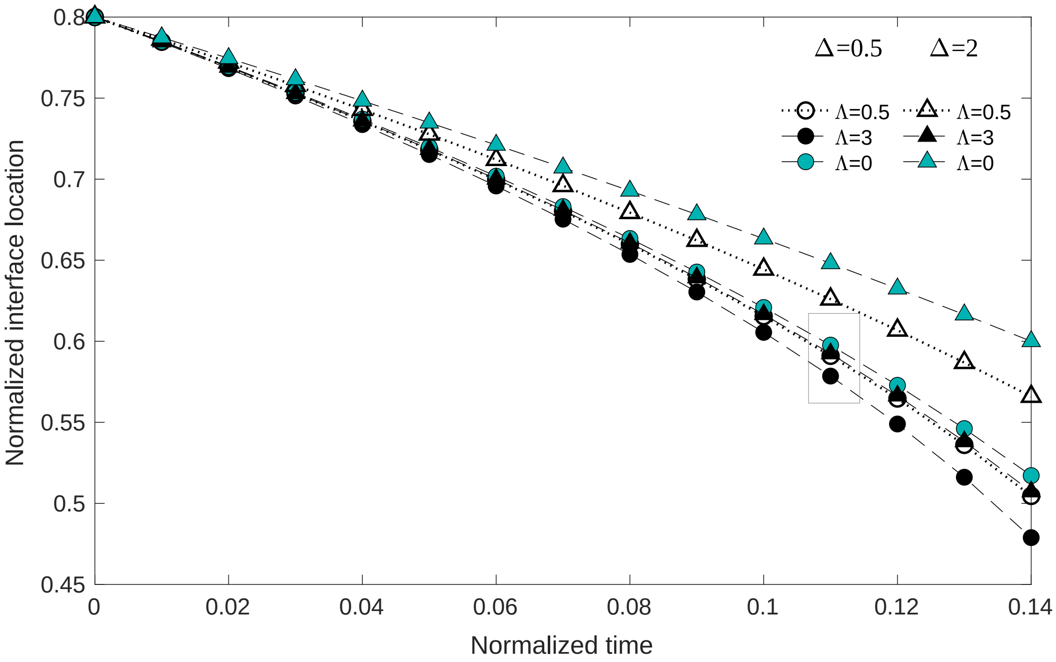

Figure 5.2: Normalized interface location, $\tilde{a}$, vs normalized time, $\tilde{t}$. Three solutions are presented, corresponding to $\Lambda = 0, 0.5, 3$. The circles show the results for $\Delta = 0.5$; the triangles correspond to $\Delta = 2$. The remaining material parameters are selected as follows: $\Theta = 0.5$, $\Gamma = 1$, and $K_D = 0.5$. Initially, the interface is at $\tilde{a}_0 = 0.8$. The solutions were evaluated in MATLAB®.

the uncoupled solution (Λ=0) is presented together with two elastically-coupled solutions (Λ=0.5, 3). The triangles ($\Delta = 2$) illustrate the results for faster transport of B-atoms through the bulk compared to the circles ($\Delta = 0.5$); in each case, the results show that the diffusive phase growth is enhanced in the presence of elasticity. The chemical and mechanical contributions to the driving forces of diffusion and phase transformation dictate the interface growth; the interplay is especially noted in the two cases corresponding to $\Delta = 0.5$, $\Lambda = 0.5$, and $\Delta = 2$, $\Lambda = 3$, where the two sets of material parameters exhibit comparable phase growth.

5.4.4 Limit analysis

The nature of equations (4.15, 5.55) and (4.24, 5.71f) cue a limit analysis of growth kinetics involving ζ or ζ' and the thickness of the β-phase; a limit analysis was undertaken for the uncoupled core-shell model in *Section 4.3.2*. This analysis reveals reaction-dominated behavior at smaller thicknesses, and diffusion-limited behavior at greater thicknesses; in the planar case, this manifests as linear growth when reaction is dominating the kinetics, and parabolic growth when diffusion is predominant:

$$\begin{aligned} \zeta z_I \ll 1: &\quad z_I(t) = z_I^0 + \frac{J^*}{\left(C_{eq}^{\beta} - C_{eq}^{\alpha}\right)} t, \\ \zeta z_I \gg 1: &\quad \frac{z_I^2}{2} = \frac{(z_I^0)^2}{2} + \frac{J^* t}{\left(C_{eq}^{\beta} - C_{eq}^{\alpha}\right)\zeta}. \end{aligned} \tag{5.79}$$

The parameter, $1/\zeta$, can be interpreted as a critical thickness which characterizes the two growth regimes [111]. In the presence of DISs, the parameter is $1/\zeta'$, and $1/\zeta' > 1/\zeta$; however, the qualitative nature of the growth kinetics remains the same, as seen in Eqs. (5.55) and (5.71)f, and illustrated in Fig. 5.2 for the coupled spherical model.

It is noted that these linear and parabolic kinetic regimes, where the latter regime is observed at larger thicknesses and depends on the thickness, as well as the linear-to-parabolic growth transition above a critical transition thickness are characteristic of several thin film material systems including hydrides, oxides, and silicides [56, 111–113]. While there is experimental evidence for these growth behaviors, knowledge of thermodynamic driving forces is required to determine the transport coefficients quantitatively.

In this thesis, the uncoupled and elastically-coupled growth kinetics of the considered models exhibit two kinetic regimes using well-defined thermodynamic and kinetic parameters.

5.4.5 Nature of coupling

The elastically-coupled results and subsequent discussion presented in the previous sections apply when the nature of coupling is such that the coupled driving force for the phase transformation reaction remains negative. The consequences of large coupling effects are discussed in this section.

Reaction block

In the absence of deformation, the driving force for phase transformation is always negative, and given by $\Phi = -\kappa^\beta \delta C_I^\beta (C_{eq}^\beta - C_{eq}^\alpha)$.

In the presence of stress, the phase transformation driving force may not be negative, which is evident from Eq. (5.74). For the spherical case, when $\kappa^\alpha = \kappa^\beta = \kappa$, $\Phi_{\text{core-shell}}$ is given by

$$\Phi_{\text{core-shell}} = -\kappa \delta C_I (C_{eq}^\beta - C_{eq}^\alpha) + \frac{\overline{E}\Omega^2}{9} \frac{\zeta' C_{eq}^\beta}{\tilde{a} b\{\zeta'(\frac{1}{a} - \frac{1}{b}) + \frac{1}{b^2}\}} (\tilde{a} - 1)^2 (\tilde{a} + 2)(C_{eq}^\beta - C_{eq}^\alpha), \quad (5.80)$$

which vanishes when $\delta C_I = \frac{\overline{E}\Omega^2}{9\kappa} \frac{\zeta' C_{eq}^\beta}{\tilde{a} b\{\zeta'(\frac{1}{a} - \frac{1}{b}) + \frac{1}{b^2}\}} (\tilde{a} - 1)^2 (\tilde{a} + 2)$. Subsequently, the phase transformation reaction cannot proceed; this scenario is interpreted as a reaction block or lock, and also occurs in the planar case, where Φ_{bilayer} is given by

$$\Phi_{\text{bilayer}} = \llbracket \mathscr{g} \rrbracket - \mu_I \llbracket C \rrbracket + \frac{(\overline{\sigma}^\beta)^2}{\overline{E}^\beta}. \quad (5.81)$$

In the presence of reaction block, it is evident that the growth kinetics are affected; this locking effect can be interpreted as an energy threshold or barrier that must be overcome for the interface to move again.

To query the occurrence of reaction block for the selected set of points corresponding to $\Delta = 0.5$ in Fig. 5.2, specified using a grey box, we cast Eq. (5.80) into its dimensionless form using Eq. (5.77) to obtain the corresponding normalized interfacial concentration deviation when $\Phi_{\text{core-shell}} = 0$:

$$\delta\tilde{C}_w = \frac{\Lambda/\Delta}{(\Gamma/\Delta)(3\Lambda/\Delta + 2\Lambda/\Delta)} \frac{(\tilde{a}-1)^2(\tilde{a}+2)}{\tilde{a}} \frac{1}{\left(1 + 3\dfrac{(1-K_D)(\frac{1}{\tilde{a}}-1)}{(3\Lambda/\Delta + 2\Lambda/\Delta)}\right)}, \tag{5.82}$$

where the subscript w is used to emphasize that the solution corresponds to the interfacial concentration deviation when the interface is not moving, i.e., it is 'waiting'.

Λ	$\delta\tilde{C}_w$
0	0
0.5	0.04
3	0.12

Table 5.1: Estimated values of $\delta\tilde{C}_w$ for the specified set of points in Fig. 5.2 for $\Delta = 0.5$.

Table 5.1 presents the estimated values of $\delta\tilde{C}_w$ corresponding to the selection in Fig. 5.2. In the uncoupled case, the interfacial concentration vanishes, corresponding to interfacial equilibrium. In the two elastically coupled cases, it is possible for $\Phi_{\text{core-shell}}$ to vanish away from equilibrium, i.e. when $\delta\tilde{C}_w \neq 0$; when these deviations violate the key assumption, $\delta\tilde{C}_w \ll 1$, the situation is out of scope of this chapter, and we require another model.[11]

The slowing down of reaction fronts in the presence of mechanical stress as well as a complete arrest of the phase transformation reaction has been observed via in-situ TEM studies of material systems such as silicon nanowires (SiNWs) [62, 65], lithium-silicon and lithium-germanium nanoparticles and nanowires [64, 67, 68]. Analysis of such systems are of key interest to nanoscale devices and LIB technologies. However, the stress mediated kinetics affect the charging/discharging rates, thereby compromising their net capacity and performance. To describe these experimental observations, effective transport parameters are often used, which contain fitting parameters [64]. Similarly, theoretical investigations

---

[11] A kinetic model is proposed in *Chapter 8* using modeling insights derived from the full tertiary coupling considered here.

often feature effective parameters as well; for example, a surface locking instability has been proposed in the context of LIB by coupling stress with diffusion via an effective diffusivity, which contains the effects of a stress-induced energy barrier [24].

In this work, we demonstrated the deceleration effect to be a consequence of strong stress-reaction coupling using the thermodynamic concept of reaction driving force in the presence of stress. This result is revisited in *Chapter 8* to contemplate the next step in its modeling.

It is noted that we used the terminology of Freidin et al. [48, 49, 114–116], who use *reaction block* or *reaction lock* to describe this coupled effect, which they predict by considering binary coupling between stress and phase transformation within a nonclassical thermodynamics formulation.

Phase stability and hysteresis

Interfacial equilibrium entails $\Phi = 0$. In the absence of stress, this condition was described graphically in Fig. 3.2 by a common tangent to the two Gibbs energy density curves, which sections the composition range. For compositions between C^{α}_{eq} and C^{β}_{eq}, the stable state of the system comprises two phases with compositions at C^{α}_{eq} and C^{β}_{eq}, where the lever rule provides the relative proportions. This state is often referred to as the *true* equilibrium state.

When a reaction block occurs, the driving force is once again zero. This state, which is often interpreted as a *false* interfacial equilibrium [117], raises the question of phase stability in the presence of stress, particularly under cyclic conditions.

Crucially, stress has modified the two-phase field. When a solution to the interfacial and chemical equilibrium exists, a two-phase field is possible even in the presence of stress, as shown by the blocked state. Nevertheless, a state with stress holds more energy, and is subsequently metastable compared to a stress-free state. During an isothermal cyclic operation, the α to β phase transformation reaction experiences an energy barrier. This energy threshold can be interpreted as a metastability barrier that leads to hysteresis.

Other impeding effects in the literature

In physical metallurgical literature, which includes metal hydride systems, well-known impeding effects, often in the presence of stresses, include *solute pinning*, *solute drag*, *solute trapping* [118], and *interface pinning* [86], where solute particles refer to point defects or impurity atoms and trapping sites include grain boundaries, dislocations and second-phase particles, i.e. the microstructure is at the forefront in these studies. These effects require sophisticated models; at present, they are modeled using diffusion equations by invoking pinning potentials, trapping energies, and effective diffusivities, which require experimental data to fit the parameters. To model trapping, chemical reactions are often used with diffusion.

Recently, interface pinning has been proposed to be the source of hysteresis between the absorption and desorption of hydrogen in palladium-hydride systems in their bulk form, which exhibits defects [86].

The modeling of reaction block, interface pinning, and trapping to investigate phase stability and the mechanism of hysteresis in bulk and nanoscale materials are active areas of research in metal hydrogen systems and lithium-ion batteries [81, 83, 86, 119].

5.4.6 Model validity

The QSS model applies when $\delta C \ll (C_{eq}^{\beta} - C_{eq}^{\alpha})$. As δC^{β} is nonhomogeneous, the validity of the steady-state condition can be expressed in terms of λ_{QSS}, the ratio of the maximum deviation resulting from the B-atoms in the bulk to those at the interface [23]; $\lambda_{QSS} \ll 1$ for the steady-state assumption to hold, as seen in *Section 4.3.4*. This condition indicates that the analysis assumes (a) slow interface kinetics and (b) limited bulk solubility. When there are no limitations to the solubility of the bulk phase, the phase interface is stationary and the kinetics of the problem are described by a transient diffusion problem.

The linear kinetic models, governed by linear irreversible thermodynamics (LIT), rely on the *local equilibrium hypothesis*, which states that at any given time, each material point or cell exhibits equilibrium, however, this equilibrium state differs from that of its neighbouring cells thereby allowing mass and energy transfer. The upshot of this hypothesis is that it enables the use of equilibrium thermostatics concepts of *Chapter 2*, while imposing restrictions on the systems and processes because it is only valid for large length and time scales. This hypothesis is typically characterized by the Deborah number, De, which is a ratio of the time required for equilibration within one cell to the macroscopic characteristic time; when $De \ll 1$, the local equilibrium assumption is valid [120].

Finally, the underlying thermostatic framework is based on the internal energy density as a function of the small strain tensor, entropy density, and concentration: $\mathscr{u} = \mathscr{u}(\boldsymbol{\epsilon}, \mathscr{s}, C)$, as seen in *Section 2.2*. This is a constitutive assumption for the deformed continuum that further dictates the material and mechanics that can be studied within this framework.

5.5. Summary

Chapters 3-5 presented the formulation and analyses of moving boundary problems, derived using linear kinetic models guided by equilibrium thermostatics. The quasi-steady state approximation permits closed-form analytical solutions for concentration, growth kinetics, and elastic stresses in a spherical and planar particle, which offer a rich variety of physical insights. Specifically, it was demonstrated for the first time within this framework that the derived growth kinetics compare qualitatively to classical empirical models, and contain thermodynamic-kinetic parameters instead of fitting parameters. The effects of stress-diffusion and stress-reaction coupling are derived. Stress-enhanced diffusion was deduced and coupling conditions for stress-induced reaction blocking were derived. Reaction blocking, phase stability, and hysteresis are interrelated concepts that were discussed within this framework. While some of these phenomena have been investigated separately, the deductions presented in these chapters, which lend themselves to physical and modeling insights, are presented for the first time using a consolidated theoretical approach based on both thermodynamics and kinetics.

Furthermore, the systematic layout of the formulation and the accompanying assumptions provide insights into possible nonclassical extensions as well as the constraints of the models in the realm of real devices and materials. For example, it is possible to apply the formulation of these chapters to explore diffusion in rubbery polymers, which exhibit Fickian-type diffusion. However, to describe non-Fickian transport, which can occur when diffusion is accompanied by substantial macromolecular relaxations, one needs to modify and extend at the foundational level because the local equilibrium hypothesis is no longer valid. Subsequently, glassy polymers, which exhibit non-Fickian characteristics cannot be studied within this framework.

Similarly, to explore the system behavior under conditions of strong coupling, it is required to extend the kinetics and mechanics to consider nonlinear diffusion and nonlinear elasticity. For example, for larger concentrations, and subsequently strong coupling, which is encountered in both metal hydrides and lithium-ion batteries, the kinetics of diffusion exhibit nonlinearities. It is noted that while the assumptions of the present chapter do not include large concentrations, the exploration of the full tertiary coupling, enabled by these simplifying assumptions, offers several kinetic modeling insights, which are highlighted in *Chapter 8*, including a nonlinear diffusion equation that may be best suited to model the coupled phenomenon of reaction block. Likewise, relaxing the assumption of constant elastic parameters to include concentration-dependent elastic modulus also generates nonlinear kinetics. In [121], Yang derived the diffusion equation for regular binary solid solutions using a thermodynamic model; however, to obtain closed-form expressions, this diffusion equation was simplified by assuming that the effect of stress on diffusion of the solute can be ignored, and that the solid solution is ideal.

In many scenarios, nonlinear diffusion equations, specifically, the effective diffusivities, which are nonlinear functions of the solute concentration, need to be analyzed. These nonlinear diffusivities are rich in information, including pertinent length and time scales; however, extracting these characteristics from the nonlinear equation is nontrivial and requires sophisticated tools of analysis, including asymptotics and renormalization.

Chapter 6

Phase equilibrium and stability of an elastically stressed thin-film bilayer

This open chapter explores the effects of elasticity on the solution thermodynamics of a thin-film bilayer.

When lattice misfit occurs between phases, coherency strains are generated, which play an important role in thermodynamics because they influence the solubility and stability of the phases. This topic can be an entire thesis in its own right; indeed, there are extensive publications, including those of W. C. Johnson and P. W. Voorhees, contemporaries of Larché and Cahn, that investigate the thermodynamics of coherent equilibrium and the stability of the phases at and away from equilibrium in various elastically stressed systems [78–80,122–160]. Several of these studies were motivated by the Cahn-Larché model in [123].

This chapter considers a thin-film bilayer model to explore the effects of the elastic stresses in the film, which are given by

$$\overline{\sigma}^{\beta} = \overline{E}^{\beta}\frac{1}{3}\big(\Omega^{\alpha}\Delta C^{\alpha} - \Omega^{\beta}\Delta C^{\beta}\big), \tag{6.1}$$

where ΔC is analogous to temperature changes in heat transfer problems, and $\Omega^{\alpha} \neq \Omega^{\beta}$, i.e. the material parameter, Ω, is assumed to be constant but has different values in the two phases. Equation (6.1) can be obtained using the derivations of *Sections 5.3.1 and 5.3.2.*

6.1. Equilibrium thermostatics

At a given temperature, the total Helmholtz energy of the thin-film bilayer is given by [123]

$$F = V_A\Big[(1-x)\not{f}^{\alpha}(C,0) + x\not{f}^{\beta}(C,0) + x(1-x)\phi^{\beta}\Big], \tag{6.2}$$

where V_A denotes the volume occupied by the A-atoms, x is the volume fraction of the β-phase, $x = V^{\beta}/V_A$, $\not{f}$ denotes the Helmholtz energy density, and ϕ^{β} is the strain energy density of the thin-film β-phase. For single phases, i.e. when x is 0 or 1, the last term vanishes.

Since a thin-film of β-phase is assumed, $x \ll 1$; subsequently, the last term can be simplified to $x\phi^{\beta}$, and the total energy is given by

$$\begin{aligned} F &= V_A\Big[(1-x)\not{f}^{\alpha}(C,0) + x\not{f}^{\beta}(C,0) + x\phi^{\beta}\Big], \\ F &= V_A\Big[(1-x)\not{f}^{\alpha}(C,0) + x\not{f}^{\beta}(C,\sigma)\Big], \end{aligned} \tag{6.3}$$

where $\not{f}(C,\sigma) = \not{f}(C,0) + \phi$ for the β-phase; this derivation is presented in *Appendix F*.

The equation for a constant overall composition of the B-atoms, C_o, is given by

$$xC^{\beta} + (1-x)C^{\alpha} = C_o. \tag{6.4}$$

The conditions for chemical and interface equilibrium can be obtained by minimizing the total energy of the system, subjected to the constraint of constant overall composition, which is incorporated via a Lagrange multiplier:

$$\begin{aligned} \frac{\partial}{\partial C^{\alpha}}(F' - \lambda(xC^{\beta} + (1-x)C^{\alpha} - C_o)) &= 0, \\ \frac{\partial}{\partial C^{\beta}}(F' - \lambda(xC^{\beta} + (1-x)C^{\alpha} - C_o)) &= 0, \\ \frac{\partial}{\partial x}(F' - \lambda(xC^{\beta} + (1-x)C^{\alpha} - C_o)) &= 0, \end{aligned} \tag{6.5}$$

where $F' = F/V_A$. Equation (6.5)a simplifies to

$$\frac{\partial F'}{\partial C^\alpha} - \lambda(1-x) = 0. \tag{6.6}$$

The first term is given by $\frac{\partial F'}{\partial C^\alpha} = (1-x)\frac{\partial \not{f}^\alpha}{\partial C^\alpha} + x(1-x)\frac{\partial \phi^\beta}{\partial C^\alpha} = (1-x)\Big(\frac{\partial \not{f}^\alpha}{\partial C^\alpha} + x\frac{\partial \phi^\beta}{\partial C^\alpha}\Big)$. Thus, Eq. (6.6) is satisfied by

$$\begin{aligned} &x = 1 \\ &\quad \text{or} \\ &\lambda = \frac{\partial \not{f}^\alpha}{\partial C^\alpha} + x\frac{\partial \phi^\beta}{\partial C^\alpha}. \end{aligned} \tag{6.7}$$

Similarly Eq. (6.5)b simplifies to

$$\begin{aligned} &x = 0, \\ &\quad \text{or} \\ &\lambda = \frac{\partial \not{f}^\beta}{\partial C^\beta}(C,\sigma), \end{aligned} \tag{6.8}$$

where $x \ll 1$ is used to simplify.

The results, $x = 0$ and $x = 1$, correspond to single phases. The two-phase solution for chemical equilibrium corresponds to Eqs. (6.7)b and (6.8)b.

6.1.1 Two-phase equilibrium when $\Omega^\alpha = 0$

Assuming $\Omega^\alpha = 0$, we obtain

$$\lambda = \frac{\partial \not{f}^\alpha}{\partial C^\alpha}, \tag{6.9}$$

where Eq. (6.7) was simplified. As λ is a Lagrange multiplier, it is constant and given by

$$\lambda = \frac{\partial \mathscr{f}^{\alpha}(C,0)}{\partial C^{\alpha}} = \frac{\partial \mathscr{f}^{\beta}(C,\sigma)}{\partial C^{\beta}}. \tag{6.10}$$

This equation represents the chemical equilibrium, where λ is identified with the chemical potential, μ.

Equation (6.5)c simplifies to

$$\mathscr{f}^{\beta}(C,\sigma) - \mathscr{f}^{\alpha}(C,0) - \lambda(C^{\beta} - C^{\alpha}) = 0, \tag{6.11}$$

where $x \ll 1$ is used to simplify. This equation represents the interfacial equilibrium for a planar coherent interface.

6.2. Coherent concentration field

The coherent equilibrium, if it exists, corresponds to the concentration field, C^{η} ($\eta = \alpha, \beta$), and non-zero thin-film stresses. Assuming a two-phase stress-free (SF) state exists, we assume that the coherent equilibrium is close to this SF state, whose concentrations are denoted C_0^{η}. This implies we can undertake the following linearization:

$$\begin{aligned} C^{\eta} &= C_0^{\eta} + \Delta C^{\eta}, \\ \mu^{\eta}(C,0) &= \mu^{\eta}(C_0^{\eta},0) + \chi^{\eta}\Delta C^{\eta}, \qquad \eta = \alpha, \beta \\ \mathscr{f}^{\eta}(C,0) &= \mathscr{f}^{\eta}(C_0^{\eta},0) + \mu_0^{\eta}\Delta C^{\eta}, \end{aligned} \tag{6.12}$$

where μ_0 and χ are respectively the first and second derivatives of the Helmholtz energy density with respect to concentration in the absence of stress; both are evaluated at the SF concentrations.

To solve for the coherent equilibrium compositions, C^{α} and C^{β}, we require two equations, which are provided by the chemical and interfacial equilibrium conditions. The chemical equilibrium condition, Eq. (6.10), is simplified for $\Omega^\alpha = 0$:

$$\begin{aligned} \frac{\partial \not{f}^{\alpha}(C,0)}{\partial C^\alpha} &= \frac{\partial \not{f}^{\beta}(C,0)}{\partial C^\beta} + \frac{\partial \phi^\beta}{\partial C^\beta}, \\ \mu^\alpha(C,0) &= \mu^\beta(C,0) + \frac{2}{9}\overline{E}^{\beta}(\Omega^\beta)^2 \Delta C^\beta, \end{aligned} \tag{6.13}$$

and subsequent linearizations are as follows:

$$\begin{aligned} \mu^\alpha(C_0^\alpha,0) + \chi^\alpha \Delta C^\alpha &= \mu^\beta(C_0^\beta,0) + \chi^\beta \Delta C^\beta + \frac{2}{9}\overline{E}^{\beta}(\Omega^\beta)^2 \Delta C^\beta, \\ \mu^\alpha(C_0^\alpha,0) + \chi^\alpha \Delta C^\alpha &= \mu^\beta(C_0^\beta,0) + \chi'^\beta \Delta C^\beta, \end{aligned} \tag{6.14}$$

where $\chi'^\beta = \chi^\beta + (2/9)\overline{E}^{\beta}(\Omega^\beta)^2$.

The SF chemical equilibrium corresponds to $\mu_0 = \mu^\alpha(C_0^\alpha, 0) = \mu^\beta(C_0^\beta, 0)$. Thus, Eq. (6.14) simplifies to

$$\chi^\alpha \Delta C^\alpha = \chi'^\beta \Delta C^\beta. \tag{6.15}$$

Similarly, simplifying the interfacial equilibrium, Eq. (6.11), using linearization, and incorporating Eq. (6.15) and the SF interfacial equilibrium condition, i.e.,

$\not{f}^{\beta}(C_0^\beta, 0) - \not{f}^{\alpha}(C_0^\alpha, 0) - \mu_0(C_0^\beta - C_0^\alpha) = 0$, we obtain two solutions for ΔC^α and ΔC^β:

$$\begin{aligned} &\Delta C^\alpha = \Delta C^\beta = 0, \\ &\quad\text{or} \\ &\frac{\Delta C^\beta}{C_0^\beta} = \frac{1-\hat{C}}{\left[\dfrac{\overline{E}^{\beta}(\Omega^\beta)^2}{9\chi'^\beta} - (1-\hat{\chi})\right]}, \end{aligned} \tag{6.16}$$

where $\hat{C} = C_0^\alpha / C_0^\beta$, $\hat{\chi} = \chi'^\beta / \chi^\alpha$, and $\Delta C^\alpha = \dfrac{\chi'^\beta}{\chi^\alpha}\Delta C^\beta$. The first result is a trivial solution corresponding to the SF solution; the second result corresponds to coherent equilibrium in the presence of stress.

In summary, we have two solutions for the equilibrium concentration field: stress-free solution, C_0, and elastically-stressed solution, C. This raises the question of stability of the concentration field in the presence of stress. To gain insight, we consider the relative linear stability of the phases corresponding to the two solutions.

6.3. Relative stability of phases

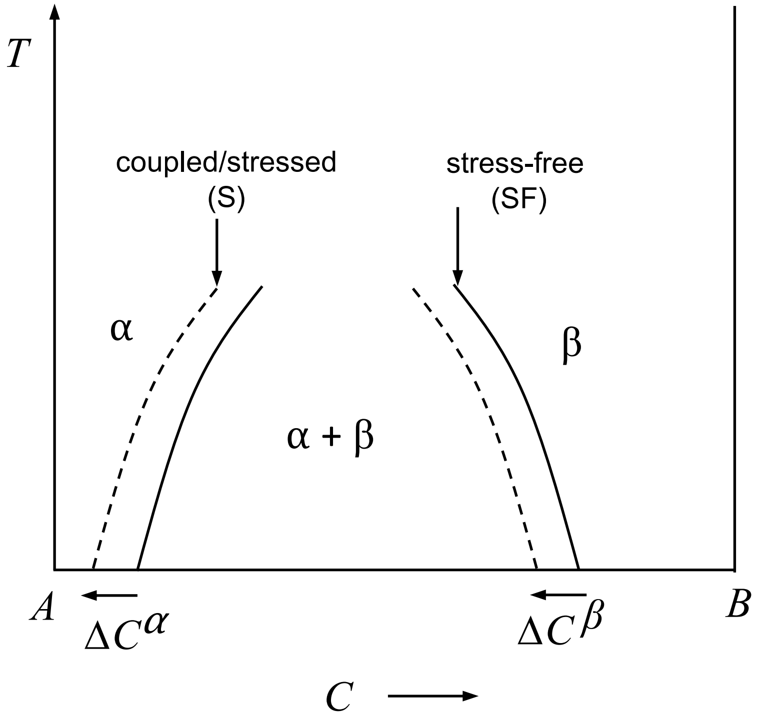

Figure 6.1: Schematic phase boundaries of the thin-film bilayer corresponding to the two equilibrium solutions. The solid lines correspond to the stress-free (SF) solution. The dashed lines correspond to the stressed solution (S), given by Eqs. (6.15) and (6.16)b. The shift in the phase boundaries or solubilities indicates the effects of the film stress on relative stability; when the β-phase is stabilized by the stress, the α-phase is destabilized.

The β-phase is stabilized by the stress when ΔC^{β} is negative, i.e., the stressed $\alpha+\beta/\beta$ phase boundary is on the left of the corresponding SF boundary. Because of Eq. (6.15), the stressed $\alpha/\alpha+\beta$ phase boundary is also on the left of the SF boundary. A schematic of these two solutions is displayed in Fig 6.1.

6.4. Graphical analyses and discussion

The following stability considerations are undertaken graphically.

6.4.1 Stability considerations for open systems at constant temperature

In open systems, the overall composition of the B-atoms, C_o, is an external variable that is changed by varying the prescribed partial pressure of the mobile B-atoms in the gaseous phase, which is related to their chemical potential in the solid phases, and provides the driving force for the absorption and desorption of B-atoms.

Absorption at constant temperature

Consider the process of absorption at constant temperature, as shown in Fig. 6.2a. Initially, the solid is in its single α-phase. The pressure of the gas is increased, which increases the chemical potential of the B-atoms, and subsequently, the overall composition. The solid continues to exist in the α-phase until the concentration of the B-atoms is such that it is energetically more favorable to phase transform; this two phase $\alpha+\beta$ field is delineated by phase boundaries.

In classical thermodynamics, there is only one solution to the phase boundaries, determined by the SF concentrations. Here, there are two possible solutions for the $\alpha/\alpha+\beta$ phase boundary. However, when starting from the α-phase, the SF phase boundary is stable compared to the stressed solution, as per *Section 6.3*. Thus, the two-phase solution under absorption of B-atoms by the α-phase corresponds to SF equilibrium.

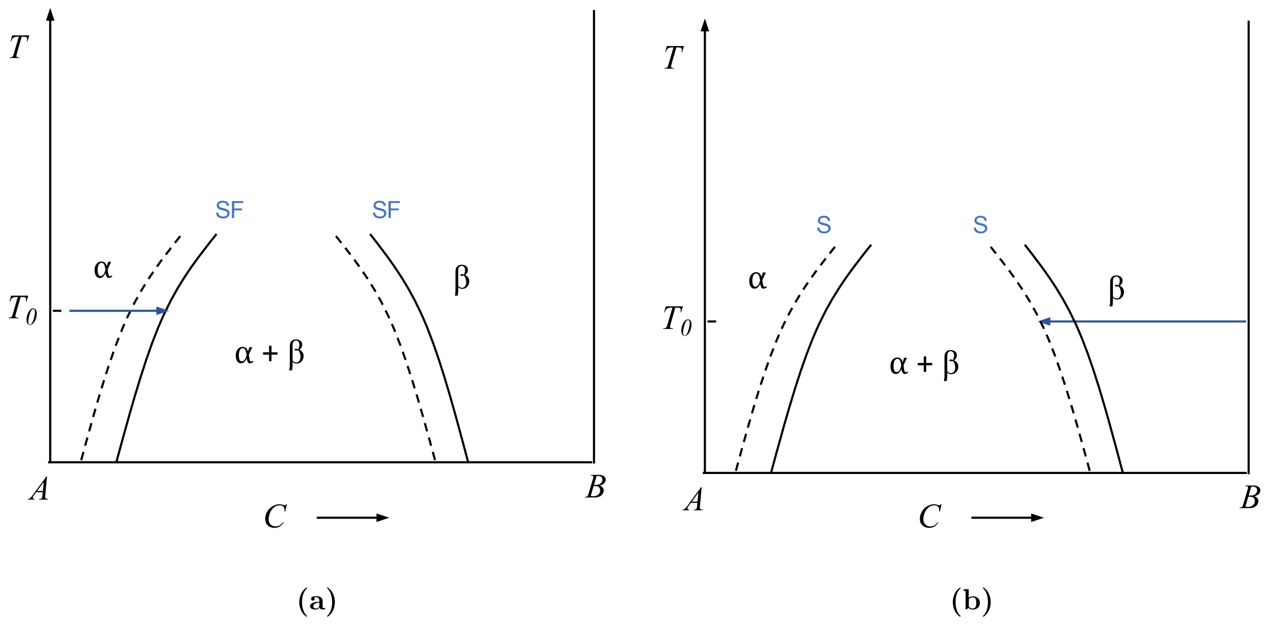

(a) (b)

Figure 6.2: Schematic phase boundaries of the thin-film bilayer corresponding to the absorption (desorption) of B-atoms at constant temperature, T_0, are given by the SF (S) solutions.

Desorption at constant temperature

Similarly, the stable solution corresponding to the desorption of the β-phase is the stressed solution, as shown in Fig. 6.2b.

Absorption-Desorption offset

The absorption and desorption of B-atoms exhibit an offset induced by stress, and consequently, the partial pressure of B-atoms required for absorption (SF) is greater than the partial pressure that drives desorption (S). This offset may be interpreted as a macroscopic energy barrier that must be overcome (by increasing the chemical potential of the gas and thereby the overall composition of the B-atoms) for the phase transformation to proceed; else the phase transformation reaction is locked.

Hysteresis

The absorption-desorption offset and the associated energy barrier are indicators of isothermal hysteresis, which appears to be an intrinsic property of the system as it is deduced solely based on the existence of two metastable solutions. The thermodynamic path is not conservative because it is path-dependent (and therefore history-dependent), as indicated by Fig. 6.2 and the subsequent discussion of absorption and desorption. Furthermore, the nature of the hysteresis appears to be rate-independent because it cannot be decreased by slowing down the rates of absorption and desorption.

Stability of the two-phase field

The stress-free two-phase field corresponds to an α-phase that is relatively stable than the β-phase; the elastically stressed two-phase field corresponds to a β-phase that is relatively stable than the α-phase.

Consequently, the two-phase field becomes unstable for the open system because of the two metastable solutions. During absorption, once the energy barrier is overcome, the α to β phase transformation proceeds spontaneously until all the α-phase is converted to β, and vice versa for desorption. Therefore, equilibrium coexistence of α- and β-phases is not possible under open conditions.

6.4.2 Stability considerations for closed systems at constant temperature

Closed systems have a fixed number of B-atoms, and thereby a constant overall composition of the B-atoms, which is given by C_o.

If we undertake a temperature scan on the solvus side, i.e. the dilute phase boundary side, of the phase diagram, we once again encounter an offset, as shown in Fig. 6.3. Here, we obtain a temperature offset: the solvus temperature required for heating is greater than the solvus temperature required for cooling. Thus, the closed systems must also overcome an energy barrier for the reaction to proceed. However, unlike open systems, closed systems at a given operating temperature are in an arrested state, and cannot access other favorable states. Subsequently, there is no spontaneous phase transition and the closed thin-film bilayer system is able to exhibit two-phase equilibrium.

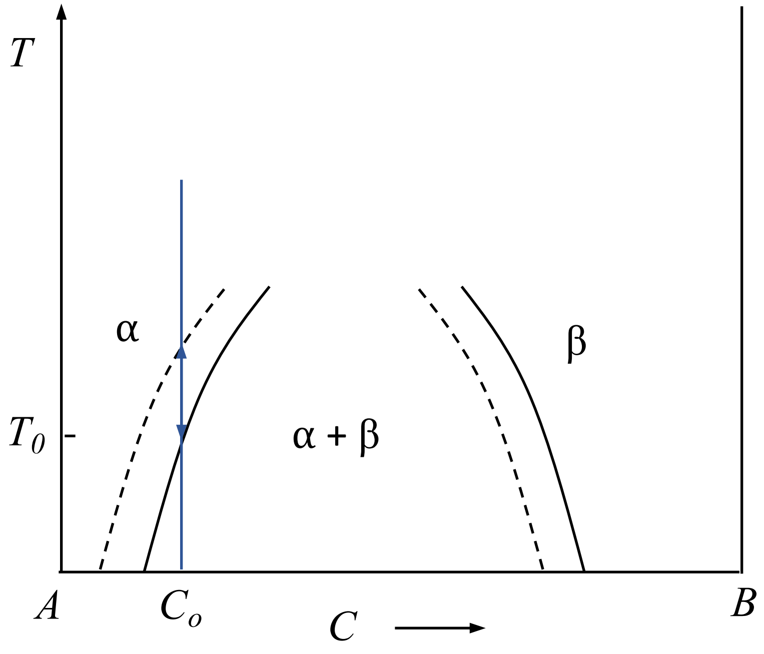

Figure 6.3: Schematic illustration of a temperature scan in a closed thin-film bilayer system. The relationship to heating and cooling are indicated in blue, corresponding to a temperature offset.

6.4.3 Palladium-hydrogen system

To corroborate the deductions of the above analyses, we seek material systems that can be approximated by the physical model considered here, namely, a binary system exhibiting two isostructural[12] solid phases, where the absorption of B-atoms generates volume expansion of

---

[12] Isostructural or isomorphic phases differ only in their composition.

the A-lattice, and the mobile B-atoms occupy interstitial positions. Metal-hydride systems are suitable candidates, particularly the palladium-hydrogen system, as the partial molar volume of its α-phase is close to zero, i.e. the lattice parameters of this phase are close to the undeformed A-lattice or Pd-lattice.

The hydrogenation of palladium entails reactions at its surface, where the hydrogen gas is split catalytically, and subsequently, the atomic hydrogen intercalates into the metal. The chemical potential of the hydrogen atoms is controlled by the hydrogen pressure; at low pressures, we observe the dilute solid solution or the α-$\mathrm{PdH_x}$ phase (at 298 K, H/Pd atom ratio is less than $\sim$0.015), where the hydrogen atoms occupy random interstitial octahedral sites in palladium. The lattice constant of this phase is 3.894 Å. The lattice constant of pure Pd is 3.889 Å; subsequently α-$\mathrm{PdH_x}$ features a light expansion of the lattice. When the hydrogen gas pressure is increased, $\alpha \rightarrow \beta$ phase transformation occurs, which entails an expanded lattice with $\sim$3.7% expansion in the lattice constant, and a H/Pd ratio that is larger than $\sim$0.6 [71]. The hydrogen pressure corresponding to the $\alpha \rightarrow \beta$ phase transition occurs at a higher hydrogen pressure than the reverse reaction, leading to hysteresis, a ubiquitous characteristic of metal hydrides in general.

The temperature-composition phase diagram of the Pd-H system was determined experimentally by a few researchers [87, 161, 162] based on hydrogenation (absorption) and dehydrogenation (desorption) data. These papers established two sets of solubility curves or phase boundaries corresponding to the two palladium hydride interstitial alloys.

It is noted that figures 5, 1, and 7 in [161], [162], and [87] respectively, exhibit an absorption-desorption offset that is qualitatively comparable to that of Fig. 6.2. For example, Fig. 5 of Flanagan and Oates [161], displayed in Fig. 6.4, shows the plot of phase boundary composition using r, denoting the ratio of the hydrogen concentration to the Pd concentration; the temperatures are normalized with respect to the critical temperature. Figure 7 of Wicke and Blaurock [87], displayed in Fig. 6.5, shows a similar trend. These

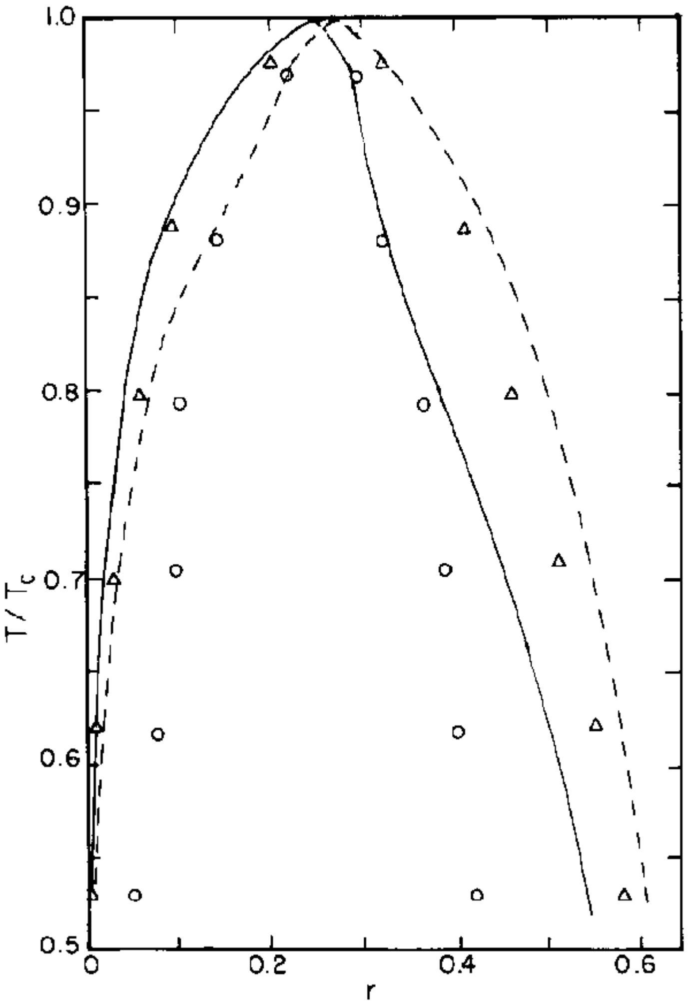

Figure 6.4: Phase boundary compositions for the Pd-H system: dashed plot corresponds to hydride formation, solid lines represent hydride decomposition [161]. Reprinted from “The effect of hysteresis on the phase diagram of Pd-H," by T. B. Flanagan and W. A. Oates, 1983, Journal of the Less-Common Metals, 92, p. 137. 2022 by "Surabhi Joshi". Reprinted with permission.

publications attributed the observed offset to hysteresis, however, its origin was extensively discussed and debated.

Finally, several experiments have reported that hysteresis in hydrogen absorbing alloys is reproducible over thousands of cycles [79, 163, 164].

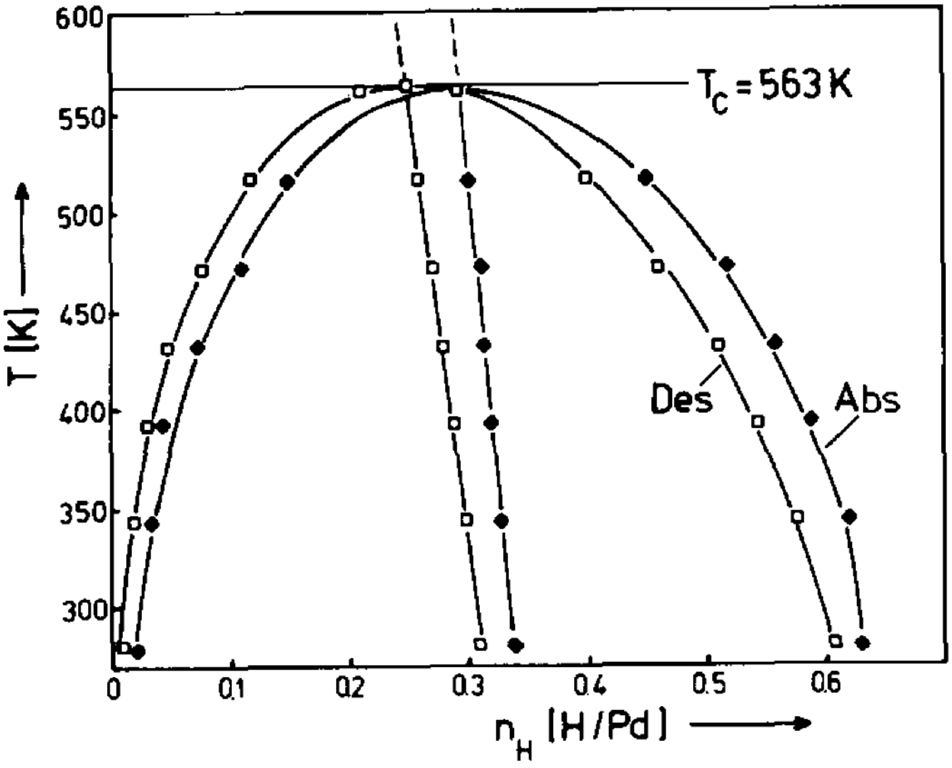

Figure 6.5: Phase boundary compositions for Pd-H showing the absorption and desorption behavior of palladium hydride [87]. Reprinted from "New experiments on and interpretations of hysteresis effects of Pd-D2 and Pd-H2," by E. Wicke, J. Blaurock, 1987, Journal of the Less Common Metals, 130, p. 360. 2022 by "Surabhi Joshi". Reprinted with permission.

The existence of the two-phase field was not questioned in these studies; this is where these experiments differ from the stability analysis of the open system in *Section 6.4.1.* However, it is noted that the analyses and solubility curves in this chapter correspond to a defect-free particle unlike the experiments cited thus far which use palladium samples in bulk form, i.e. containing several particles, each of which undergoes phase transitions during the processes of absorption and desorption; furthermore some of these particles may be defective, i.e. contain interfaces that are semicoherent and incoherent.

Dionne et al. [71] conducted several in-situ experiments on palladium nanocrystals using the tools of environmental electron microscopy and spectroscopy. These single particle experiments shed light on the phase transition processes with nanometer resolution. Their single-crystalline nanoparticles, which included cubes, did not exhibit phase coexistence in equilibrium, which matches our deductions.

The Schwarz–Khachaturyan (S-K) thermodynamic theory considered open interstitial systems that form coherent interstitial phases, such as coherent hydrides, in the host lattice, which is assumed to be elastically isotropic and its lattice parameters vary linearly with concentration. They employed a strain energy equation based on Eshelby's model [165], which assumes the solute atoms are misfitting elastic spheres that are coherently inserted into a matrix that forms the parent phase. Their model [78] established that isostructural phase transformations in such systems may be characterized by a macroscopic energy barrier that makes two-phase equilibrium impossible in open coherent systems; their graphical considerations entailed curves of free energy and chemical potential vs concentration. In 2020, Schwarz et al. [80] confirmed their theoretical conclusions, namely, the presence of ubiquitous hysteresis under open conditions, and no hysteresis in closed systems. This was possible via atomistic experiments, which enabled the study of the Pd-H system in its single crystalline form without any material defects, as well as the study of closed systems, both of which are challenging to conduct in real experiments.

6.4.4 Thermomechanical equilibrium

It is noted that the elastically-coupled analyses of the driven systems in *Chapters 4* and *5* assumed *stress-free thermochemical equilibrium* as the starting point, which was set up in *Section 3.9.* The systems did not exhibit any initial stress; stresses were generated as the systems were driven away from equilibrium. However, the L-C equilibrium framework does not exclude stresses; such a *thermomechanical* or *thermo-chemo-mechanical* equilibrium state satisfies all the equilibrium conditions: thermal, mechanical, chemical, and interfacial equilibrium, as demonstrated in *Section 2.2 Equilibrium Thermostatics.* For systems with coherent interfaces, the stressed equilibrium is called coherent equilibrium, an active area of theoretical and experimental research, especially at small scales.

6.5. Summary

> “When we are not sure, we are alive.”
>
> Graham Greene

When elastic stresses in two-phase binary solids extend (or reduce) the range of solubility of both phases, it is concluded undoubtedly that the stresses have a stabilizing (destabilizing) effect on the solution thermodynamics. For example, an overall stabilizing effect of stresses in this study would correspond to the coherent $\alpha/\alpha{+}\beta$ phase boundary shifting to the right of the corresponding SF boundary, and $\alpha{+}\beta/\beta$ phase boundary displacing to the left of the SF boundary. This situation is familiar to many models in this literature [122,132,148,160].

However, in this chapter, the nature of the shifts, which are implied by Eq. (6.15), differ from the above scenario. Subsequently, at first glance, we cannot be sure of the stability of the thermomechanical equilibrium.

To gain an understanding of the stress-induced effects on phase equilibria, a graphical approach was undertaken to explore the (a) relative stability of the two phases, (b) absorption and desorption behavior of the B-atoms under open conditions at a given operating temperature, and (c) the absorption and desorption behavior of the closed system.

These thought experiments reveal several pertinent aspects; in particular, the stress-induced absorption-desorption offset is identified as the source of thermodynamic hysteresis, which forms a fundamental limit to cyclic operations because of its rate-independent nature. Furthermore, the graphical analyses compare qualitatively to the Pd-H system, which was illustrated for the first time.

Nevertheless, to study this system quantitatively, several foundational assumptions must be revisited and revised, requiring a new framework thermodynamically, and mechanically. For example, in the presence of elastic strains, the total energy of the system is no longer additive because the strain energy term varies nonlinearly with the volume fractions of the coexisting phases. Ergodicity is not applicable either because the state of the system depends on the history; indeed, this lack of ergodicity lends the hysteresis its rate-independent character [80]. Consequently, the key assumptions in classical thermodynamics of phase transitions, additivity and ergodicity, are violated. Physically, this is because of the presence of long-range or nonlocal interactions, which is a consequence of the elastic stresses, as seen in Eq. (6.1), which represents the average stress experienced by the thin film or β-phase; the thin-film stress depends on the material parameter, Ω, and concentration of the α-phase. In the absence of such nonlocal effects, the equations for mechanical equilibrium can be decoupled from equations for chemical equilibrium, and a quantitative approach can be undertaken, for example, in [130], Johnson and Voorhees analyzed a spherical system, assuming a substitutional binary two-phase system. Likewise, in [132], Johnson and Chiang consider a two-phase thin-film system on a rigid substrate, modeled by imposing a set of displacement boundary conditions along the film's edge; subsequently, the free energy of a phase does not depend on the presence of the second phase.

In this chapter, we were able to speculate on the system behavior by assuming $\Omega^{\alpha} = 0$, and the stressed state is close to a stress-free state, which is assumed to exist. The latter assumption enabled linearization of the conditions for chemical and phase equilibria, and the concentration field in the presence of stress was derived. A coherent phase diagram was presented where the new growing phase is stabilized by the stress, and formed the basis for the subsequent graphical analyses.

Subsequently, it was concluded that the key consequence of elastic coupling in isostructural phase transformations is the appearance of hysteresis in coherent open systems, which appears to be an inherent characteristic, leading to entropy production. This kind of fundamental mechanism of energy dissipation is redolent of thermoelastic damping (TED), a mechanism of material damping which occurs ubiquitously in resonators due to the coupling of temperature and strain in a solid via the thermal expansion coefficient [166].

This reproducible thermodynamic hysteresis that continues to persist with vanishing kinetics is observed experimentally in several phase transforming systems including metal hydrides and lithium-ion batteries. In electrochemical systems, the subsequent residual voltage is called a zero-current offset [20, 71, 74–76]; this zero-current hysteresis is predicted even for a single particle [83]. Similarly, the lack of phase coexistence shown in this chapter is also observed in nanostructured Li-insertion compounds that undergo volume expansion when lithium-ions are inserted, such as TiO_2 and $FePO_4$ [167].

Chapter 7

Transient diffusion analysis of a viscoelastic thin-film bilayer

This chapter considers unsteady diffusion in both phases of the thin-film bilayer, and viscoelastic deformation in the thin film. It is assumed that both phases undergo small deviations from equilibrium, and the phase boundary is stationary and does not move.

The transient diffusion problem entails solving the concentration deviations from equilibrium, which are given by $\delta C(z,t)$.

7.1. Boundary conditions

Two flux conditions are specified. The first condition prescribes the flux of B-atoms at $z = 0$:

$$\begin{aligned} J\bigg|_{z=0} &= J^*, \\ \frac{\partial \delta C^\beta}{\partial z}\bigg|_{z=0} &= -\frac{J^*}{M^\beta C^\beta_{eq} \kappa^\beta}. \end{aligned} \tag{7.1}$$

The second outer boundary, $z = z_o$, is impermeable, i.e., the flux is 0:

$$\begin{aligned} J\bigg|_{z=z_o} &= 0, \\ \frac{\partial \delta C^\alpha}{\partial z}\bigg|_{z=z_o} &= 0. \end{aligned} \tag{7.2}$$

Equations (3.5)a, (3.28), and (3.31) were used to simplify the flux boundary conditions.

7.2. Interface model

The first interface condition is given by

$$[\![J]\!] = 0, \tag{7.3}$$

which is a continuity equation at the interface in the absence of any sources and sinks.

The interface experiences diffusion of B-atoms on both sides, both from and to each phase. Subsequently, the interface is no longer in chemical equilibrium. This interfacial description requires a model for the interface that accounts for the diffusion in the presence of different equilibrium concentrations of the two phases. Subsequently, the second interface condition is given by

$$-J_I = V_0(C_I^\alpha - \frac{C_{eq}^\alpha}{C_{eq}^\beta} C_I^\beta), \tag{7.4}$$

which relates the interfacial concentrations to the local flux; this general description is derived in *Appendix C.2.* based on the first-order kinetic model of the interface.

7.3. Diffusion analysis

The goal of the transient diffusion analysis is to derive the concentration field in the planar system for small deviations from equilibrium, where Eq. (3.5) describes the unsteady diffusion in the bilayer, which is taking place in the presence of a sharp phase interface.

Using Eqs. (3.5), (3.28), and (3.31) for the β-phase, the diffusion equation simplifies to

$$\begin{aligned} \frac{\partial \delta C^\beta(z,t)}{\partial t} &= M^\beta (C_{eq}^\beta + \delta C^\beta) \kappa^\beta \frac{\partial \delta C^\beta(z,t)}{\partial z}, \\ &= D'^\beta \frac{\partial^2 \delta C^\beta(z,t)}{\partial z^2}, \end{aligned} \tag{7.5}$$

where $D'^{\beta} \equiv M^{\beta} C^{\beta}_{eq} \kappa^{\beta}$. Similarly, for the α-phase, the diffusion equation is given by

$$\frac{\partial \delta C^{\alpha}(z,t)}{\partial t} = D'^{\alpha} \frac{\partial^2 \delta C^{\alpha}(z,t)}{\partial z^2}, \tag{7.6}$$

where $D'^{\alpha} \equiv M^{\alpha} C^{\alpha}_{eq} \kappa^{\alpha}$.

7.3.1 Extended separation of variables method

The transient diffusion problem for the composite system consists of the partial differential equations (PDEs) (7.5) and (7.6) with two interface conditions and two boundary conditions. Initially, the phases are in equilibrium.

To solve the concentration field in a composite system subjected to two flux boundary conditions, the method of variable transformation is applied. This method splits the solution into three components to account for the nonhomogeneous boundary conditions, homogeneous boundary conditions, and the initial conditions. Subsequently, for each phase, the following variable transformations are used [168]:

$$\delta C(z,t) = v(t) + w(z) + u(z,t), \tag{7.7}$$

where $u(z,t)$ satisfies the homogeneous boundary conditions, and is given by

$$u(z,t) = Z(z)T(t). \tag{7.8}$$

Substituting Eq. (7.7) into the diffusion equation, we obtain

$$\frac{\partial u}{\partial t} + \frac{dv}{dt} = D'\Big(\frac{d^2 w}{dz^2} + \frac{\partial^2 u}{\partial z^2}\Big). \tag{7.9}$$

As $u(z,t)$ satisfies the homogeneous boundary conditions and PDE, the corresponding PDE is given by

$$\frac{\partial u}{\partial t} = D' \frac{\partial^2 u}{\partial z^2}. \tag{7.10}$$

Thus, from Eqs. (7.9) and (7.10), we obtain

$$\frac{1}{D'}\frac{dv}{dt} = \frac{d^2w}{dz^2}, \tag{7.11}$$

where the LHS is a function of time and the RHS is a function of z, therefore, the above equation must be equal to a constant; here, we set it equal to w_1:

$$\begin{aligned} \frac{dv}{dt} &= w_1, \\ D'\frac{d^2w}{dz^2} &= w_1. \end{aligned} \tag{7.12}$$

By integrating the above equations, we obtain the following expressions for $v(t)$ and $w(z)$:

$$\begin{aligned} v(t) &= w_1 D' t + v_1, \\ w(z) &= w_1 \frac{z^2}{2} + w_2 z + w_3, \end{aligned} \tag{7.13}$$

where w_1, w_2, and v_1 are unknown constants to be determined. As $v(t)$ satisfies the initial condition, i.e. $v(t = 0) = 0$, we obtain $v_1 = 0$.

To derive $u(z, t)$, we substitute Eq. (7.8) into Eq. (7.10). Separating the variables leads to

$$\frac{d^2Z}{dz^2} = \frac{1}{D'}\frac{dT}{dt} = -\lambda^2, \tag{7.14}$$

where the LHS is a function of z, and the RHS is a function of time, hence, the equation must be equal to a constant; furthermore, this constant must be negative because the concentration cannot increase exponentially with time in the absence of a source term in the PDE, Eq. (7.10). Thus, from Eq. (7.14), we obtain two ODEs, which can be solved to obtain the two components of $u(z, t)$:

$$\begin{aligned} Z(z) &= A\cos(\lambda z) + B\sin(\lambda z), \\ T(t) &= Ce^{-D'\lambda^2 t}, \end{aligned} \tag{7.15}$$

where λ, A, B, and C are unknown constants.

The subsequent sections apply Eqs. (7.7), (7.8), (7.13), and (7.15) to the thin film and substrate with the corresponding boundary conditions, interface conditions, and initial conditions.

7.3.2 Thin film

The deviation in the concentration of the B-atoms in the thin film is given by

$$\delta C^{\beta}(z,t) = v^{\beta}(t) + w^{\beta}(z) + u^{\beta}(z,t), \tag{7.16}$$

where

$$\begin{aligned} v^{\beta}(t) &= w_1^{\beta} D'^{\beta} t, \\ w^{\beta}(z) &= w_1^{\beta} \frac{z^2}{2} + w_2^{\beta} z + w_3^{\beta}, \\ u^{\beta}(z,t) &= Z^{\beta}(z) T^{\beta}(t) = C^{\beta} e^{-D'^{\beta}(\lambda^{\beta})^2 t}(A^{\beta}\cos(\lambda^{\beta} z) + B^{\beta}\sin(\lambda^{\beta} z)). \end{aligned} \tag{7.17}$$

Applying the nonhomogeneous flux boundary condition at $z = 0$, Eq. (7.1), which is accounted for by $w^{\beta}(z)$, given by Eq. (7.17)b, we obtain

$$w_2^{\beta} = -\zeta C_{eq}^{\beta}. \tag{7.18}$$

It is noted that $Z^{\beta}(z)$, which is part of $u^{\beta}(z,t)$, the homogeneous flux boundary condition, i.e. Eq. (7.1) with RHS equal to 0, corresponds to $\left.\frac{\partial u^{\beta}}{\partial z}\right|_{z=0} = 0$; this equation is used with Eq. (7.17)c to obtain

$$Z^{\beta}(z) = A^{\beta}\cos(\lambda^{\beta} z). \tag{7.19}$$

Thus, $u^{\beta}(z,t)$ simplifies to

$$u^{\beta}(z,t) = F^{\beta} e^{-D'^{\beta}(\lambda^{\beta})^2 t}\cos(\lambda^{\beta} z), \tag{7.20}$$

where $F^\beta \equiv A^\beta C^\beta$.

7.3.3 Substrate

Applying the same procedure to the substrate, we obtain

$$\delta C^\alpha(z,t) = v^\alpha(t) + w^\alpha(z) + u^\alpha(z,t), \tag{7.21}$$

where

$$\begin{aligned} v^\alpha(t) &= w_1^\alpha D'^\alpha t, \\ w^\alpha(z) &= w_1^\alpha \frac{z^2}{2} + w_2^\alpha z + w_3^\alpha, \\ u^\alpha(z,t) &= Z^\alpha(z)T^\alpha(t) = C^\alpha e^{-D'^\alpha(\lambda^\alpha)^2 t}(A^\alpha \cos(\lambda^\alpha z) + B^\alpha \sin(\lambda^\alpha z)). \end{aligned} \tag{7.22}$$

Applying the boundary condition, Eq. (7.2), we obtain

$$\begin{aligned} w_2^\alpha &= -w_1^\alpha z_o, \\ Z^\alpha(z) &= A'^\alpha \cos(\lambda^\alpha(z - z_o)), \end{aligned} \tag{7.23}$$

where $A'^\alpha = \dfrac{A^\alpha}{\cos(\lambda^\alpha(z_o)}$. Thus, $u^\alpha(z,t)$ simplifies to

$$u^\alpha = F^\alpha e^{-D'^\alpha(\lambda^\alpha)^2 t} \cos(\lambda^\alpha(z - z_o)), \tag{7.24}$$

where $F^\alpha \equiv A^\alpha C^\alpha$.

7.3.4 Interface conditions

The continuity of flux across the interface is given by Eq. (7.3); simplifying this condition using Eqs. (3.5)a, (3.28), and (3.31), we obtain

$$\frac{\partial \delta C^\alpha}{\partial z}\bigg|_{z_I} = \frac{D'^\beta}{D'^\alpha}\frac{\partial \delta C^\beta}{\partial z}\bigg|_{z_I}, \tag{7.25}$$

which can be further simplified using Eqs. (7.16), (7.17), (7.20)-(7.22), and (7.24) to obtain

$$w_1^\alpha(z_I-z_o)-\lambda^\alpha F^\alpha e^{-(\lambda^\alpha)^2 D'^\alpha t}\sin(\lambda^\alpha(z-z_o)) = \Big(\frac{D'^\beta}{D'^\alpha}\Big)\Big(w_1^\beta z_I-\zeta C_{eq}^\beta-\lambda^\beta F^\beta e^{-(\lambda^\beta)^2 D'^\beta t}\sin(\lambda^\beta z_I)\Big). \tag{7.26}$$

For the above equality to hold for arbitrary time, the following conditions must hold:

$$-\lambda^\alpha F^\alpha e^{-(\lambda^\alpha)^2 D'^\alpha t}\sin(\lambda^\alpha(z-z_o)) = \Big(\frac{D'^\beta}{D'^\alpha}\Big)F^\beta e^{-(\lambda^\beta)^2 D'^\beta t}\sin(\lambda^\beta z_I), \tag{7.27}$$

and,

$$\begin{aligned} e^{-(\lambda^\alpha)^2 D'^\alpha t} &= e^{-(\lambda^\beta)^2 D'^\beta t}, \\ (\lambda^\alpha)^2 D'^\alpha &= (\lambda^\beta)^2 D'^\beta, \\ \frac{\lambda^\alpha}{\lambda^\beta} &= \sqrt{\frac{D'^\beta}{D'^\alpha}}. \end{aligned} \tag{7.28}$$

Equation (7.28) can be used to simplify Eq. (7.27):

$$-\lambda^\alpha F^\alpha \sin(\lambda^\alpha(z-z_o)) = -\lambda^\beta \frac{D'^\beta}{D'^\alpha}F^\beta \sin(\lambda^\beta z_I). \tag{7.29}$$

Subsequently, Eq. (7.26) simplifies to[13]

$$\begin{aligned} w_1^\alpha(z_I-z_o) &= \frac{D'^\beta}{D'^\alpha}\Big(w_1^\beta z_I-\zeta C_{eq}^\beta\Big), \\ w_1^\alpha &= \frac{\frac{D'^\beta}{D'^\alpha}}{(z_I-z_o)}\Big(w_1^\beta z_I-\zeta C_{eq}^\beta\Big). \end{aligned} \tag{7.30}$$

---

[13] $\zeta C_{eq}^\beta = \frac{J^*}{D'^\beta}$

The second interface condition, Eq. (7.4), is similarly simplified using Eqs. (3.5)a, (3.28), and (3.31) to obtain

$$\begin{aligned}\frac{\partial(\delta C^\alpha)}{\partial z}\Big|_{z_I} &= \frac{V_0}{D'^\alpha}\Big(\delta C_I^\alpha - (\frac{C_{eq}^\alpha}{C_{eq}^\beta})\delta C_I^\beta\Big),\\ \frac{dw^\alpha}{dz}\Big|_{z_I} + T^\alpha(t)\frac{dZ^\alpha}{dz}\Big|_{z_I} &= \frac{V_0}{D'^\alpha}\Big(w^\alpha(z_I) - \Big(\frac{C_{eq}^\alpha}{C_{eq}^\beta}\Big)w^\beta(z_I) + Z^\alpha(z)T^\alpha(t)\\ &\quad - \Big(\frac{C_{eq}^\alpha}{C_{eq}^\beta}\Big)Z^\beta(z)T^\beta(t) + v^\alpha(t) - \Big(\frac{C_{eq}^\alpha}{C_{eq}^\beta}\Big)v^\beta(t)\Big),\end{aligned} \tag{7.31}$$

where Eqs. (7.16), (7.17), (7.20)-(7.22), and (7.24) were used to expand the concentration terms. For the above equality to hold for arbitrary time, the following condition must hold:

$$T^\alpha(t)\frac{dZ^\alpha}{dz}\Big|_{z_I} = \frac{V_0}{D'^\alpha}\Big(Z^\alpha(z)T^\alpha(t) - \Big(\frac{C_{eq}^\alpha}{C_{eq}^\beta}\Big)Z^\beta(z)T^\beta(t) + v^\alpha(t) - \Big(\frac{C_{eq}^\alpha}{C_{eq}^\beta}\Big)v^\beta(t)\Big). \tag{7.32}$$

Dividing by $T^\alpha(t)$, we obtain

$$\frac{dZ^\alpha}{dz}\Big|_{z_I} = \frac{V_0}{D'^\alpha}\Big(Z^\alpha(z) - \Big(\frac{C_{eq}^\alpha}{C_{eq}^\beta}\Big)Z^\beta(z)\frac{C^\beta}{C^\alpha} + \frac{v^\alpha(t)}{T^\alpha(t)} - \Big(\frac{C_{eq}^\alpha}{C_{eq}^\beta}\Big)\frac{v^\beta(t)}{T^\alpha(t)}\Big). \tag{7.33}$$

For the above equality to hold for arbitrary time, the following conditions must hold:

$$\begin{aligned}\frac{dZ^\alpha}{dz}\Big|_{z_I} &= \frac{V_0}{D'^\alpha}\Big(Z^\alpha(z) - \Big(\frac{C_{eq}^\alpha}{C_{eq}^\beta}\Big)Z^\beta(z)\frac{C^\beta}{C^\alpha}\Big),\\ \frac{V_0}{D'^\alpha}\Big(\frac{v^\alpha(t)}{T^\alpha(t)} &- \Big(\frac{C_{eq}^\alpha}{C_{eq}^\beta}\Big)\frac{v^\beta(t)}{T^\alpha(t)}\Big) = 0.\end{aligned} \tag{7.34}$$

Using Eqs. (7.31) and (7.34)a, we obtain

$$\frac{dw^\alpha}{dz}\Big|_{z_I} = \frac{V_0}{D'^\alpha}\Big(w^\alpha(z_I) - \Big(\frac{C_{eq}^\alpha}{C_{eq}^\beta}\Big)w^\beta(z_I)\Big). \tag{7.35}$$

Using Eqs. (7.17) and (7.22) in (7.35), we obtain

$$w_3^\beta = \frac{C_{eq}^\beta}{C_{eq}^\alpha}\Big[w_1^\alpha\frac{z_I^2}{2} + w_2^\alpha z_I + w_3^\alpha - \frac{D'^\alpha}{V_0}(w_1^\alpha z_I + w_2^\alpha)\Big]. \tag{7.36}$$

Equation (7.34)b simplifies to

$$v^{\alpha}(t) - \Big(\frac{C^{\alpha}_{eq}}{C^{\beta}_{eq}}\Big)v^{\beta}(t) = 0, \tag{7.37}$$

which can be expressed in terms of two unknown constants, w^{α}_1 and w^{β}_1 using Eqs. (7.17)a and (7.22)a; subsequently, we obtain

$$w^{\alpha}_1 = \Big(\frac{C^{\alpha}_{eq}}{C^{\beta}_{eq}}\Big)\Big(\frac{D'^{\beta}}{D'^{\alpha}}\Big)w^{\beta}_1. \tag{7.38}$$

Equations (7.30) and (7.38) generate a solution for w^{β}_1:

$$w^{\beta}_1 = \frac{\zeta C^{\beta}_{eq}}{\Big(z_I\big(1 - \frac{C^{\alpha}_{eq}}{C^{\beta}_{eq}}\big) + \frac{C^{\alpha}_{eq}}{C^{\beta}_{eq}}z_o\Big)}. \tag{7.39}$$

Equation (7.34)a is expanded using Eqs. (7.19) and (7.23):

$$F^{\alpha} = F^{\beta}\Big(\frac{V_0}{D'^{\alpha}}\Big)\Big(\frac{C^{\alpha}_{eq}}{C^{\beta}_{eq}}\Big)\frac{\cos(\lambda z_I)}{\Big\{\frac{V_0}{D'^{\alpha}}\cos(\lambda^{\alpha}(z - z_I)) + \lambda^{\alpha}\sin(\lambda^{\alpha}(z - z_I))\Big\}}. \tag{7.40}$$

Using Eqs. (7.29) and (7.40), we obtain a transcendental equation for the eigenvalues:

$$\begin{gathered}
\frac{\tan(\lambda^{\beta}z_I)(V_0 + \lambda^{\alpha}D'^{\alpha}\tan(\lambda^{\alpha}(z_I - z_o)))}{\tan(\lambda^{\alpha}(z_I - z_o))} = V_0\frac{C^{\alpha}_{eq}}{C^{\beta}_{eq}}\sqrt{\frac{D'^{\alpha}}{D'^{\beta}}},\\
\frac{\tan(\lambda^{\beta}z_I)(V_0 + \lambda^{\beta}\sqrt{D'^{\alpha}D'^{\beta}}\tan(\lambda^{\beta}\sqrt{\frac{D'^{\beta}}{D'^{\alpha}}}(z_I - z_o)))}{\tan(\lambda^{\beta}\sqrt{\frac{D'^{\beta}}{D'^{\alpha}}}(z_I - z_o))} = V_0\frac{C^{\alpha}_{eq}}{C^{\beta}_{eq}}\sqrt{\frac{D'^{\alpha}}{D'^{\beta}}},
\end{gathered} \tag{7.41}$$

where Eq. (7.28)c was used to express the equation in terms of λ^{β} only. This equation has multiple solutions for λ^{β}, and subsequently, λ^{α}; thus, by principle of superposition, $u^{\alpha}(z,t)$ and $u^{\beta}(z,t)$ are series solutions given by $\sum_{n=1}^{\infty} Z^{\alpha}T^{\alpha}$, and $\sum_{n=1}^{\infty} Z^{\beta}T^{\beta}$ respectively.

To summarize, the concentration deviations are given by

$$\begin{aligned}\delta C^{\alpha}(z,t) &= w_1^{\alpha}\frac{z^2}{2} + w_2^{\alpha}z + w_3^{\alpha} + w_1^{\alpha}D'^{\alpha}t + \sum_{n=1}^{\infty} F_n\lambda^{\beta}\sin(\lambda^{\beta}z_I)\cos(\lambda^{\alpha}(z-z_o))e^{-D'^{\alpha}(\lambda^{\alpha})^2t},\\ \delta C^{\beta}(z,t) &= w_1^{\beta}\frac{z^2}{2} + w_2^{\beta}z + w_3^{\beta} + w_1^{\beta}D'^{\beta}t + \sum_{n=1}^{\infty} F_n\lambda^{\alpha}\frac{D'^{\alpha}}{D'^{\beta}}\sin(\lambda^{\alpha}(z-z_o))\cos(\lambda^{\beta}z)e^{-D'^{\beta}(\lambda^{\beta})^2t},\end{aligned} \tag{7.42}$$

where $F_n = \dfrac{F^{\alpha}}{\lambda^{\beta}\sin(\lambda^{\beta}z_I)} = \dfrac{F^{\beta}}{\lambda^{\alpha}\sin(\lambda^{\alpha}(z_I-z_o)\frac{D'^{\alpha}}{D'^{\beta}}}$ using Eq. (7.29). The eigenvalues are given by the transcendental equation; w_1^{α}, w_2^{α}, w_1^{β}, w_2^{β} are known from Eqs. (7.38), (7.39), (7.23)c, and (7.18); w_3^{β} is given by Eq. (7.36) and depends on w_3^{α}.

Thus, there are two outstanding constants in Eq. (7.42): w_3^{α} and F_n; these will be determined using initial conditions.

7.3.5 Initial conditions

The initial conditions are given by

$$\begin{aligned}\delta C^{\alpha}(z,0) &= 0,\\ \delta C^{\beta}(z,0) &= 0.\end{aligned} \tag{7.43}$$

The initial condition can be applied in the integral form:

$$\int_0^{z_I} \delta C^{\beta}(z,0)dz + \int_{z_I}^{z_o} \delta C^{\alpha}(z,0)dz = 0, \tag{7.44}$$

which is expanded using Eq. (7.42), leading to

$$\int_0^{z_I} w^{\beta}(z)dz + \int_{z_I}^{z_o} w^{\alpha}(z)dz + \sum_{n=1}^{\infty} F_n\Big(\int_0^{z_I} f^{\beta}(z)dz + \int_{z_I}^{z_o} f^{\alpha}(z)dz\Big) = 0, \tag{7.45}$$

where $f^{\alpha}(z)$ and $f^{\beta}(z)$ are eigenfunctions in the series expansion, and are given by

$$\begin{aligned}f^{\alpha}(z) &= \lambda^{\beta}\sin(\lambda^{\beta}z_I)\cos(\lambda^{\alpha}(z-z_o)),\\ f^{\beta}(z) &= \lambda^{\alpha}\frac{D'^{\alpha}}{D'^{\beta}}\sin(\lambda^{\alpha}(z-z_o))\cos(\lambda^{\beta}z).\end{aligned} \tag{7.46}$$

Simplifying the integrals of Eq. (7.45) , we obtain w_3^α:

$$w_3^\alpha = -w_1^\alpha \frac{1}{(z_o - z_I)} \Big[\frac{z_I^3}{6} + \Big(\frac{1}{\zeta} \Big(\frac{C_{eq}^\alpha}{C_{eq}^\beta} \Big) (z_I - z_o) - \frac{z_I}{\zeta} \Big) z_I + \Big(\frac{C_{eq}^\alpha}{C_{eq}^\beta} \Big) \Big(\frac{D'^\beta}{D'^\alpha} \Big) \Big(\frac{z_o^3 - z_I^3}{6} - z_o \frac{(z_o^2 - z_I^2)}{2} \Big) \Big]. \tag{7.47}$$

To solve for the coefficient of the series, F_n, we use the following equation:

$$F_n = -\frac{\int_{z_I}^{z_o} w^\alpha(z) f_n^\alpha(z) dz + \hat{C} \int_0^{z_I} w^\beta(z) f_n^\beta(z) dz}{\int_{z_I}^{z_o} w^\alpha(z) (f_n^\alpha(z))^2 dz + \hat{C} \int_0^{z_I} w^\beta(z) (f_n^\beta(z))^2 dz}, \tag{7.48}$$

where $\hat{C} \equiv \dfrac{C_{eq}^\alpha}{C_{eq}^\beta}$ is a *discontinuous-weighting function* for our composite system, which makes the eigenfunctions orthogonal [169]. The derivations of this weighting function and Eq. (7.48) are provided in *Appendix H.* Applying Eq. (7.48) leads to the series coefficient for the bilayer:

$$F_n = -\frac{2\zeta C_{eq}^\alpha}{\hat{D}\lambda^\beta} \frac{\sin(\lambda^\beta z_I) \sin(\lambda^\alpha (z_I - z_o)) \Big[\dfrac{\lambda^\beta z_I^2}{2(z_I(1-\hat{C}) + \hat{C} z_o)} - \lambda^\beta z_I + 1 \Big]}{\Big[\sin^2(\lambda^\beta z_I)(z_o - z_I - \dfrac{\sin(2\lambda^\alpha (z_I - z_o))}{2\lambda^\alpha}) + \frac{\hat{C}}{\hat{D}^2} \sin^2(\lambda^\alpha (z_I - z_o))(z_I + \frac{\sin(2\lambda^\beta z_I)}{2\lambda^\beta}) \Big]}. \tag{7.49}$$

This completes the semi-analytical solution to the transient diffusion problem.

7.4. Viscoelastically-coupled analysis

This section considers viscoelastic deformation in the thin film. However, incorporating viscoelasticity, and thereby, new mechanics and material response compared to our analyses so far, requires a visit to the foundations of continuum mechanics and the underlying principles used to build the constitutive theories of elasticity and fluid mechanics.

7.4.1 Foundations of constitutive equations

The response of a material to an imposed loading (mechanical, chemical, or thermal) is described mathematically by constitutive equations or response functions.

For linear isotropic elasticity, the constitutive equation is given by Hooke's law: $\boldsymbol{\sigma} = \lambda \mathrm{tr}\boldsymbol{\epsilon}\boldsymbol{I} + 2\mu\boldsymbol{\epsilon}$, where λ and μ are the Lamé elastic moduli and are related to material parameters. Linear viscous fluids are described using Newton's viscous constitutive law, which is given by $\sigma = \eta \frac{d\epsilon}{dt}$, where η denotes the coefficient of viscosity.[14]

These constitutive functions are restricted by several physical principles, which include the principles of determinism, local action, and material frame-indifference. The principle of determinism states that past events determine the present. According to the principle of local action, the response of the material at a point is influenced by what's occurring in a small region about that point. The principle of material frame-indifference or objectivity imposes that all physical variables requiring constitutive relations remain the same in all reference frames; such entities are called objective tensors. Finally, a constitutive relation must obey the second law of thermodynamics [170].

7.4.2 Viscoelastic mechanics and material model

Viscoelastic or rheological materials exhibit both elastic and viscous-like characteristics, and the relationship between stress and strain depends on time.[15] To model the viscoelastic material response, memory effects must also be incorporated.

In this thesis, it is assumed that the β-phase exhibits linear viscoelastic behavior at the operating temperature, and can be described by Maxwell's rheological model. This selected material model consists of a spring (Hookean element) and dashpot (viscous or Newton element) in series as shown in Fig. 7.1; the corresponding 1D constitutive equation is given

---

[14] On notation: η was used as an index in the previous chapters; here it is used for the coefficient of viscosity.

[15] In the elastic solutions, time does not appear explicitly (only via the interface position); stresses depend on the instantaneous value of the interface position.

by

$$\tau\dot{\sigma} + \sigma = \eta\dot{\epsilon}, \tag{7.50}$$

where the time constant of the model is given by $\tau = \frac{\eta}{E}$ and represents the relaxation time, and ϵ is the total mechanical strain, which is equal to the sum of the elastic and viscous strains [171].

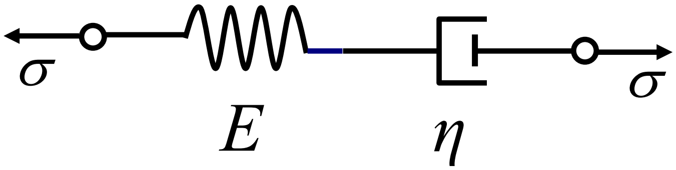

Figure 7.1: Schematic of the Maxwell model of viscoelasticity comprising a spring (or a Hookean element) in series with a dashpot (or a Newtonian viscous element). The model exhibits a relaxation time. There are no inertial effects.

7.4.3 Correspondence principle

The general partial differential equation describing the stress-strain behavior in a viscoelastic material is position- and time-dependent. Instead of solving this formidable equation directly, Laplace transform can be applied to the field equations and boundary conditions to derive the viscoelastic stresses.

The correspondence principle compares the Laplace transformed field equations of viscoelasticity to the corresponding elastic field equations; because these equations exhibit the same form, the solution to the elastic problem that is compatible with the transformed boundary conditions can be used to solve the original problem by transform inversion. This method of applying the correspondence between the elastic and viscoelastic equations to solve viscoelastic stress analysis problems is well-established and also known as the *elastic-*

viscoelastic analogy [172]. In its classical form, the elastic-viscoelastic analogy only holds for time-independent or stationary boundary conditions [171, 173].

Before applying the analogy, two key steps are typically undertaken: the stress-strain-time constitutive equation for viscoelastic materials is extended to three dimensions, and the stress and strain tensors are decomposed into their dilatational (or mean) and deviatoric contributions respectively. This decomposition is typically undertaken because most materials behave elastically under hydrostatic conditions. Subsequently, only the deviatoric parts are affected by the presence of viscoelasticity; in the presence of volumetric strain, the pertinent constitutive relation, in its general form, is given by[16] [172]

$$\begin{aligned} P_m s_{ij} &= 2Q_m e_{ij}, \\ P_m\Big(\sigma_{ij} - \frac{\sigma_{kk}}{3}\delta_{ij}\Big) &= 2Q_m\Big(\epsilon_{ij} - \frac{\epsilon_{kk}}{3}\delta_{ij} - C\Omega\delta_{ij}\Big), \end{aligned} \tag{7.51}$$

where s_{ij} and e_{ij} are the deviatoric components of stress and strain respectively, ϵ represents the total strain tensor which consists of the mechanical strain and the diffusion-induced strain, and P_m and Q_m are model-dependent operators given by

$$\begin{aligned} P_m &= \sum_{k=0}^{m} a_k \frac{\partial^k}{\partial t^k}, \\ Q_m &= \sum_{k=0}^{n} b_k \frac{\partial^k}{\partial t^k}, \end{aligned} \tag{7.52}$$

where a_k and b_k are material constants. For the Maxwell model, $P_m = \frac{1}{G}\frac{\partial}{\partial t} + \frac{1}{\eta}$ and $Q_m = \frac{\partial}{\partial t}$, where G is the shear modulus[17] [166].

The Laplace transformed viscoelastic equations of mechanical equilibrium, strain-displacement relation, prescribed traction and/or displacement boundary conditions, and constitutive equations correspond to the elastic equations [172]. Thus, by comparing the

---

[16] The numerical factor 2 is introduced for convenience [172].

[17] For linear isotropic elasticity, $P_m = 1$ and $Q_m = G$.

elastic equation involving the deviatoric components, $\sigma_{ij}^{ed} = 2G\epsilon_{ij}^{ed}$, to the Laplace transform of Eq. (7.51), $P_m(s)\mathcal{L}\{\sigma_{ij}^{d}\} = 2Q_m\mathcal{L}\{\epsilon_{ij}^{d}\}$, it is deduced that replacing the shear modulus of the elastic problem with $\frac{Q_m(s)}{P_m(s)}$ generates the same form as the Laplace transformed viscoelastic equations. For the Maxwell material:

$$G(s) = \frac{Q_m(s)}{P_m(s)} = \frac{s}{\dfrac{s}{G} + \dfrac{1}{\eta}} = \frac{G\eta s}{(G + \eta s)}. \tag{7.53}$$

When the solution to the elastic problem is available, it can be readily used by replacing the shear modulus as described above to obtain the Laplace transformed viscoelastic equation. Inverting this equation then provides the viscoelastic solution. This method is undertaken in *Section 7.4.4* to obtain the viscoelastic stresses in the thin film.

7.4.4 Viscoelastic stress analysis

The viscoelastic stress analysis is undertaken using the classical quasi-static correspondence principle or elastic-viscoelastic analogy.

Using the elastic solution, Eq. (5.61)d, the Laplace transform of the viscoelastic solution is given by

$$\mathcal{L}\{\overline{\sigma}_V^{\beta}(z,t)\} \approx \overline{E}_V^{\beta}\frac{\Omega}{3}\mathcal{L}\{\delta C^{\alpha}(z,t) - \delta C^{\beta}(z,t)\}, \tag{7.54}$$

where the subscript V denotes the viscoelastic entity. $\overline{E}_V^{\beta}$ is the *transformed* biaxial modulus, and its value depends on the choice of the viscoelastic material; for a Maxwell material model, it is given by Eq. (45) [172]:

$$\overline{E}_V = \frac{E_V}{1 - \nu_V} = \frac{18KG\eta s}{(3K(G + \eta s) + 4G\eta s)}, \tag{7.55}$$

where K is the bulk modulus. For isotropic elasticity, the bulk and shear moduli are given by [105]

$$\begin{aligned} K &= \frac{E}{3(1-2\nu)}, \\ G &= \frac{E}{2(1+\nu)}, \end{aligned} \tag{7.56}$$

which can be used to simplify Eq. (7.55):

$$\overline{E}_V = \frac{6\overline{E}\eta s}{(\overline{E}+6\eta s)} = \frac{\overline{E}s}{\left(s+\dfrac{\overline{E}}{6\eta}\right)}. \tag{7.57}$$

Substituting Eq. (7.57) in Eq. (7.54), we obtain

$$\begin{aligned} \mathcal{L}\{\overline{\sigma}_V^\beta(z,t)\} &= \frac{s}{\left(s+\dfrac{\overline{E}^\beta}{6\eta}\right)}\overline{E}^\beta\frac{\Omega}{3}\mathcal{L}\{\delta C^\alpha(z,t)-\delta C^\beta(z,t)\}, \\ \mathcal{L}\{\overline{\sigma}_V^\beta(z,t)\} &= \frac{s}{\left(s+\dfrac{\overline{E}^\beta}{6\eta}\right)}\mathcal{L}\{\overline{\sigma}_E^\beta(z,t)\}, \end{aligned} \tag{7.58}$$

where the Laplace transform of the elastic solution was identified and substituted based on Eq. (5.61); the subscript E denotes this elastic solution. Next, we use Laplace transform operations to simplify, starting with the numerator, which is simplified using the derivative rule; the subsequent expression is given by

$$\mathcal{L}\{\overline{\sigma}_V^\beta(z,t)\} = \frac{1}{\left(s+\dfrac{\overline{E}^\beta}{6\eta}\right)}\left(\mathcal{L}_\pm\left\{\frac{d\overline{\sigma}_E^\beta}{dt}\right\}+\overline{\sigma}_E^\beta(t=0)\right). \tag{7.59}$$

Taking the inverse of the Laplace transform on both sides, we obtain

$$\begin{aligned}\overline{\sigma}_V^\beta(z,t) &= \mathcal{L}^{-1}\Big[\frac{1}{\big(s+\dfrac{\overline{E}^\beta}{6\eta}\big)}\Big(\mathcal{L}_\pm\Big\{\frac{d\overline{\sigma}_E^\beta}{dt}\Big\}+\overline{\sigma}_E^\beta(t=0)\Big)\Big],\\ &= \mathcal{L}^{-1}\Big[\frac{\mathcal{L}_\pm\Big\{\dfrac{d\overline{\sigma}_E^\beta}{dt}\Big\}}{\big(s+\dfrac{\overline{E}^\beta}{6\eta}\big)}\Big]+\overline{\sigma}_E^\beta(t=0)e^{-\frac{\overline{E}^\beta}{6\eta}t},\\ &= \mathcal{L}^{-1}\Big[G(s)F(s)\Big]+\overline{\sigma}_E^\beta(t=0)e^{-\frac{\overline{E}^\beta}{6\eta}t},\end{aligned} \tag{7.60}$$

where $F(s)=\frac{1}{\left(s+\frac{\overline{E}^\beta}{6\eta}\right)}$ and $G(s)=\mathcal{L}_\pm\Big\{\dfrac{d\overline{\sigma}_E^\beta}{dt}\Big\}$. The first term on the right hand side of Eq. (7.60) is simplified using the convolution rule which states that [174]

$$G(s)F(s)=\mathcal{L}(g(t)f(t))=\mathcal{L}((g*f)(t))=\mathcal{L}\{\int_0^t g(x)f(t-x)\}. \tag{7.61}$$

Using Eq. (7.61) in Eq. (7.60), we obtain

$$\overline{\sigma}_V^\beta(z,t)=\int_0^t \frac{d\overline{\sigma}_E^\beta}{du}e^{-\frac{\overline{E}^\beta}{6\eta}(t-u)}du+\overline{\sigma}_E^\beta(t=0)e^{-\frac{\overline{E}^\beta}{6\eta}t}. \tag{7.62}$$

For an initially stress-free system that subsequently experiences diffusion-induced viscoelastic stresses, $\overline{\sigma}_E^\beta(t=0)=0$; thus $\sigma_{xx}^\beta=\sigma_{yy}^\beta=\overline{\sigma}_V^\beta$:

$$\begin{aligned}\overline{\sigma}_V^\beta(z,t) &= \int_0^t \frac{d\overline{\sigma}_E^\beta}{du}e^{-\frac{\overline{E}^\beta}{6\eta}(t-u)}du,\\ &= \overline{\sigma}_E^\beta-\frac{\overline{E}^\beta}{6\eta}\int_0^t \overline{\sigma}_E^\beta(z,u)e^{-\frac{\overline{E}^\beta}{6\eta}(t-u)}du.\end{aligned} \tag{7.63}$$

Equation (7.63) represents the viscoelastic (Maxwell) stress distribution in a thin film of thickness z_I at a given time t.

7.4.5 Mass transport in the viscoelastic layer

Sections 7.3 and *7.4.4* describe the viscoelasically-coupled transient diffusion in the thin-film bilayer.

Assuming one-way coupling between diffusion and deformation, the viscoelastic stresses in the thin film, induced by diffusion of B-entities, do not influence diffusion. Thus, the modified Fick's equation for diffusion, Eq. (3.5), is still applicable. Subsequently, the results of *Section 7.3* provide the solution to the concentration field. Figure 7.2 illustrates these solutions, Eq. (7.42), by showing the results for the concentration deviation in the two phases. For further clarification, Fig. 7.3 shows the effects of $\hat{C}$. The semi-analytical solutions were evaluated in MATLAB®.

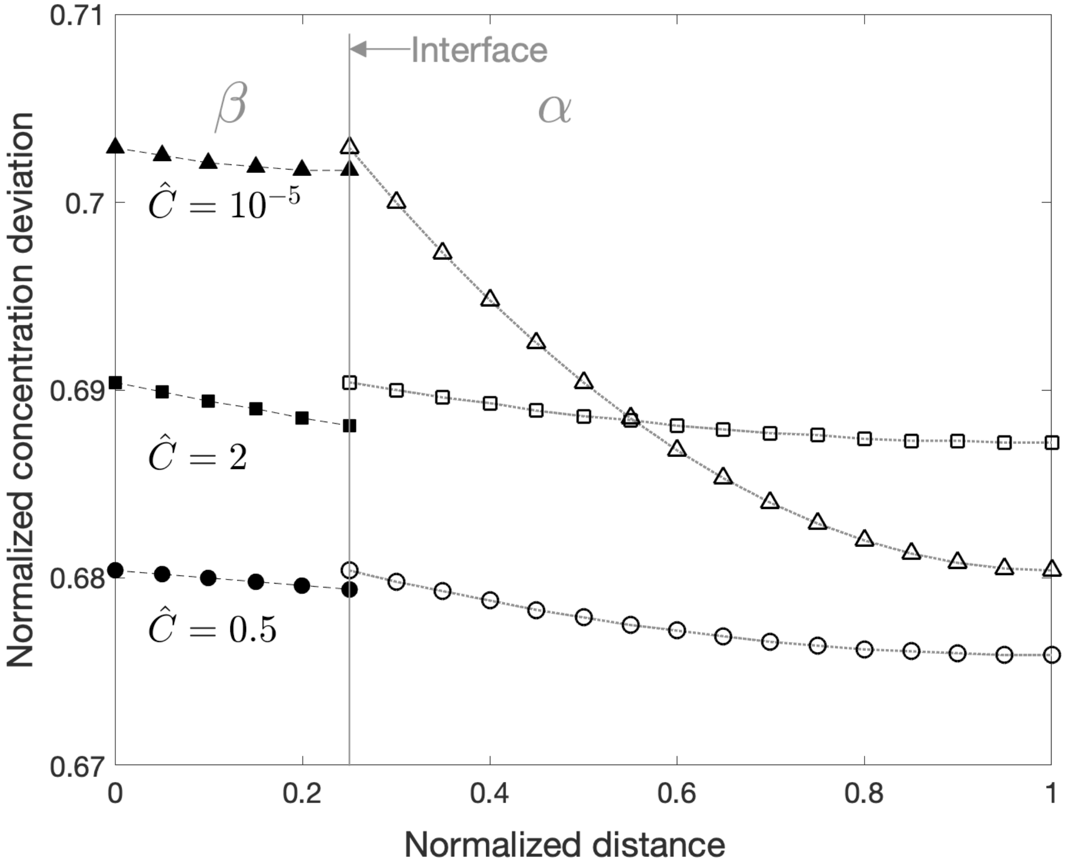

Figure 7.2: Normalized concentration deviations, $\delta C/C_{eq}$, in the two phases at time 2.7 s in the presence of a general interface, located at $z_I/z_o = 0.25$. The prescribed flux is 0.01 mol/m^{2}s, V_0 is 500 m/s, and the diffusivity ratio, $D'^{\beta}/D'^{\alpha} = 2$. This figure shows three cases corresponding to different ratios of equilibrium concentrations.

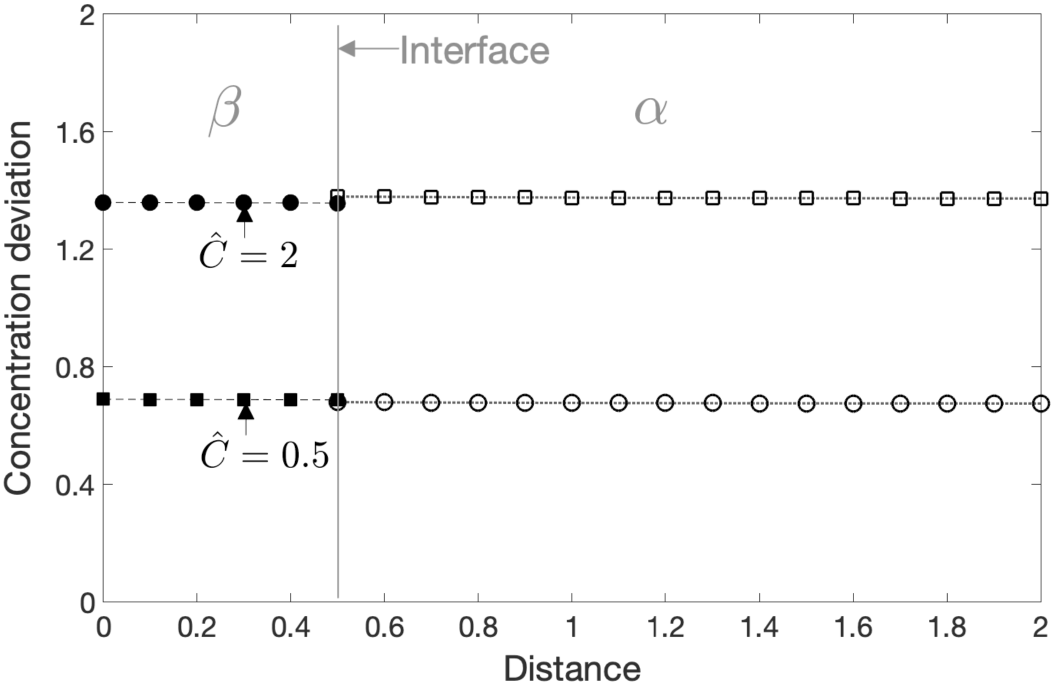

Figure 7.3: Concentration deviation, δC vs distance, z, for two cases of $\hat{C}$. The interface exhibits a concentration jump that is transposed from the $\hat{C} = 0.5$ case to the $\hat{C} = 2$ case.

7.5. Discussion

This chapter considered transient concentration fields that are interacting at the interfaces; subsequently, the interface is no longer in interfacial equilibrium.

The flux, J^*, is applied at $z = 0$, and the simplified Robin condition is approximated as a Neumann condition; i.e., it is assumed that $\zeta z_I \ll 1$. The second boundary condition is also a flux condition; consequently, the classical solution methods of PDEs cannot be applied to this composite problem.

For a single layer subject to two flux boundary conditions, the solution to the diffusion equation can be derived using the classical method of Laplace transformation [175]. Subramanian and White [168] have demonstrated that this solution to the single layer problem can also be derived using the method of variable transformation, which splits the solution into three components to account for the nonhomogeneous boundary conditions, homogeneous boundary conditions, and the initial conditions [168]. Furthermore, this latter method can be easily applied to a bilayer system; subsequently, it is used to solve for the concentration field.

7.5.1 Interface boundary condition

The interface boundary condition (IBC) given by Eq. (7.4) describes the transfer of B-atoms at the interface. It is given by

$$-J_I = V_0(C_I^\alpha - K_D C_I^\beta), \tag{7.64}$$

where the discontinuous weighting function, $\hat{C}$, is identified with K_D, which denotes the partition ratio for the system under consideration; it is also known as the distribution constant, and represents the ratio of concentrations of a component in two phases at equilibrium [176].[18] Thus, the interface can be interpreted as a membrane and the IBC contains the pertinent membrane transport parameters related to diffusion, partitioning, and permeation; in this model, the characteristic velocity, V_0 [m/s], represents the permeability of the membrane, and characterizes its diffusing ability of the solute.

The concentrations are not continuous at the interface, i.e. there is imperfect contact at the interface because the interface exhibits a resistance called the mass transfer resistance, which is manifested as a discontinuity in the chemical potential and hence the concentrations. The equation also displays a discontinuity in the diffusivity as well as represents a semi-permeable

---

[18] It is noted that this dimensionless material parameter appeared in *Chapters 5* and *6* as well.

membrane with a finite permeability between 0 (impermeable) and ∞ (fully permeable). Considering a few limiting cases can provide more insight into the physics of this general interface model.

Partition ratio = 1

Partitioning occurs because of a chemical potential difference between the two phases. In the absence of partitioning, the B-entities are able to move freely through the interface. Thus, in the limiting case where both phases exhibit the same equilibrium capacities, $C_{eq}^{\alpha} = C_{eq}^{\beta}$, the interface condition simplifies to

$$-J_I = V_0(C_I^{\alpha} - C_I^{\beta}), \tag{7.65}$$

which exhibits semi-permeability but without any chemical potential jump. When $V_0 = 0$ (i.e. zero permeability), the above equation simplifies to a perfectly reflecting condition with the flux at the interface equal to 0.

Fully permeable membrane

When $V_0 \to \infty$, (i.e. fully permeable) the general interface condition simplifies to

$$C_I^{\alpha} - \frac{C_{eq}^{\alpha}}{C_{eq}^{\beta}} C_I^{\beta} = 0, \tag{7.66}$$

where partitioning still occurs.

Perfect contact

In the absence of partitioning, Eq. (7.66) simplifies to $C_I^{\alpha} = C_I^{\beta}$, i.e. the interfacial concentrations are equal and there is perfect contact.

7.5.2 Model validity

Both Fickian diffusion, Eq. (7.5), as well as the simplified boundary condition at $z{=}0$ are valid for small times and small thicknesses, $\zeta z_I \ll 1$. For later times as well as larger thicknesses, the effects of the viscoelastic stresses on diffusion can no longer be ignored; subsequently non-Fickian diffusion models must be invoked.

7.5.3 Viscoelastic thin film

In this chapter, the diffusion-induced deformation is viscoelastic, i.e. diffusion can loosen the network structure of the β-phase, which has the constitution of a Maxwell fluid, and can now flow according to Eq. (7.50). The stress relaxation is diffusion-controlled.

The system exhibits a relaxation time, which is given by $\tau_r = 6\eta/\overline{E}^{\beta}$. The normalized time is given by $t/\tau_r = \overline{E}^{\beta} t/6\eta$; as this normalized time increases, the viscoelastic stresses decrease and subsequently vanish as the normalized time approaches infinity. Thus the system eventually relaxes to equilibrium. Consequently, there is no material degradation as the film/substrate interface is stationary and the film returns to its stress-free state with time.

The presence of viscoelasticity introduces a time lag between the elastic and viscoelastic stress that is characterized by the viscosity, η. For systems exhibiting large values of η, the time lag is negligible, and the stress is elastic. Furthermore, Eq. (7.63)b shows that the Maxwell type viscoelasticity reduces the magnitude of the stresses when $\overline{\sigma}^{\beta}_{E}(z,t)$ is of the same sign for all times, for a given value of z.

7.5.4 Thermodynamic framework

The presence of viscoelasticity implies that the framework of linear irreversible thermodynamics (LIT) or thermodynamics of irreversible processes (TIP) is no longer applicable because it relies on the postulate of local equilibrium hypothesis (*Section 5.4.6*); subsequently, the kinetic models of this framework are unable to capture the material behavior described by the Maxwell model. The simplest extension of the LIT formulation is the *Internal Variable Theory (IVT)* or *Thermodynamics of Internal Variables (TIV).* This nonclassical framework expands the state space of classical thermostatics to include internal or hidden variables that account for the internal order that characterizes the material under study. For the Maxwell material, by identifying the internal variable with the viscous strain, the rheological model given by Eq. (7.50), can be derived within this IVT formulation. It is noted that the IVT framework replaces the local equilibrium hypothesis of LIT with a generalized axiom called the hypothesis of the *local accompanying state (LAS)*, which postulates an accompanying (fictitious) equilibrium state to each non-equilibrium state [120].

In this chapter, we used a continuum mechanics concept, namely, the correspondence between elasticity and viscoelasticity, to prepare a partially-coupled model. This approach also allowed us to sidestep the thermodynamic considerations described above. However, to extend and develop the model further thermodynamically, the foundations must be revisited.

7.5.5 Moving boundary

To incorporate a moving boundary in the absence of deformation, one can prescribe the interfacial kinetics, $z_I = kt^2$, where k is a kinetic parameter.

In the presence of viscoelastic deformation, moving boundaries pose a problem because the classical elastic-viscoelastic analogy cannot be applied as the underlying Laplace transformation is defined for stationary boundaries. However, for the thin-film bilayer under study, the mechanical conditions at the interface correspond to a trivial solution. Subsequently, the classical correspondence principle still applies in the presence of partial coupling and the moving boundary can be prescribed. However, such models may be of limited utility when the effect of viscoelastic stress on diffusion must be considered as the film grows, requiring nonclassical theories such as IVT.

7.6. Summary

Viscous and viscoelastic effects appear in several thin-film applications including silicon oxide processing and polymer technologies, where they accompany diffusion and reactions. Polymers are increasingly used as coatings, barriers, and membranes in organic electronics and controlled drug delivery technologies; in the latter application, design considerations include concentration profiles of the drug at various times [177].

This chapter formulated a viscoelasically-coupled unsteady diffusion problem in a thin-film bilayer. *Sections 7.3* and *7.4* describe the solution, which is semi-analytical, and valid for small times and thicknesses. The problem is partially-coupled as the stress does not affect diffusion.

To illustrate the pharmaceutical application of controlled drug release with respect to the system under study, we consider the following scenario: the applied flux is used to inject the desired amount of solute (drug) into the thin film; the flux is then turned off, and the system sealed. The film has undergone viscoelastic deformation during the diffusion of the drug. When the system is in contact with the target environment, the drug is released (desorption), and the film gets restored to its stress-free state. Thus, the drug or solute can be stored for later release.

The thin-film bilayer model also featured a general interface. Physically, this sharp interface represents a thin membrane that is permeable to the small and mobile B-atoms. In problems of membrane transport, processes of diffusion and permeability play a key role. For example, in applications where the film acts as a protective layer against the B-entities, it is desirable to have an impermeable interface and an inert film with respect to phase transformation.

The IBC given by Eq. (7.4) is a general interface condition that combines many types of interfaces; it includes discontinuity in diffusivity, discontinuity in chemical potential (imperfect contact), and semi-permeability. Such interfaces are of interest in studies of living cell membranes, where the transport of small ions or molecules occurs by diffusion across the membranes; the diffusion of these species is often described by Fick's equations.

Furthermore, the IBC, derived in this work using simple kinetic considerations, resembles the modified Kedem-Katchalsky (K-K) equation in the absence of convection [178, 179]; the K-K equation is well-known equation in biological literature to describe transport of substances across biological membranes. Finally, it is noted that the mass transfer resistance exhibited by this interface is analogous to thermal or contact resistance in heat conduction literature [180–182], and charge transfer resistance in battery literature [183].

Incorporating viscoelasticity, and thereby, new mechanics and material response, required a visit to the foundations of continuum mechanics and the underlying principles used to build the constitutive theories of elasticity and fluid mechanics. While the L-C framework used in previous chapters is no longer valid in the presence of viscoelasticity, it was possible to forgo these thermodynamic considerations at present because the problem is partially-coupled and the mechanics can be derived using the classical correspondence principle. Thus, we were able to analyze the diffusion-induced stresses within the framework of linear viscoelasticity and the concentration field within the framework of classical thermodynamics for the planar bilayer of Fig. 5.1 with the film exhibiting viscoelastic (Maxwell) deformation. Nevertheless, the systematic set up of the model led to the following modeling insights: partially-coupled analyses of systems that feature a moving boundary and non-trivial mechanical BCs at the interface require an extended version of the correspondence principle [173], and a fully-coupled diffusion-reaction-deformation analysis requires a reformulated thermodynamic framework. The IVT formulation can be used for small deformation and material models such as the Maxwell model, however for large deformation as well as complex materials, further extensions may be necessary. For example, the Hookean spring of the Maxwell model can be generalized to accommodate larger deformation. Similarly, the Maxwell model, which features a single relaxation time, may be generalized to exhibit a distribution of relaxation times.

Chapter 8

Modeling insights and implications

> “Men can do nothing without the
> make-believe of a beginning.
> Even science, the strict measurer, is
> obliged to start with a make-believe
> unit, and must fix on a point in the
> stars’ unceasing journey when his
> sidereal clock shall pretend that time is
> at Nought.”
>
> George Eliot

We began our modeling exploration by selecting a thermodynamic framework that provided a natural extension of classical thermodynamics. Most models are thermodynamic, few kinetic even though the latter are most useful to technological applications. In this thesis, we used the Larché-Cahn theory as the starting point, and applied and extended it to model the growth kinetics in two geometries as well as predict the effects of diffusion-induced stresses.

However, solely kinetic models are often utilized to estimate the key kinetic parameters. Indeed, Fick’s first law of diffusion is a phenomenological equation based on experiments.

Modeling the chemical kinetics of diffusion and reaction in solids, particularly the growth behavior, was the motivation for this thesis and will continue to drive our research, with kinetics at the forefront. Therefore, this chapter takes the kinetic viewpoint to develop further modeling insights and set up future work. First, let's consider two illustrative semi-infinite planar problems with a prescribed surface concentration.

8.1. Fickian diffusion with a moving interface

Consider a semi-infinite supersaturated α-phase. Initially, this phase occupies the spatial range: $0 \leq z < \infty$. When the boundary, $z = 0$, is subjected to a concentration C^*, a sharp interface develops and propagates into the α-phase; this interface divides the α-phase from the β-phase that is growing at the surface and at time t, occupies the region $0 \leq z \leq S(t)$, where $S(t)$ denotes the location of the interface.

It is assumed that the concentration changes in the semi-infinite α-phase, which acts like a reservoir, can be ignored; subsequently, only the β-phase experiences diffusion of B-atoms. The Fickian diffusion equation is given by

$$\frac{\partial C^\beta}{\partial t} = D^\beta \frac{\partial^2 C^\beta}{\partial z^2}. \tag{8.1}$$

The mass balance condition at the interface is given by

$$-D^\beta \frac{\partial C^\beta}{\partial z}\Big|_{S(t)} = (C^\beta_{eq} - C^\alpha_{eq}) \frac{dz}{dt}\Big|_{S(t)}, \tag{8.2}$$

where it is assumed that the interfacial concentrations are constants, and correspond to the equilibrium values.

An exact solution to this semi-infinite diffusion problem is given by [11]

$$\begin{aligned} C^\beta(z,t) &= C^* + c_1 \operatorname{erf}\Big(\frac{z}{2\sqrt{Dt}}\Big), \\ \frac{C^\beta(z,t) - C^*}{C^\beta_{eq} - C^*} &= \frac{\operatorname{erf}(\gamma z/S)}{\operatorname{erf}(\gamma)}, \end{aligned} \tag{8.3}$$

where c_1 is determined by the interfacial boundary condition: $C^* + c_1 \operatorname{erf}(S/(2\sqrt{Dt})) = C_{eq}^{\beta}$; as the interfacial concentration is assumed to be constant, it cannot depend on time, i.e. $S/(2\sqrt{Dt}) = \gamma$, a constant, which is to be determined by the transcendental equation resulting from Eq. (8.2):

$$\sqrt{\pi}\gamma \operatorname{erf}(\gamma) e^{\gamma^2} = \varepsilon \equiv \frac{(C^* - C_{eq}^{\beta})}{(C_{eq}^{\beta} - C_{eq}^{\alpha})}. \tag{8.4}$$

For small values of γ, the error function is given by [184]

$$\operatorname{erf}(\gamma) = \frac{2}{\sqrt{\pi}} e^{-\gamma^2} \sum_{n=0}^{\infty} \frac{2^n \gamma^{2n+1}}{(2n+1)!!}.$$

Subsequently, Eq. (8.4) simplifies to

$$\sum_{n=0}^{\infty} \frac{(2\gamma^2)^{n+1}}{(2n+1)!!} = \varepsilon. \tag{8.5}$$

A general series such as

$$\sum_{n=1}^{\infty} a_n (\gamma^2)^n = \varepsilon$$

can be reversed to

$$\gamma^2 = \sum_{n=1}^{\infty} b_n = \varepsilon^n,$$

where $b_1 = 1/a_1$, $b_2 = -a_2/a_1^3$, and $b_3 = (2a_2^2 - a_1 a_3)/a_1^5$ [185]. Subsequently, we obtain

$$\gamma^2 = \frac{\varepsilon}{2} - \frac{\varepsilon^2}{16} + \frac{7\varepsilon^3}{90}. \tag{8.6}$$

8.1.1 Control parameter

Equation (8.4) illustrates the kinetic parameter that controls the diffusion behavior of the solution:

$$\varepsilon = \frac{(C^* - C^\beta_{eq})}{(C^\beta_{eq} - C^\alpha_{eq})} = \frac{(C^* - C^\beta_{eq})}{aC_A}, \tag{8.7}$$

where the latter equation is applicable to stoichiometric reactions; a is the stochiometric coefficient.

This supersaturation ratio is a key parameter that controls the growth kinetics as well as the validity of steady state diffusion models, as seen in the subsequent sections.

8.1.2 Pseudo-steady state solution

The pseudo-steady state (PSS) or quasi-steady state (QSS) approximation represents a suitable estimate of the time-dependent solution when $\varepsilon \ll 1$.

Using a boundary fixing transformation, $y = z/S(t)$ [186], Eq. (8.3)b can be written as

$$\frac{C^\beta(z,t) - C^*}{C^\beta_I - C^*} = \frac{\operatorname{erf}(\gamma y)}{\operatorname{erf}(\gamma)} = \frac{\int_0^{\gamma y} e^{-\eta^2} d\eta}{\int_0^{\gamma} e^{-\eta^2} d\eta}, \tag{8.8}$$

which is simplified using the Taylor expansion for the exponential function, resulting in the PSS solution to the concentration, which is given by

$$\begin{aligned} \frac{C^\beta(z,t) - C^*}{C^\beta_I - C^*} &= \frac{z}{S(t)}\big(1 + \frac{\gamma^2}{3}\big), \\ \frac{C^\beta_{\mathrm{PSS}}(z,t) - C^*}{C^\beta_I - C^*} &\approx \frac{z}{S(t)}, \end{aligned} \tag{8.9}$$

when $\varepsilon \ll 1$. The location of the interface is given by

$$S_{\mathrm{PSS}}(t) = \sqrt{2\epsilon D t}. \tag{8.10}$$

Equations (8.9) and (8.10) demonstrate that the PSS solution forms an upper bound on the concentration and a lower bound on the interface position.

8.1.3 Growth kinetics

The reaction interface location exhibits parabolic behavior, i.e. $S(t) = \mathcal{O}(t^{1/2})$. It is noted that the short-time behavior of the interface speed is not physical because the velocity, $dS(t)/dt \to \infty$ as $t \to 0^+$.

8.1.4 Summary

The presented problem and the subsequent analyses were guided by heat conduction literature.

Chapters 4 and *5* employed quasi-steady state analyses. The implication of steady state diffusion was discussed in *Section 5.4.6* and illustrated further in the above problem.

Fickian diffusion in the absence of any reaction kinetics contains no natural length or time scales, leading to a self-similar solution, as seen in Eq. (8.3). The growth of the β-phase is parabolic, which has an effect on the small-time limit behavior, namely that the model does not exhibit physical behavior in this limit. This 'blow up' in finite time is a key deficiency of this model, and is typically overcome in kinetic models by including reaction kinetics.

Chapter 3 presented a moving boundary formulation using a thermodynamic-kinetic approach where the driving force for phase transformation was identified from the equilibrium thermostatics framework of *Chapter 2*, and related to the velocity of the interface to describe the phase transformation reaction. This procedure led to the kinetic model given by Eq. (3.7). Consequently, reaction kinetics arise naturally in this model formulation.

The research methodology of *Chapter 3* was used in the uncoupled and elastically-coupled analyses of *Chapters 4* and *5* respectively, leading to linear-parabolic growth kinetics in the planar problem instead of solely parabolic growth. The implications of the linear-parabolic growth kinetics were discussed in *Section 5.4.4* via a limit analysis, which demonstrated that at small times, the planar interface grows linearly. Subsequently, the small-time asymptotic behavior in the presence of reaction kinetics, $S(t) = \mathcal{O}(t)$, is stable. Thus, including reaction kinetics in the model has a regularizing effect.

8.2. Concentration effects as moving interfaces

Consider diffusion in both phases in the presence of a perfect interface, which entails continuous concentrations and fluxes across the interface. Assuming the diffusivity has different values in different ranges of the local concentration, the two regions, α and β correspond to regions of low and high concentrations respectively.

The equations for determining the concentrations, $C(z,t)$, in the two regions are assumed to be given by Fick's law with different diffusivities. Thus, two different mechanisms of diffusion occur with diffusivity D^{β} (D^{α}) in region β (α) defined by the concentration range $C < C_S$ ($C \geq C_S$), where C_S is the concentration at the moving boundary, $z = S(t)$. Subsequently, the conditions of this transient problem are given by

$$\begin{aligned} C^{\alpha}(z,0) &= C_a, \\ C^{\beta}(0,t) &= C_b, \\ -D^{\beta}\frac{\partial C^{\beta}}{\partial z} &= -D^{\alpha}\frac{\partial C^{\alpha}}{\partial z} \text{ at } z = S(t), \end{aligned} \tag{8.11}$$

where C_a and C_b are prescribed concentrations corresponding to the initial condition and the boundary condition respectively; Eq. (8.11)c is an interfacial boundary condition, representing continuous flux across the interface. Since the interface is moving because of the effects of diffusion, the kinetics follow a parabolic law; subsequently, $S(t) = k\sqrt{t}$, where k is unknown and to be determined. The solution to the concentration field is given by [187]

$$\begin{aligned} C^\beta(z,t) &= C_b + B_\beta \operatorname{erf}\Big(\frac{z}{2\sqrt{D^\beta t}}\Big), \\ C^\alpha(z,t) &= C_a + B_\alpha \operatorname{erfc}\Big(\frac{z}{2\sqrt{D^\alpha t}}\Big), \end{aligned} \tag{8.12}$$

where erfc denotes the complementary error function, and B_β and B_α are constants given by $B_\beta = (C_S - C^\beta)/\operatorname{erf}(k/2\sqrt{D^\beta})$ and $B_\alpha = (C_S - C^\alpha)/\operatorname{erfc}(k/2\sqrt{D^\alpha})$, determined using the interfacial boundary condition. The parabolic growth kinetic parameter is determined using $(C_S - C_b)/(\sqrt{\pi}K_b e^{K_b^2} \operatorname{erf} K_b) + (C_S - C_a)/(\sqrt{\pi}K_a e^{K_a^2} \operatorname{erfc} K_a) = 0$, where $K_a = k/2\sqrt{D^\alpha}$ and $K_b = k/2\sqrt{D^\beta}$.

8.2.1 Vanishing diffusivity at low concentrations

If we set $D^\alpha = 0$, C^α stays 0, and the above formulation can be used to solve for the concentration distribution in the β-phase. Furthermore, the distribution of the local concentration can be expressed in terms of the local reaction: $-DC_z = C_S S_t$, where the derivatives are denoted using subscripts.

That is, using this local reaction instead of the diffusion equation, $C_t^\beta = D^\beta C_{zz}^\beta$, provides the same result for $D^\alpha = 0$. Thus, it is possible to interpret the immobilization reaction as a pure diffusion process, where $D = 0$ over $0 \leq C < C_S$ with D changing sharply at C_S.

8.2.2 Summary

Transient diffusion problems with discontinuous properties arise in composite barriers and multilayer applications.

The presented problem assumes a perfect interface, which entails equal capacities or equilibrium concentrations of the two phases; it can be derived from the general semi-permeable sharp interface model that was presented in *Chapter 7* and is derived in *Appendix C.2.*.

Chapter 7 considered a transient diffusion problem with two layers and a general semi-permeable interface. Unlike the classical methods of solution, an extended separation of variables was required. The problem was solved in the presence of a viscoelastic thin film; the interface was stationary. This problem can be extended to incorporate parabolic growth, as demonstrated by the kinetic problem presented above.

Analyses of macroscopic local diffusion processes and immobilization reactions often postulate discontinuities in diffusivities [5, 187]. The correspondence between diffusion and local reaction models is noted above; this feature, which is valuable for experimental models and analyses, is developed further in the subsequent sections.

8.3. Effective kinetic parameters

Experimental modeling frequently involves effective kinetic parameters to fit the measurements. These heuristic models describe experimental observations by invoking nonlinearity via the transport parameters to describe the complex kinetics that arise because of the effects of deformation, microstructure, trapping, and porosity.

For example, measurements of growth kinetics in silicon nanowires (SiNWs) undergoing lithium diffusion and reaction are fitted to empirical kinetic coefficients to explain the observed blocking of the phase transformation reaction, which is attributed to the effects of stress [188]. Liu et al. showed that the measured data could be fitted using either an effective diffusivity or an effective interface rate coefficient, both involving stretched exponentials; for instance, the effective diffusivity was given by $D = D_0 e^{-(pX_r/X_i)^q}$, where D_0 is the stress-free diffusivity, X_r denotes the radius of the SiNW and X_i is its initial radius, p and q are fitting parameters [188].

Power-law diffusivities, $D(C) = D_0 C^m$, describe the kinetics in a wide range of phenomena, including the diffusivities of many elements at high concentrations; m denotes the power-law exponent and is constant. For example, the diffusion of dopants, such as boron and phosphorous, in silicon can be modeled using power-law diffusivities with $m=1$ and $m=2$ respectively [189].

8.3.1 Summary

Chapter 5 presented the effective diffusivity for ideal solutions in the presence of elastic stress:

$$D_{\text{eff}}(C) = D_0\Big(1 + \frac{2}{9}\frac{\overline{E}\Omega^2}{RT}C\Big). \tag{8.13}$$

The derivation entailed Vegard's law, which assumes that the diffusion-induced strains vary linearly with concentration. Consequently, for higher concentrations and subsequent stronger elastic coupling, an extension of Vegard's law and hence the effective diffusivity is required. Power-law diffusivities may prove to be suitable candidates.

Chapter 5 also predicted reaction blocking in the presence of *strong* coupling, which is delineated in *Section 5.4.5.* This effect of stress is often known as *self-limiting lithiation* in battery literature.

8.4. Nonlinear degenerate diffusion

Moving boundary problems can be described within the framework of nonlinear degenerate diffusion, where free boundaries arise via the theory rather than the formulation. The manifestation of interfaces is a consequence of the degeneracy.

The porous medium equation is a well known example of a nonlinear degenerate equation; the one-dimensional nondimensionalized form is given by[19] [190]

$$C_t = (C^m C_z)_z. \tag{8.14}$$

This model governs a wide range of physical phenomena, including gas percolation in porous media, spreading of a thin film under gravity, and saturated flow in thin regions in porous media [191, 192]. Subsequently, a vast and rich mathematical literature is available.

8.4.1 Waiting time solutions

Waiting time solutions of nonlinear degenerate diffusion equations feature interfaces that do not move immediately but after a finite time period known as waiting time, t_w.

Two-parameter family of weak solutions of Eq. (8.14) for $t > 0$ exhibit a moving free boundary at $z = at^b$, where $a > 0$ and $b > 1$. Under appropriate initial data, these solutions exhibit a finite waiting time [191].

8.4.2 Summary

The reaction block phenomenon, predicted in *Chapter 5*, alters the growth kinetics in a nontrivial manner, requiring another framework. Thinking in terms of diffusivity, guided by Eq. (8.13), concentration-dependent diffusivities depending on higher orders can be selected, where the exponent depends on the material system under study.

Furthermore, it is inferred that the waiting time solutions may capture the reaction block phenomenon in a reasoned manner because the analysis of the consequent nonlinear equation within the framework of nonlinear mathematics can be used to derive error estimates and

---

[19] For our planar system, C in this model represents a normalized concentration of B-atoms.

bounds of concentrations, diffusivities, and waiting times. These estimates may be used to analyze experimental data.

8.5. Non-Fickian diffusion for viscoelasticity

Transport phenomena in polymer-penetrant systems entail diffusion of solvents in the polymer's entanglement network. When these systems exhibit glassy regions, non-Fickian transport occurs.

Consider a semi-infinite polymer-penetrant system exhibiting two viscoelastic phases that are distinguished by C, the concentration of the penetrant: glassy ($0 \leq C \leq C_S$) and rubbery ($C_S \leq C \leq C_{\mathrm{sat}}$), where C_{sat} denotes the saturation threshold of the polymer and C_S denotes the concentration at the moving boundary or the concentration at which the phase transition, i.e. rubber to glassy transition, takes place.

A non-Fickian diffusion formulation that postulates a generalized flux to account for the viscoelastic effects on diffusion is given by [193]

$$\begin{aligned} C_t &= \left[D(C)C_z + \tilde{E}\tilde{\sigma}_z\right]_z, \\ \tilde{\sigma}_t + \tilde{\beta}(C)\tilde{\sigma} &= \tilde{\mu}C + \tilde{\nu}C_t, \end{aligned} \tag{8.15}$$

where the second term of Eq. (8.15)a represents the contribution of the relaxation process to the diffusive flux, $\tilde{E}$, $\tilde{\mu}$, and $\tilde{\nu}$ are positive constants, $\tilde{\beta}(C)$ is the inverse of the relaxation time, assumed to be constant in each material phase, and $\tilde{\sigma}$, which can be interpreted as a stress, is a convenient artifice that is introduced to simplify the formulation; its evolution is described by Eq. (8.15)b [194].

Desorption of saturated films of polymers can lead to the formation of a thin skin of the polymer with glassy properties. Subsequently, a non-Fickian formulation is required that accounts for the effects of viscoelasticity on diffusion; by applying the above moving boundary model, Edwards [193] predicted the phenomenon of *trapping skinning*, in which an increase in the driving force for desorption decreases the accumulated flux.

8.5.1 Summary

Chapter 7 considered a viscoelastic thin film on an elastic substrate. This formulation can model coatings, barriers, and membranes, where the general semi-permeable interface allows the desired diffusion profile to be designed.

Polymer-penetrant systems that exhibit glassy regions cannot ignore the effects of viscoelasticity on diffusion because of their long relaxation times. To model diffusion with viscoelastic effects, one possible thermodynamic approach is discussed in *Chapter 7*.

Undertaking a kinetic approach in the context of viscoelasticity entails approximating the chemical potential to account for the effects of viscoelasticity on diffusion, as seen in the above example from [193]; it is noted that the assumed chemical potential of Eq. (8.15)a can be interpreted as an extension of Eq. (3.20).

Using the constitutive equation given by Eq. (8.15)b, which can be interpreted as an extension of the Maxwell material, Eq. (7.50), their work predicted the phenomenon of *trapping skinning* or *solvent trapping* during desorption. Physically, this blocking effect of viscoelastic stress on diffusion is analogous to *reaction block* or *solute trapping* in the context of elastically-coupled effects (*Chapter 5*).

8.6. Discussion

In this thesis, the analyses of the previous chapters illustrated a range of physical phenomena that result from the diffusion-reaction-deformation coupling; however, when applying any model, the following items must be addressed:

- model validity

- errors and bounds
- control parameters
- comparison to experiments
- pertinent length or time scales
- asymptotic regimes

The previous chapters discussed some of these aspects. This chapter attempted to expand them further as well as demonstrate additional modeling characteristics by considering five illustrative planar problems, guided by heat conduction and applied mathematical literature in addition to the thermodynamic foundation and analyses of this thesis. This exercise revealed several unifying aspects that link these vast fields. A systemized vetting of the pertinent features was undertaken to build understanding and shape future work.

Chapter 9

Conclusions and future work

> "Complex models are rarely useful (except for those writing their dissertation)."
>
> V.I. Arnold

In this study, the simplest models and assumptions were used to systematically derive, present, and unify key modeling ideas thermodynamically, kinetically, and mathematically.

9.1. Contribution to original knowledge

By applying and extending the rigorous equilibrium thermostatics framework of Larché and Cahn to binary two-phase systems, a consolidated theoretical approach, comprising linear kinetic models guided by the L-C theory is presented. The contributions are as follows.

- Closed-form analytical solutions are presented for composition and elastic stresses in a core-shell particle and a thin-film bilayer under conditions of steady-state diffusion.
- For the first time, the classical (uncoupled) stress-free growth kinetics of the spherical core-shell particle and planar bilayer are derived within this formulation, containing well-defined thermodynamic and kinetic quantities instead of fitting parameters.

The growth kinetics exhibit two kinetic regimes, where the limiting behavior is characterized by the critical thickness parameter, $1/\zeta'$ ($1/\zeta$ in the absence of stress), which depends on the material parameters, and the applied flux.

The selected theoretical approach also provided the thermodynamic framework to study the elastically-coupled effects systematically.

- The elastically-coupled parameters that influence the two growth kinetic regimes are identified, and the nature of coupling is defined to subsequently address the consequences of strong coupling.
- The coupled phenomena of stress-induced reaction blocking and hysteresis were predicted for the first time within this framework.
- Stability of the reaction front and isothermal hysteresis are discussed using the conceptual tools of thermodynamic driving force for phase transformations in the presence of stress, and the associated energy barrier. In particular, the thermodynamic origin of hysteresis in the planar bilayer is deduced using graphical analyses and stability arguments, which represent a novel look at the highly debated origins of the ubiquitous hysteresis that is characteristic of several material systems, including the palladium-hydrogen system.

These gaps in knowledge may have persisted in the literature because the original L-C thermostatics theory is general and involves multiple components and phases, which gave rise to alternative energy approaches to investigate equilibrium problems. For example, Puls [77] remarks:

> "Beginning in the 1970s, a series of comprehensive studies were carried out by Larché and Cahn [14–18] to determine the general conditions for thermo-chemical equilibrium and diffusion in multi-component crystalline solids self-stressed by coherency strains. The important contribution of these authors

> was the development of a rigorous thermodynamic framework dealing with the linkage between composition and stress in coherently stressed solids. However, the very generality of this treatment, involving lengthy and complex relationships and requiring the introduction of many new physical parameters, seems to have obscured recognition of some unusual and potentially important physical characteristics of phase equilbria in such solids. These features were recognized in two important papers by Williams [26, 27], who based his thermodynamic analysis of the effect of coherency strains on a simpler, more intuitive approach."

Indeed, such an alternative energy approach was used as the basis in *Chapter 6* to investigate coherent equilibrium. However, kinetic formulations in the literature have not utilized the full extent of the original and lengthy L-C theory, which was our starting point to model the phase growth kinetics.

- This thesis applied the L-C thermostatics framework directly to a binary two-phase system, and presented it explicitly for the first time.

To explore bilayer mass transfer problems involving viscoelasticity, the techniques of classical elastic-viscoelastic correspondence principle and extended separation of variables were applied to a partially-coupled formulation.

- A protocol containing both viscoelasticity and transient diffusion is devised. The interface model, derived from simple kinetic considerations, describes a general semi-permeable sharp interface, and is identified with the modified Kedem-Katchalsky (K-K) equation.

The coupled phenomena of stress-enhanced diffusion, reaction blocking, and hysteresis as well as their modeling are of immediate relevance to technology and experimental analyses. To facilitate further progress in this direction, a kinetic point of view is adopted to present the salient points pertinent to the modeling of transport phenomena, guided by the literature in multiple disciplines. Once again, simple kinetic formulations are undertaken for this reflective analysis.

- The correspondence between modeling diffusion and immobilization reactions is noted for a moving boundary problem. Subsequently, the stress-enhanced diffusion result of *Chapter 5* is revisited to motivate power-law diffusivities for higher concentrations and consequently, stronger coupling, which directs us to nonlinear degenerate diffusion.
- A survey of the theory of nonlinear degenerate diffusion reveals that power-law diffusivities exhibit waiting time solutions, a mathematical analog of reaction blocking! It is noted that this conclusion was drawn by considering the full tertiary coupling between diffusion, reaction, and deformation, as illustrated by the concept map in Fig. 9.1.

This transfer of knowledge forms the final contribution of this work, and provides a natural starting point for future experimental modeling research, which largely employs heuristic effective diffusivities at present. That is, the framework of nonlinear mathematics lends itself to (a) modeling reaction as part of the diffusion theory, (b) extracting kinetic information from effective diffusivities, which are the transport quantities that get measured in experiments, and (c) estimating the effective diffusivities, waiting times, and concentration solutions, as well as their bounds.

Furthermore, this reflection encapsulates the multidisciplinary approach involving thermodynamics, kinetics, and mathematics, and demonstrates the combined capacity of these fields for modeling insights.

The key contributions of this thesis and their underlying links are presented visually in Fig. 9.1.

9.2. Modeling implications and extensions

> "Coming back to where you started is
> not the same as never leaving."
>
> Terry Pratchett

This work can be extended in multiple directions. Broadly, there are two key areas for further investigation of the tertiary coupling:

9.2.1 Modeling of diffusion-reaction-deformation phenomena using nonclassical frameworks

Nonclassical formulations of mechanics, thermodynamics, and kinetics are active areas of research worldwide with an abundant and growing literature.

By enriching the description of the deformed continuum, these nonclassical frameworks can enhance the system resolution to characterize their complex behavior in the presence of additional considerations such as surface effects, charges, porosity, plasticity, fracture, and viscoelastic diffusion. The literature survey in *Chapter 2* cited extensions of the L-C framework with respect to some of these extensions. However, by applying and extending the L-C framework to investigate the effects of coupling in considerable detail, we are in a better position to revisit and assess the vast literature of nonclassical mechanics and thermodynamics, and substantiate their utility in studying coupled effects in elastic and viscoelastic applications.

For example, selecting, applying, and extending a suitable nonclassical thermodynamic framework to account for viscoelastic diffusion is an important area for future research, and can lend itself to predicting the subsequent coupled phenomena, including the phenomenon of trapping skinning, which was discussed in *Chapter 8*. While the Maxwell model of viscoelasticity can be derived within the TIV framework in the absence of diffusion [195] using the notion of internal variables, extending IVT as well as other nonclassical thermodynamic frameworks to include diffusion is nontrivial and an open area of thermodynamics research.

An example of a nonclassical framework that deviates from the classical Gibbsian thermodynamics and its extensions is the formulation that employs the notions of a chemical potential tensor and an equilibrium concentration that depends on the current state. This framework has been applied to describe the thermodynamic phenomenon of reaction block [48] in the absence of diffusion and has also included viscoelasticity in recent publications [196].

9.2.2 Estimating solutions and parameters of approximate (asymptotic) nonlinear models

Approximate models, constructed using nonlinear kinetics, can be used to describe the system behavior away from equilibrium. Often, the driving forces in the nonlinear diffusion and reaction equations are guided by their linear analogs, which serve as building blocks for the nonlinear model. An example of this approach from the literature was described in *Section 8.15*, which entails an extension of Eq. (3.20).

While these nonlinear models contain unknown kinetic parameters, the utility of the asymptotic approach lies in their immediate application to experiments by providing the range of validity of the kinetic parameters, as opposed to merely extracting them by fitting experimental data.

Chapter 8 made a preliminary link between the phenomenon of stress-induced reaction block, predicted in this work using L-C thermodynamics, and the waiting time solution, which exists for weak solutions of nonlinear degenerate diffusion equations. It would be of interest to explore this connection further for experimental modeling. For example, revisiting the literature survey of LIBs in *Chapter 2*, it is noted that the self-limiting effect of stress, i.e. reaction block, observed in LIB experiments has been found to exhibit a stretched exponential behavior [64]; similarly, the self-limiting behavior in silicon oxidation has also been explored using the self-same power-law ansatz [197]. Consequently, the framework of nonlinear degenerate diffusion, which entails stretched exponentials, lends itself to kinetic models, solutions, and theories that are of utility in the analysis of experimental data.

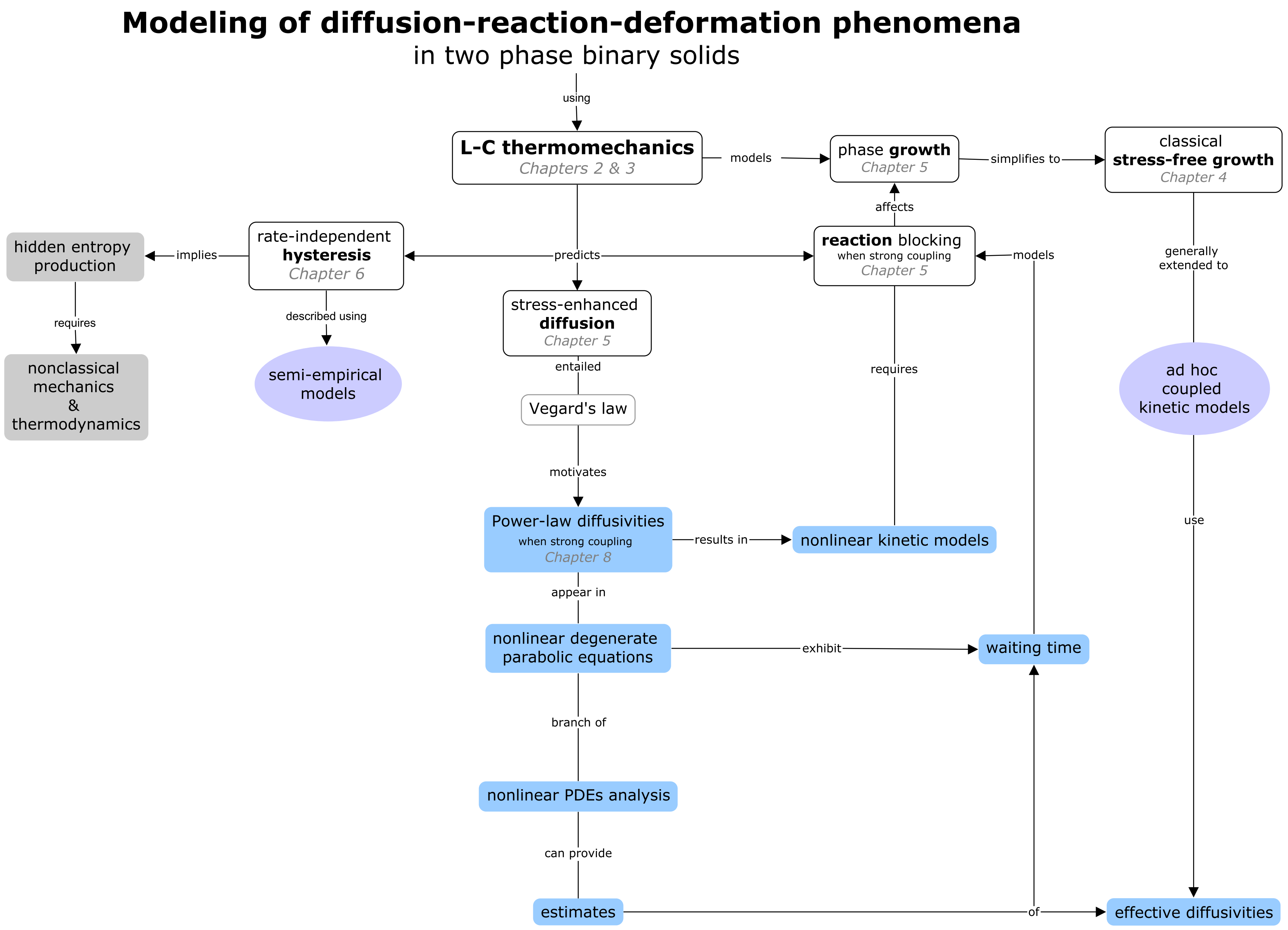

Figure 9.1: Concept map showing the key results and their connections, as well as their links to experimental models (violet), and thermodynamic (grey) and kinetic (blue) extensions. The growth kinetics equations are emphasized in *Chapters 4* and *5*.

Bibliography

[1] A. Fick, "Ueber Diffusion," *Annalen der Physik*, vol. 170, pp. 59-86, 1855.

[2] J. W. Gibbs, *Scientific Papers*, Dover Publications, pp. 55-353, 1961.

[3] R. Hooke, *De Potentia Restitutiva, or of Spring. Explaining the Power of Springing Bodies*, London, 1678.

[4] R. W. Balluffi, S. M. Allen, and W. C. Carter, *Kinetics of Materials*, John Wiley Sons, 2005.

[5] J. Crank, *The Mathematics of Diffusion*, Clarendon Press Oxford, 1975.

[6] M. E. Gurtin, E. Fried, and L. Anand, *The Mechanics and Thermodynamics of Continua*, Cambridge University Press, 2010.

[7] M. E. Glicksman, *Diffusion in Solids: Field Theory, Solid-State Principles, and Applications*, Wiley, 1999.

[8] L. E. Malvern, *Introduction to the Mechanics of a Continuous Medium*, Prentice-Hall, 1969.

[9] H. Mehrer, *Diffusion in Solids: Fundamentals, Methods, Materials, Diffusion-Controlled Processes*, Springer-Verlag Berlin Heidelberg, 2007.

[10] D. A. Porter, K. E. Easterling, and M. Sherif, *Phase Transformations in Metals and Alloys*, CRC Press, 2009.

[11] P. G. Shewmon, *Diffusion in solids*, Wiley-TMS, 1991.

[12] E. B. Tadmor, R. E. Miller, and R. S. Elliott, *Continuum Mechanics and Thermodynamics*, Cambridge, 2012.

[13] D. Bistri, A. Afshar, C. V. Di Leo, "Modeling the chemo-mechanical behavior of all-solid-state batteries: a review," *Meccanica*, vol. 56, pp. 1523–1554, 2021.

[14] D. Grazioli, M. Magri, and A. Salvadori, "Computational modeling of Li-ion batteries," *Computational Mechanics*, vol. 58, pp. 889–909, 2016.

[15] R. Mohtadi, S-i. Orimo, "The renaissance of hydrides as energy materials," *Nature Review Materials*, vol. 2, no. 16091, 1-15, 2017.

[16] Y. Zhao, P. Stein, Y. Bai, M. Al-Siraj, Y. Yang, B-X Xua, "A review on modeling of electro-chemo-mechanics in lithium-ion batteries," *Journal of Power Sources*, vol. 413, pp. 259-283, 2019.

[17] B. Key, R. Bhattacharyya, M. Morcrette, V. Seznec, J.-M. Tarascon, and C. P. Grey, "Real-Time NMR Investigations of Structural Changes in Silicon Electrodes for Lithium-Ion Batteries," *American Chemical Society*, vol. 131, no. 26, pp. 9239-9249, 2009.

[18] V. A. Sethuraman, M. J. Chon, M. Shimshak, N. Van Winkle, P. R. Guduru, "In situ measurement of biaxial modulus of Si anode for Li-ion batteries," *Electrochemistry Communications*, vol. 12, pp. 1614-1617, 2010.

[19] B. Key, M. Morcrette, J.-M. Tarascon, and C. P. Grey, "Pair Distribution Function Analysis and Solid State NMR Studies of Silicon Electrodes for Lithium Ion Batteries: Understanding the (De)lithiation Mechanisms," *Journal of the American Chemical Society*, vol. 133, no. 3, pp. 503-512, 2011.

[20] M. T. McDowell, S. W. Lee, W. D. Nix, Y. Cui, "25th Anniversary Article: Understanding the lithiation of silicon and other alloying anodes for lithium-ion batteries," *Advanced Materials*, vol. 25, no. 36, pp. 4966-4985, 2013.

[21] M. T. McDowell, S. W. Lee, J. T. Harris, B. A. Korgel, C. Wang, W. D. Nix, Y. Cui, "In situ TEM of two-phase lithiation of amorphous silicon nanospheres," *Nano Letters*, vol. 13, no. 2, pp. 758-764, 2013.

[22] L.A. Berla, S.W. Lee, Y. Cui, W. D. Nix, "Mechanical behavior of electrochemically lithiated silicon," *Journal of Power Sources*, vol. 273, pp. 4151, 2015.

[23] A. F. Bower, P. R. Guduru, and E. Chason, “Analytical solutions for composition and stress in spherical elastic-plastic lithium-ion electrode particles containing a propagating phase boundary,” *International Journal of Solids and Structures*, vol. 69-70, pp. 328-342, 2015.

[24] H. Haftbaradaran, H. Gao, W. Curtin, "A surface locking instability for atomic intercalation into a solid electrode," *Applied Physics Letters*, vol. 96, pp. 091909-1-091909-3, 2010.

[25] T. K. Bhandakkar and H. J. Gao, "Cohesive Modeling of Crack Nucleation Under Diffusion Induced Stresses in a Thin Strip: Implications on the Critical Size for Flaw Tolerant Battery Electrodes," *International Journal of Solids and Structures*, vol. 47, no. 10, pp. 14241434, 2010.

[26] B. S. Bokstein, M. I. Mendelev, and D. J. Srolovitz, *Thermodynamics and Kinetics in Materials Science: A Short Course, Oxford University Press*, 2005.

[27] J. Hirschfelder, C. F. Curtiss, R. Bird, *Molecular Theory of Gases and Liquids*, Wiley, 1954.

[28] A.D. Drozdov, "Viscoplastic response of electrode particles in Li-ion batteries driven by insertion of lithium," *International Journal of Solids and Structures*, vol. 51, no. 3–4, pp. 690-705, 2014.

[29] J. C. M. Li, R. A. Oriani, and L. S. Darken, "The thermodynamics of stressed solids," *Zeitschrift für Physikalische Chemie Neue Folge*, vol. 49, pp. 271-290, 1966.

[30] J. C. M. Li, F. V. Nolfi Jr., C. A Johnson, "Diffusional equilibrium of substitutional atoms in a stressed solid," *Acta Metallurgica*, vol. 19, no. 8, pp. 749-752, 1971.

[31] F. Larché and J. W. Cahn, "A linear theory of thermochemical equilibrium of solids under stress," *Acta Metallurgica*, vol. 21, pp. 1051-1063, 1973.

[32] F. Larché and J. W. Cahn, "Thermochemical equilibrium of multiphase solids under stress," *Acta Metallurgica*, vol. 26, pp. 1579-1589, 1978.

[33] F. Larché and J. W. Cahn, "Thermochemical equilibrium of multiphase solids under stress," *Acta Metallurgica*, vol. 26, pp. 1579–1589, 1978.

[34] F. Larché and J. W. Cahn, "The effect of self-stress on diffusion in solids," *Acta Metallurgica*, vol. 30, pp. 1835-1845, 1982.

[35] F. Larché and J. W. Cahn, "Overview no. 41 The interactions of composition and stress in crystalline solids," *Acta Metallurgica*, vol. 33, no. 3, pp. 331-357, 1985.

[36] C. H. Wu, "The role of Eshelby stress in composition-generated and stress-assisted diffusion," *Journal of the Mechanics and Physics of Solids*, vol. 49, pp. 1771-1794, 2001.

[37] Z. Cui, F. Gao, and J. Qu, "A finite deformation stress-dependent chemical potential and its applications to lithium ion batteries," *Journal of the Mechanics and Physics of Solids*, vol. 60, no. 7, pp. 1280-1295, 2012.

[38] A. B. Freidin, I. K. Korolev, S. P. Aleshchenko, and E. N. Vilchevskaya, "Chemical affinity tensor and chemical reaction front propagation: theory and FE-simulations," *International Journal of Fracture*, vol. 202, pp. 245-259, 2016.

[39] A. F. Bower, P. R. Guduru, and V. A. Sethuraman, "A finite strain model of stress, diffusion, plastic flow, and electrochemical reactions in a lithium-ion half-cell," *Journal of Mechanics and Physics of Solids*, vol. 59, no. 4, pp. 804-828, 2011.

[40] A. F. Bower and P. R. Guduru, "A simple finite element model of diffusion, finite deformation, plasticity and fracture in lithium ion insertion electrode materials," *Modelling and Simulation in Materials Science and Engineering*, vol. 20, no. 045004, pp. 1-20, 2012.

[41] A. F. Bower, E. Chason, P. R. Guduru, and B. W. Sheldon, "A continuum model of deformation, transport and irreversible changes in atomic structure in amorphous lithium silicon electrodes," *Acta Materialia*, vol. 98, pp. 229-241, 2015.

[42] G. Bucci, Y. -M Chiang, W. C. Carter, "Formulation of the coupled electrochemical-mechanical boundary-value problem, with applications to transport of multiple charged species," *Acta Materialia*, vol. 104, pp. 33-51 2016.

[43] R. Deshpande, Y. -T. Cheng, M. W. Verbrugge, and A. Timmons, "Diffusion Induced Stresses and Strain Energy in a Phase-Transforming Spherical Electrode Particle," *Journal of The Electrochemical Society*, vol. 158, no. 6, pp. A718-A724, 2011.

[44] Z. Cui, F. Gao, and J. Qu, "Interface-reaction controlled diffusion in binary solids with applications to lithiation of silicon in lithium-ion batteries," *Journal of Mechanics and Physics of Solids*, vol. 61, pp. 293-310, 2013.

[45] M. Poluektov, A. B. Freidin, and L. Figiel, "Modelling stress-affected chemical reactions in non-linear viscoelastic solids with application to lithiation reaction in spherical Si particles," *International Journal of Engineering Science*, vol. 128, pp. 44–62, 2018.

[46] L. Anand, "A Cahn-Hilliard-type theory for species diffusion coupled with large elastic-plastic deformations," *Journal of the Mechanics and Physics of Solids*, vol. 60, no. 12, pp. 1983-2002, 2012.

[47] L. Chen, F. Fan, L. Hong, J. Chen, Y. Z. Ji, S. L. Zhang, T. Zhu, and L. Q. Chen, "A Phase-Field Model Coupled with Large Elasto-Plastic Deformation: Application to Lithiated Silicon Electrodes," *Journal of The Electrochemical Society*, vol. 161, no. 11, pp. F3164-F3172, 2014.

[48] A. B. Freidin, "On the chemical affinity tensor for chemical reactions in deformable materials," *Mechanics of Solids*, vol. 50, pp. 260–285, 2015.

[49] A.B. Freidin, E.N. Vilchevskaya, I.K. Korolev, "Stress-assist chemical reactions front propagation in deformable solids," *International Journal of Engineering Science*, vol. 83, pp. 57-75, 2014.

[50] M. E. Gurtin and A. I. Murdoch, "A continuum theory of elastic material surfaces," *Archive for Rational Mechanics and Analysis*, vol. 57, pp. 291–323, 1975.

[51] W. W. Mullins and R. F. Sekerka, "On the thermodynamics of crystalline solids," *The Journal of Chemical Physics*, vol. 82, pp. 5192-5202, 1985.

[52] W. C. Johnson, and J. Iwan D. Alexander, "Interfacial conditions for thermomechanical equilibrium in two-phase crystals," *Journal of Applied Physics*, vol. 59, pp. 2735-2746, 1986.

[53] P. Cermelli, and S. Sellers, "Multi-phase equilibrium of crystalline solids," *Journal of the Mechanics and Physics of Solids*, vol. 48, no. 4, pp. 765-796, 2000.

[54] H. Schmalzried, *Chemical Kinetics of Solids*, VCH Publishers, 1995.

[55] A. M. Ginstling and V. I. Brounshtein, "Concerning the Diffusion Kinetics of Reactions in Spherical Particles," *Journal of Applied Chemistry of the USSR*, vol. 23, 1950, pp. 1327-1338.

[56] B. E. Deal and A. S. Grove, "General Relationship for the Thermal Oxidation of Silicon," *Journal of Applied Physics*, vol. 36, pp. 3770–3778, 1965.

[57] T. Higuchi, "Rate of release of medicaments from ointment bases containing drugs in suspensions," *Journal of Pharmaceutical Sciences*, vol. 50, no. 10, pp. 874-875, 1961.

[58] Khawam, and D. R. Flanagan, "Solid-state kinetic models: basics and mathematical fundamentals," *Journal of Physical Chemistry B*, vol. 110, no. 35, pp. 17315-17328, 2006.

[59] J. Siepmann, and N. A. Peppas, "Higuchi equation: Derivation, applications, use and misuse," *International Journal of Pharmaceutics*, vol. 418, no. 1, pp. 6-12, 2011.

[60] D. -B. Kao, J. P. McVittie, W. D. Nix and K. C. Saraswat, "Two-dimensional thermal oxidation of silicon. II. Modeling stress effects in wet oxides," *IEEE Transactions on Electron Devices*, vol. 35, no. 1, pp. 25-37, 1988.

[61] H. Coffin, C. Bonafos, S. Schamm, N. Cherkashin, G. Ben Assayag, and A. Claverie, "Oxidation of Si nanocrystals fabricated by ultralow-energy ion implantation in thin SiO_2 layers," *Journal of Applied Physics*, vol. 99, pp. 044302-1-044302-9, 2006).

[62] C. Büttner, and M. Zacharias, "Retarded oxidation of Si nanowires," *Applied Physics Letters*, vol. 89, pp. 263106-1-263106-3, 2006.

[63] Y. F. Gao, M. Cho, M. Zhou, "Mechanical reliability of alloy-based electrode materials for rechargeable Li-ion batteries," *Journal of Mechanical Science and Technology*, vol. 27, pp. 1205–1224, 2013.

[64] X. H Liu, F. Fan, H. Yang, S. Zhang, J. Y. Huang, T. Zhu, "Self limiting lithiation in silicon nanowires," *ACS Nano*, vol. 7, no. 2, pp. 1495-1503, 2013.

[65] U. Khalilov, G. Pourtois, A. C. T. van Duin, and E. C. Neyts, "Self-Limiting Oxidation in Small-Diameter Si Nanowires," *Chemistry of Materials*, vol. 24, no. 11, pp. 2141-2147, 2012.

[66] Y. Lu, A. K. Soh, Y. Ni, et al. "Understanding size-dependent migration of a two-phase lithiation front coupled to stress," *Acta Mechanica*, vol. 230, pp. 303–317, 2019.

[67] M. T. McDowell, I. Ryu, S. W. Lee, C.-M. Wang, W. D. Nix, and Y. Cui, "Studying the Kinetics of Crystalline Silicon Nanoparticle Lithiation with In Situ Transmission Electron Microscopy," *Advanced Materials*, vol. 24, pp. 6034-6041, 2012.

[68] H. Yang, W. Liang, X. Guo, C.-M. Wang, S. Zhang, "Strong kinetics-stress coupling in lithiation of Si and Ge anodes," *Extreme Mechanics Letters*, vol. 2, pp. 1-6, 2015.

[69] K. Zhang, Y. Li, F. Wang, B. Zheng, and Fuqian Yang, "A phase-field study of the effect of local deformation velocity on lithiation-induced stress in wire-like structures," *Journal of Physics D: Applied Physics*, vol. 52, no. 14, pp. 145501-1-145501-16, 2019.

[70] S. Wagner, P. Klose, V. Burlaka, K. Nörthemann, M. Hamm, A. Pundt, "Structural Phase Transitions in Niobium Hydrogen Thin Films: Mechanical Stress, Phase Equilibria and Critical Temperatures," *Chemphyschem*, vol. 20, no. 14, pp. 1890-1904, 2019.

[71] J. A. Dionne, "Inside out — Visualizing dynamic chemical transformations in situ with nanometer-scale resolution," *MRS Bulletin*, vol. 42, pp. 743–751, 2017.

[72] R. Griessen, N. Strohfeldt, and H. Giessen, "Thermodynamics of the hybrid interaction of hydrogen with palladium nanoparticles," *Nature Materials*, vol. 15, pp. 311–317, 2016.

[73] F. Hayee, T. C. Narayan, N. Nadkarni, et al., "In-situ visualization of solute-driven phase coexistence within individual nanorods," *Nature Communications*, vol. 9, no. 1775, pp. 1-8, 2018.

[74] S. Syrenova, C. Wadell, F. A. Nugroho, T. A. Gschneidtner, Y. A. Diaz Fernandez, G. Nalin, D. Świtlik, F. Westerlund, T. J. Antosiewicz, V. P. Zhdanov, K. Moth-Poulsen, and C. Langhammer, "Hydride formation thermodynamics and hysteresis in individual Pd nanocrystals with different size and shape," *Nature Materials*, vol. 14, no. 12, pp. 1236-1244, 2015.

[75] W. Dreyer, J. Jamnik, C. Guhlke et al. "The thermodynamic origin of hysteresis in insertion batteries," *Nature Materials*, vol. 9, pp. 448–453, 2010.

[76] V. A. Sethuraman, V. Srinivasan, and J. Newman, "Analysis of Electrochemical Lithiation and Delithiation Kinetics in Silicon," *Journal of The Electrochemical Society*, vol. 160, no. 2, pp. A394-A403, 2013.

[77] M. P. Puls, *The Effect of Hydrogen and Hydrides on the Integrity of Zirconium Alloy Components*, Springer-Verlag, 2012.

[78] R. B. Schwarz and A. G. Khachaturyan, "Thermodynamics of Open Two-Phase Systems with Coherent Interfaces," *Physical Review Letters*, vol. 74, no. 13, 1995.

[79] R.B. Schwarz and A. K. Khachaturyan "Thermodynamics of open two-phase systems with coherent interfaces: application to metal-hydrogen systems," *Acta Materialia*, vol. 54, no. 2, pp. 313–323, 2006.

[80] R.B. Schwarz, A. K. Khachaturyan, A. Caro, et al. "Coherent phase decomposition in the Pd–H system," *Journal of Materials Science*, vol. 55, pp. 4864–4882, 2020.

[81] A. B. Freidin and Victor A. Eremeyev, "On Kinetic Nature of Hysteresis Phenomena in Stress-Induced Phase Transformations," in: H. Altenbach, A. Belyaev, V. Eremeyev,

A. Krivtsov, A. Porubov (eds) *Dynamical Processes in Generalized Continua and Structures. Advanced Structured Materials*, vol 103. Springer Cham., 2019.

[82] W. Dreyer, C. Guhlke, R. Huth, "The behavior of a many-particle electrode in a lithium-ion battery," *Physica D: Nonlinear Phenomena*, vol. 240, no. 12, pp. 1008-1019, 2011.

[83] S. Hulikal and A. Bower, "On the Role of Heterogeneity in Phase-Transforming Electrodes: Origin of Zero-Current Hysteresis," *Journal of the Electrochemical Society*, vol. 164, no. 7, pp. A1401-A1411, 2017.

[84] T.B. Flanagan, C.-N. Park, W.A. Oates, "Hysteresis in solid state reactions," *Progress in Solid State Chemistry*, vol. 23, no. 4, pp. 291-363, 1995.

[85] A. R. Ubbelohde "Some Properties of the Metallic State. I. Metallic Hydrogen and Its Alloys." *Proceedings of the Royal Society of London. Series A, Mathematical and Physical Sciences*, vol. 159, no. 897, pp. 295–306, 1937.

[86] N. J. Weadock, P. W. Voorhees, and B. Fultz, "Interface pinning causes the hysteresis of the hydride transformation in binary metal hydrides," *Physical Review Materials*, vol. 5, no. 1, 013604, 2021.

[87] E. Wicke, J. Blaurock, "New experiments on and interpretations of hysteresis effects of Pd-D2 and Pd-H2," *Journal of the Less Common Metals*, vol. 130, pp. 351-363, 1987.

[88] P. Sutardja and W. G. Oldham, "Modeling of stress effects in silicon oxidation," *IEEE Transactions on Electron Devices*, vol. 36, no. 11, pp. 2415-2421, 1989.

[89] C. Rafferty, *Stress effects in silicon oxidation—simulation and experiments (Ph.D. dissertation)*, Tech. rep. Stanford University, 1989.

[90] V. Senez, D. Collard, B. Baccus, M. Brault, and J. Lebailly, "Analysis and application of a viscoelastic model for silicon oxidation," *Journal of Applied Physics*, vol. 76, pp. 3285-3296, 1994.

[91] V. S. Rao and T. J. R. Hughes, "On modelling thermal oxidation of Silicon I: theory," *International Journal for Numerical Methods in Engineering*, vol. 47, pp. 341-358, 2000.

[92] C. D. Krzeminski, X.-L. Han, and G. Larrieu, "Understanding of the retarded oxidation effects in silicon nanostructures," *Applied Physics Letters*, vol. 100, pp. 263111-1-263111-4, 2012.

[93] J. D. Evans and J. R. King, "Stress-Dependent Local Oxidation of Silicon," *SIAM Journal on Applied Mathematics*, vol. 77, no. 6, pp. 2012-2039, 2017.

[94] S. T. Kelly, and B. M. Clemens, "Moving interface hydride formation in multilayered metal thin films," *Journal of Applied Physics*, vol. 108, pp. 013521-1-013521-6, 2010.

[95] C. A. Pico, and M. G. Lagally, "Kinetics of titanium silicide formation on single-crystal Si: Experiment and modeling," *Journal of Applied Physics,* vol. 64, pp. 4957-4967, 1988.

[96] C. Perrin, D. Mangelinck, F. Nemouchi, J. Labar, C. Lavoie, C. Bergman, P. Gas, "Nickel silicides and germanides: Phases formation, kinetics and thermal expansion," *Materials Science and Engineering: B*, vol. 154–155, pp. 163-167, 2008.

[97] P. Gas and F.M. d'Heurle, "Formation of silicide thin films by solid state reaction," *Applied Surface Science*, vol. 73, 153-161, 1993.

[98] R. A. Adams, *Calculus: A complete course*, Pearson Canada, 2006.

[99] H. I. Aaronson, *Lectures on the Theory of Phase Transformations*, TMS Publications, 1999.

[100] J. Crank, *Free and Moving Boundary Problems*, Oxford Science Publications, 1984.

[101] R. M. Jones, *Mechanics Of Composite Materials*, Taylor Francis Group, 1999.

[102] C. H. Hseuh, "Modeling of elastic deformation of multilayers due to residual stresses and external bending," *Journal of Applied Physics*, vol. 91, pp. 9652-9656, 2002.

[103] A. F. Bower, *Applied Mechanics of Solids*, CRC Press, 2010.

[104] F. Yang, "Interaction between diffusion and chemical stresses," *Materials Science and Engineering: A*, vol. 409, no. 1–2, pp. 153-159, 2005.

[105] P. C. Chou and N. J. Pagano, *Elasticity - Tensor, Dyadic, and Engineering Approaches*, Dover Publications, 1992.

[106] W.-S. Zhang, X.-W. Zhang, Z.-L. Zhang, "Steady concentration distribution of hydrogen in elastic membranes during hydrogen diffusion," *Journal of Alloys and Compounds*, vol. 302, no. 1–2, pp. 258-260, 2000.

[107] M. J. Aziz, "Pressure and Stress Effects on Diffusion in Si," *Defect and Diffusion Forum*, vol.153-155, pp. 1-10, 1997.

[108] B. Yang, Y.-P. He, J. Irsa, C. A. Lundgren, J.B. Ratchford, and Y.-P. Zhao, "Effects of composition-dependent modulus, finite concentration and boundary constraint on Li-ion diffusion and stresses in a bilayer Cu-coated Si nano-anode," *Journal of Power Sources*, vol. 204, pp. 168-176, 2012.

[109] G. Bucci, S. P. Nadimpalli, V. A. Sethuraman, A. F. Bower, and P. R. Guduru, "Measurement and modeling of the mechanical and electrochemical response of amorphous Si thin film electrodes during cyclic lithiation," *Journal of Mechanics and Physics of Solids*, vol. 62, pp. 276-294, 2014.

[110] N. Swaminathan, S. Balakrishnan and K. George, "Elasticity and Size Effects on the Electrochemical Response of a Graphite, Li-Ion Battery Electrode Particle," *Journal of Electrochemical Society*, vol. 163, pp. A488-A498, 2016.

[111] V. I. Dybkov, *Reaction Diffusion and Solid State Chemical Kinetics, Materials Science Foundations series*, Trans Tech Publications Limited, 2010.

[112] E. Hadjixenophontos, K. Zhang, A. Weigel, P. Stender, and G. Schmitz, "Hydrogenation of Pd/Mg films: A quantitative assessment of transport coefficients," *International Journal of Hydrogen Energy*, vol. 44, pp. 27862-27875, 2019.

[113] F. Nemouchi, D. Mangelinck, C. Bergman, et al., "Differential scanning calorimetry analysis of the linear parabolic growth of nanometric Ni silicide thin films on a Si substrate", *Applied Physics Letters*, vol. 86, no. 041903, pp. 1-3, 2005.

[114] E. N. Vilchevskaya, and A. B. Freidin, "On Kinetics of Chemical Reaction Fronts in Elastic Solids," In: H. Altenbach, N. Morozov (eds) *Surface Effects in Solid Mechanics. Advanced Structured Materials*, vol 30, Springer, 2013.

[115] E. N. Vilchevskaya, A. B. Freidin, and N. F. Morozov, "Kinetics of the Chemical Reaction Front in Spherically Symmetric Problems of Mechanochemistry," *Doklady Physics*, vol. 60, pp. 175–179, 2015.

[116] A. Freidin, N. Morozov, S. Petrenko, et al. "Chemical reactions in spherically symmetric problems of mechanochemistry," *Acta Mechanica*, vol. 227, pp. 43–56, 2016.

[117] I. Prigogine and R. Defay, *Chemical Thermodynamics*, Longman, 1954.

[118] A. McNabb and P. K. Foster, "A New Analysis of the Diffusion of Hydrogen in Iron and Ferritic Steels," *Transactions of TMS-AIME*, vol. 227, p. 618-627, 1963.

[119] J. M. Rahm, J. Löfgren, and P. Erhart, "Quantitative predictions of thermodynamic hysteresis: Temperature-dependent character of the phase transition in Pd–H,"*Acta Materialia*, vol. 227, pp. 117697-1-117697-11, 2022.

[120] G. Lebon, D. Jou, and J. Casas-Vázquez, *Understanding Non-equilibrium Thermodynamics*, Springer-Verlag, 2008.

[121] F. Yang, "Diffusion-induced stress in inhomogeneous materials: concentration-dependent elastic modulus," *Science China Physics, Mechanics and Astronomy*, vol. 55, pp. 955–962, 2012.

[122] J. W. Cahn, "Coherent Fluctuations and Nucleation in Isotropie Solids," *Acta Metallurgica*, vol. 10, pp. 907-913, 1962.

[123] J. W. Cahn and F. C. Larché. "A simple model for coherent equilibrium," *Acta Metallurgica*, vol. 32, no. 11, pp. 1915-1923, 1984.

[124] J. W. Cahn, and F. C. Larché, "Effects of coherency constraints on phase equilibria," *MRS Proceedings*, vol. 19, pp. 311, 1982.

[125] A. L. Roitburd, "Equilibrium and phase diagrams of coherent solids," *Fizika Tverdogo Tela*, vol 26, pp. 2025-2032, 1984.

[126] J.-Y. Huh, and W.C. Johnson, "Intrinsic thermodynamic stability of stressed coherent systems," *Acta Metallurgica et Materialia*, vol. 43, no. 4, pp. 1631-1642, 1995.

[127] J. Iwan D. Alexander, and W. C. Johnson, "Thermomechanical equilibrium in solid-fluid systems with curved interfaces," *Journal of Applied Physics*, vol. 58, pp. 816-824, 1985.

[128] F. C. Larché, "The Equilibrium of Two Solid Solutions Across a Coherent Interface", in E. C. Aifantis and J. Gittus (eds.), *Phase Transformations*, 1986.

[129] W. C. Johnson, "On the inapplicability of gibbs phase rule to coherent solids," *Metallurgical and Materials Transactions A*, vol. 18, pp. 1093–1097, 1987.

[130] W. C. Johnson, and P. W. Voorhees, "Phase equilibrium in two-phase coherent solids," *Metallurgical and Materials Transactions A*, vol. 18, pp. 1213–1228, 1987.

[131] F. C. Larché, "The Role of Stresses on Phase Transformations, in J. D. Embury, G. R. Purdy (eds), *Advances in Phase Transitions*, pp. 193-203, 1988.

[132] W. C. Johnson and C. S. Chiang, "Phase equilibrium and stability of elastically stressed heteroepitaxial thin films," *Journal of Applied Physics*, vol. 64, pp. 1155-1165, 1988.

[133] W. C. Johnson, and P. W. Voorhees, "Coherent Phase diagrams," *Bulletin of Alloy Phase Diagrams*, vol. 9, pp. 208–215, 1988.

[134] P. W. Voorhees, and W. C. Johnson, "The thermodynamics of a coherent interface," *The Journal of Chemical Physics*, vol. 90, pp. 2793-2801, 1989.

[135] R. W. Cahn, "Phase equilibria under stress," *Angewandte Chemie International Edition*, vol. 28, pp. 1128-1130, 1989.

[136] W. C. Johnson, T. A. Abinandanan, and P. W. Voorhees, "The coarsening kinetics of two misfitting particles in an anisotropic crystal," *Acta Metallurgica et Materialia*, vol. 38, no. 7, pp. 1349-1367, 1990.

[137] C. S. Chiang, W. C. Johnson, "Coherent phase equilibria in systems possessing a consolute critical point," *Journal of Materials Research*, vol. 4, pp. 678–687, 1989.

[138] W. C. Johnson, P. W. Voorhees, "On the classification of phase transitions involving changes in composition," *Acta Metallurgica et Materialia*, vol. 38, no. 6, pp. 1183-1189, 1990.

[139] F. C. Larché, "Coherent phase transformations," *Annual Review of Materials Science*, vol. 20, pp. 83-99, 1990.

[140] W. C. Johnson and G. Martin, "Influence of elastic stress on the growth kinetics of planar thin-film binary diffusion couples," *Journal of Applied Physics*, vol. 68, pp. 1252-1264, 1990.

[141] Z.-K. Liu, J. Ågren, On two-phase coherent equilibrium in binary alloys, *Acta Metallurgica et Materialia*, vol. 38, no. 4, pp. 561-572, 1990.

[142] W. C. Johnson, and W. H. Müller, "Characteristics of phase equilibria in coherent solids," *Acta Metallurgica et Materialia*, vol. 39, no. 1, pp. 89-103, 1991.

[143] M. J. Pfeifer, P. W. Voorhees, "A graphical method for constructing coherent phase diagrams," *Acta Metallurgica et Materialia*, vol. 39, Issue 8, pp. 2001-2012, 1991.

[144] W. C. Johnson, and H. Schmalzried, "Gibbs-Duhem and Clausius-Clapeyron type equations for elastically stressed crystals," *Acta Metallurgica et Materialia*, vol. 40, no. 9, pp. 2337-2342, 1992.

[145] W. C. Johnson, and H. Schmalzried, "Phenomenological thermodynamic treatment of elastically stressed ionic crystals," *Journal of the American Ceramic Society*, vol. 76, pp. 1713-1719, 1993.

[146] J. Y. Huh, J. M. Howe, and W. C. Johnson, "Effect of coherency stresses on $\alpha+\alpha_2$ phase equilibria in Ti-Al alloys," *Acta Metallurgica et Materialia*, vol. 41, no. 9, pp. 2577-2588, 1993.

[147] W. C. Johnson, "Thermodynamic Equilibria in Two-Phase, Elastically Stressed Ionic Crystals," *Journal of the American Ceramic Society*, vol. 77, no. 6, pp. 1581 - 1591, 1994.

[148] J. K. Lee, and W. Tao, "Coherent phase equilibria: Effect of composition-dependent elastic strain," *Acta Metallurgica et Materialia*, vol. 42, no. 2, pp. 569-577, 1994.

[149] T.A. Abinandanan,and W.C. Johnson, "Development of spatial correlations during coarsening," *Materials Science and Engineering: B*, vol. 32, no. 3, pp. 169-176, 1995.

[150] Z. K. Liu, J. Ågren, "Thermodynamics of constrained and unconstrained equilibrium systems and their phase rules," *Journal of Phase Equilibria*, vol. 16, pp. 30–35, 1995.

[151] J. Y. Huh "A generalized thermodynamic treatment of phase equilibria in coherent multilayers," *Metals and Materials*, vol. 3, pp. 75–86, 1997.

[152] W. C. Johnson, "Effect of elastic stress on two-phase binary diffusion couples," *Metallurgical and Materials Transactions A*, vol. 28, pp. 27–38, 1997.

[153] A. L. Roytburd, and J. Slutsker, "Equilibrium two-phase microstructure at phase transformation in a constrained solid," *Materials Science and Engineering: A*, vol. 238, no. 1, pp. 23-31, 1997.

[154] A. L. Roytburd, and J. Slutsker, "Thermodynamic hysteresis of phase transformation in solids," *Physica B: Condensed Matter*, vol. 233, no. 4, pp. 390-396, 1997.

[155] W. C. Johnson, P. W. Voorhees, "Interfacial stress, interfacial energy, and phase equilibria in binary alloys," *Journal of Statistical Physics*, vol. 95, pp. 1281–1309, 1999.

[156] W. C. Johnson, "Influence of elastic stress on phase transformations," in H.I. Aaronson (ed.) *Lectures on the Theory of Phase Transformations*, TMS-AIME, pp. 35-134, 2000.

[157] Fratzl, P., Penrose, O. and Lebowitz, J.L. "Modeling of Phase Separation in Alloys with Coherent Elastic Misfit," *Journal of Statistical Physics*, vol. 95, pp. 1429–1503, 1999.

[158] W. C. Johnson, and P. W. Voorhees, "The thermodynamics of elastically stressed crystals," in H. Ehrenreich, F. Spaepen (eds) *Solid State Physics: Advances in Research and Applications*, vol. 59, pp. 1-201, 2004.

[159] A. L. Roytburd, and J. Slutsker, "Coherent phase equilibria in a bending film," *Acta Materialia*, vol. 50, no. 7, pp. 1809-1824, 2002.

[160] J. Y. Huh, H. Lee, and W. C. Johnson, "Particle size effects on the coherent phase equilibria of binary nanoparticles," *Metals and Materials International volume*, vol. 11, pp. 357–363, 2005.

[161] T. B. Flanagan and W. A. Oates, "The effect of hysteresis on the phase diagram of Pd-H, " *Journal of the Less-Common Metals*, vol. 92, pp. 131-142, 1983.

[162] T. B. Flanagan and T. Kuji, "Hysteresis in metal hydrides evaluated from data at constant hydrogen content: application to palladium-hydrogen, " *Journal of the Less-Common Metals*, vol. 152, pp. 213-226, 1989.

[163] D. Chandra, S. Bagchi, S. W. Lambert, W. N. Cathey, F. E. Lynch, R. C. Bowman Jr., “Long-term thermal cycling studies on LaNi5.2.,” *Journal of Alloys and Compounds*, vol. 199, no. 1–2, pp. 93–100, 1993.

[164] H. Nakamura, Y. Nakamura, S. Fujitani, I. Yonezu, "Cycle performance of a hydrogen-absorbing $La_{0.8}Y_{0.2}Ni_{4.8}Mn_{0.2}$ Alloy," *International Journal of Hydrogen Energy*, vol. 21, pp. 457–460, 1996.

[165] J. D. Eshelby, "The continuum theory of lattice defects," in: F. Seitz and D. Turnbull (eds.), *Progress in Solid State Physics*, Vol. 3, Academic Press, New York, pp. 79–303, 1956.

[166] B. A. Boley, and J. H. Weiner, *Theory of Thermal Stresses*, Dover Publications Inc, 1997.

[167] A. Baldi, T. C. Narayan, A. L. Koh, and J. A. Dionne, "In situ detection of hydrogen-induced phase transitions in individual palladium nanocrystals," *Nature materials*, vol. 13, pp. 1143–1148, 2014.

[168] V. R. Subramanian and R. E. White "New separation of variables method for composite electrodes with galvanostatic boundary conditions," *Journal of Power Sources*, vol. 96, no. 2, 2001, pp. 385-395, 2001.

[169] C. W. Tittle, "Boundary Value Problems in Composite Media: Quasi-Orthogonal Functions," *Journal of Applied Physics*, vol. 36, no. 4, pp. 1486-1488, 1965.

[170] E. B. Tadmor and R. E. Miller, *Modeling Materials*, Cambridge, 2011.

[171] R. Lakes, *Viscoelastic Materials*, Cambridge University Press, 2009.

[172] G. Mase, *Schaum's Outline of Continuum Mechanics*, McGraw Hill Professional, 1970.

[173] J. M. Golden, and G. A. C. Graham, *Boundary Value Problems in Linear Viscoelasticity*, Springer-Verlag Berlin Heidelberg GmbH, 1988.

[174] K. Ogata, *System Dynamics*, Pearson, 2004.

[175] H. S. Carslaw and J. C. Jaeger *Conduction of Heat in Solids*, Oxford, Clarendon Press, 1959.

[176] IUPAC. Compendium of Chemical Terminology, 2nd ed. (the "Gold Book"). Compiled by A. D. McNaught and A. Wilkinson. Blackwell Scientific Publications, Oxford (1997). Online version (2019-) created by S. J. Chalk. ISBN 0-9678550-9-8. https://doi.org/10.1351/goldbook.

[177] G. Pontrelli, and F. de Monte "Mass diffusion through two-layer porous media: an application to the drug-eluting stent," *International Journal of Heat and Mass Transfer*, vol. 50, no. 17–18, pp. 3658-3669, 2007.

[178] O. Kedem and A. Katchalsky, "Thermodynamic analysis of the permeability of biological membrane to non-electrolytes," *Biochimica et Biophysica Acta*, vol. 27, pp. 229-246, 1958.

[179] O. Farago and G. Pontrelli, "A Langevin dynamics approach for multi-layer mass transfer problems," *Computers in Biology and Medicine*, vol. 124, no. 103932, pp. 1-8, 2020.

[180] D. W. Hahn, and M. N. Özişik, *Heat Conduction*, John Wiley & Sons, Inc., 2012.

[181] H. D. Baehr, and K. Stephan, *Heat and Mass Transfer*, Springer-Verlag, 2011.

[182] G. D'Alessandro, and F. de Monte, "Multi-Layer Transient Heat Conduction Involving Perfectly-Conducting Solids," *Energies*, vol. 13, no. 24, pp. 6484-1-6484-25, 2020.

[183] B. Suthar and V. R. Subramanian,"Lithium Intercalation in Core-Shell Materials–Theoretical Analysis," *Journal of Electrochemical Society*, vol. 161, A682-A692, 2014.

[184] S. Acton, *Numerical methods that work*, Harper & Row, 1970.

[185] V. J. Lunardini and A. Aziz, "Perturbation techniques in conduction-controlled freeze-thaw heat transfer," Monograph for US Army Corps of Engineers, Cold Regions Research & Engineering Laboratory, 1993.

[186] J. M. Hill and J. N. Dewynne, *Heat Conduction*, Blackwell Scientific Publications, 1987.

[187] B. Gebhart, *Heat Conduction and Mass Diffusion*, McGraw-Hill, 1993.

[188] X. H Liu, F. Fan, H. Yang, S. Zhang, J. Y. Huang, and T. Zhu, "Self limiting lithiation in silicon nanowires," *ACS Nano*, vol. 7, no. 2, pp. 1495-1503, 2013.

[189] J. R. King, "Approximate solutions to a nonlinear diffusion equation," *Journal of Engineering Mathematics*, vol. 22, pp. 53-72, 1988.

[190] W. L. Kath, "Waiting and propagating fronts in nonlinear diffusion," *Physica 12D*, pp. 375-381, 1984.

[191] A. A. Lacey, J. R. Ockendon and A. B. Tayler, "Waiting-Time" Solutions of a Nonlinear Diffusion Equation," *SIAM Journal on Applied Mathematics*, vol. 42, no. 6, pp. 1252-1264, 1982.

[192] J. Gratton and C. Vigo, "Evolution of self-similarity, and other properties of waiting-time solutions of the porous medium equation: the case of viscous gravity currents," *European Journal of Applied Mathematics*, vol. 9, pp. 327-350, 1998.

[193] D. A. Edwards, "A Mathematical Model for Trapping Skinning in Polymers," *Studies in Applied Mathematics*, vol. 99, pp. 49-80, 1997.

[194] D. A. Edwards and D. S. Cohen, "A Mathematical Model for a Dissolving Polymer," *Aiche Journal*, vol. 41, pp. 2345-2355, 1995.

[195] G. A. Maugin, *The Thermomechanics of Nonlinear Irreversible Behaviors*, World Scientific, 1999.

[196] S. Petrenko, A. B. Freidin, and E. Charkaluk, "On chemical reaction planar fronts in an elastic–viscoelastic mechanical framework," *Continuum Mechanics and Thermodynamics*, vol. 34, pp. 137–163, 2022.

[197] M. Itoh, "Power-Law Growth of the Oxide in the Self-Limiting Oxidation of Si Nanowires," *Journal of the Physical Society of Japan*, vol. 90, no. 7, pp. 074603-1-074603-10, 2021.

Appendices

A. Phase change in the deformed state

Let $\boldsymbol{x}$ be a vector in the deformed configuration, and $\boldsymbol{X}$ be a vector in the undeformed state. The displacements and the rotations of a deformable solid are assumed infinitesimal. Thus, the deformed configuration, $\boldsymbol{x}$, is obtained by a smooth displacement, $\boldsymbol{u}$, from the undeformed configuration, $\boldsymbol{X}$, which is given by

$$\boldsymbol{x} = \boldsymbol{X} + \boldsymbol{u}. \tag{1}$$

This implies

$$\boldsymbol{F} = \frac{\partial \boldsymbol{x}}{\partial \boldsymbol{X}} = \boldsymbol{I} + \nabla_0 \boldsymbol{u}, \tag{2}$$

where ∇_0 is the gradient operator in the undeformed state, and $\boldsymbol{F}$ is called the deformation gradient, and relates an infinitesimal vector in the deformed configuration to the corresponding vector in the undeformed configuration. Mathematically, this is given by

$$d\boldsymbol{x} = \boldsymbol{F} d\boldsymbol{X}. \tag{3}$$

For small strains, the displacement gradient is given by

$$\nabla_0 \boldsymbol{u} = \boldsymbol{\epsilon} + \boldsymbol{w}, \tag{4}$$

where $\boldsymbol{\epsilon}$ is the small strain tensor, and $\boldsymbol{w}$ is the infinitesimal rotation tensor. In component form, Eq. (4) is written as: $\epsilon_{ij} + \omega_{ij} = \dfrac{\partial u_i}{\partial X_j}$.

For infinitesimal deformation, the scalar components of the infinitesimial rotation tensor satisfy the condition $w_{ij} \ll 1$, and the distinction between the reference and deformed coordinates disappears, i.e., $\nabla_0 = \nabla$, the gradient operator in the deformed state. Therefore,

$$\nabla_0 \boldsymbol{u} = \nabla \boldsymbol{u} = \boldsymbol{\epsilon}, \tag{5}$$

and Eq. (2) simplifies to

$$\boldsymbol{F} = \boldsymbol{I} + \boldsymbol{\epsilon}. \tag{6}$$

Using Eqs. (3) and (6), we obtain

$$d\boldsymbol{x} = (\boldsymbol{I} + \boldsymbol{\epsilon})d\boldsymbol{X}. \tag{7}$$

Thus, for infinitesimal strains, the displacement due to phase change in the actual configuration is given by $(\boldsymbol{I} + \boldsymbol{\epsilon})\boldsymbol{N}\delta z$, where $\boldsymbol{N}\delta z$ is the displacement due to phase change in the reference configuration.

B. Mobility of dilute solutions

The phenomenological equation for the chemical potential is given by [7]

$$\mu = \mu^0 + RT \ln(\gamma X), \tag{8}$$

where μ^0 is the chemical potential of the B-atoms under standard conditions (generally, 1.0 atm pressure and the system temperature), and γ is the activity coefficient of the B-atoms. For dilute solutions, $\gamma \approx 1$. As the thin film and substrate contain dilute amounts of the B-species, their chemical potentials can be expressed in terms of concentration using Eq. (1.3). The simplified chemical potential is given by

$$\mu \approx \mu^0 + RT \ln \frac{C}{C_A}. \tag{9}$$

The derivative of the chemical potential in the η-phase ($\eta = \alpha, \beta$) is $\nabla \mu^\eta = \dfrac{RT}{C^\eta} \nabla C^\eta$. Thus, for isotropic diffusion, Eq. (3.3)a simplifies to

$$\boldsymbol{J}^\eta = -M^\eta RT \nabla C^\eta. \tag{10}$$

Comparing Eq. (10) to Fick's first law of diffusion, $\boldsymbol{J}^\eta = -D^\eta \nabla C^\eta$, we obtain the relationship between the diffusivity and mobility for dilute solutions undergoing small deviations from equilibrium, $M^\eta = D^\eta / RT$.

C. Interface conditions

C.1. Kinetic model of the interface

The form of the kinetic model, Eq. (3.7), to describe the velocity of the interface is motivated by a standard model used in the thermodynamics of reactions of gases. Following [26], let us consider the following reaction:

$$aA + bB \rightleftarrows cC + dD, \tag{11}$$

where A, B, C, and D represent the chemical species participating in the reaction and a, b, c, and d are the stoichiometric coefficients of these species. In the forward reaction, A and B are reactants and, C and D are products.

The rate of a reaction is equal to the rate of the forward reaction minus the rate of the reverse reaction, which is expressed as

$$v = v_1 - v_2, \tag{12}$$

where v is the net rate of the reaction, and v_1 and v_2 are the rates of the forward and backward reactions respectively.

The thermodynamics of reactions of gases use the van't Hoff isotherm, which is given by [26]

$$\Delta G_T = \Delta G_T^0 + RT\Delta \ln p_i, \tag{13}$$

where p_i is the partial pressure of component i, ΔG_T is the change of the Gibbs energy, and ΔG_T^0 is called the standard change of the Gibbs energy of the reaction; $\Delta G_T = \Delta G_T^0$ when the reaction occurs under standard conditions (all species are at 1 atm). Equation (13) assumes that the system is large, i.e., the variation in the number of moles of the participating species is negligible, and does not affect their concentration or partial pressures.

The van't Hoff isotherm determines the reaction's direction: when $\Delta G_T < 0$, the forward reaction occurs; when $\Delta G_T > 0$, the backward reaction takes place.

At equilibrium, the change in Gibbs energy vanishes:

$$\begin{aligned} \Delta G_T &= 0, \\ RT \ln \frac{p_C^c p_D^d}{p_A^a p_B^b} &= -\Delta G_T^0, \end{aligned} \tag{14}$$

where the partial pressures are equilibrium partial pressures, and their ratio is given by K_p, which denotes the equilibrium constant:

$$K_p = \frac{p_C^c p_D^d}{p_A^a p_B^b}, \tag{15}$$

which is known as the law of mass action and entails equilibrium partial pressures. It is noted that ΔG_T^0, and subsequently, K_p only depend on temperature.

Thus, $RT \ln K_p = -\Delta G_T^0$; revisiting Eq. (13), we obtain

$$\begin{aligned} \Delta G_T &= -RT \ln K_p + RT \Delta \ln p_i. \\ &= RT \ln \left(\frac{1}{K_p} \frac{p_C^c p_D^d}{p_A^a p_B^b} \right), \end{aligned} \tag{16}$$

where the ln function includes instantaneous and equilibrium (via K_p) partial pressures.

Using Eqs. (12) and (16), we obtain

$$\begin{aligned} v &= v_1 - v_2, \\ &= k_1 p_A^a p_B^b - k_2 p_C^c p_D^d, \\ &= v_1\Big(1 - \frac{1}{K_p}\frac{p_C^c p_D^d}{p_A^a p_B^b}\Big) \\ &= v_1\Big(1 - e^{\frac{\Delta G}{RT}}\Big) \end{aligned} \tag{17}$$

where the reaction constant for the forward reaction is k_1 and for the backward reaction is k_2; subsequently, $K_p = \dfrac{k_1}{k_2} = \dfrac{p_C^c p_D^d}{p_A^a p_B^b}$.

Consequently, we can express the rate of the reaction near equilibrium as

$$\begin{aligned} v &\approx v_1\Big(1 - \big(1 + \frac{\Delta G}{RT} + ...\big)\Big), \\ v &\approx -v_1\frac{\Delta G}{RT}, \end{aligned} \tag{18}$$

which motivates the following kinetic model used for the interfacial reaction rate in *Chapter 3*:

$$v_I = -\frac{V_0}{RT}\frac{\Phi}{C_A}, \tag{19}$$

where v_1 is identified as the characteristic velocity and denoted using V_0, while Φ/C_A is analogous to Gibbs energy, and drives the forward reaction.

C.2. Interface resistance

The transient diffusion analysis of *Section 7.2* features mass-transfer resistance because of the presence of heterogeneity, i.e. the two phases, α and β, in the system. This interface boundary condition is derived using insights from the previous section, namely, by expressing

Eq. (12) in terms of concentration:

$$\begin{aligned} v &= v_{\alpha\to\beta} - v_{\beta\to\alpha} \\ &= k_\alpha C_I^\alpha - k_\beta C_I^\beta \\ &= v_{\alpha\to\beta}\Big(1 - \frac{k_\beta C_I^\beta}{k_\alpha C_I^\alpha}\Big) \\ &= v_{\alpha\to\beta}\Big(1 - \frac{C_{eq}^\alpha C_I^\beta}{C_{eq}^\beta C_I^\alpha}\Big) \\ &= v_1\Big(1 - \frac{C_{eq}^\alpha}{C_{eq}^\beta}\frac{C_I^\beta}{C_I^\alpha}\Big), \end{aligned} \tag{20}$$

where $v_{\beta\to\alpha}$ and $v_{\beta\to\alpha}$ denote the rates of the forward ($\alpha \to \beta$) and backward ($\beta \to \alpha$) reactions respectively, and k_α and k_β denote the corresponding coefficients; $v_1 = v_{\alpha\to\beta}$.

Next, we express the net rate of the interfacial reaction in terms of the local flux. For the planar system, the direction of the z-coordinate is shown in Fig. 3.1; subsequently, the flux of B-atoms on the α-side of the system across the interface is opposite to the z-direction, and we obtain

$$\begin{aligned} -\frac{J_I^\alpha}{C_I^\alpha} &= v_1\Big(1 - \frac{C_{eq}^\alpha}{C_{eq}^\beta}\frac{C_I^\beta}{C_I^\alpha}\Big), \\ J_I &= -V_0\Big(C_I^\alpha - \frac{C_{eq}^\alpha}{C_{eq}^\beta}C_I^\beta\Big), \end{aligned} \tag{21}$$

where $J_I = J_I^\alpha = J_I^\beta$ as per Eq. (7.3).

D. Axisymmetric mechanics

Assuming axisymmetry, the constitutive relations are given by [103, 166]

$$\begin{aligned}\epsilon^e_{rr} &= \frac{\sigma_{rr}}{E} - \frac{\nu(\sigma_{\theta\theta} + \sigma_{\phi\phi})}{E},\\ &= \frac{\sigma_{rr}}{E} - \frac{2\nu}{E}\sigma_{\theta\theta},\end{aligned} \tag{22}$$

and

$$\begin{aligned}\epsilon^e_{\theta\theta} &= \frac{\sigma_{\theta\theta}}{E} - \frac{\nu(\sigma_{rr} + \sigma_{\phi\phi})}{E},\\ &= \frac{\sigma_{\theta\theta}}{E} - \frac{\nu(\sigma_{rr} + \sigma_{\theta\theta})}{E},\\ &= -\frac{\nu}{E}\sigma_{rr} + \frac{(1-\nu)}{E}\sigma_{\theta\theta},\end{aligned} \tag{23}$$

where the superscript e denotes elastic. Using Eqs. (22) and (23), we obtain

$$\begin{aligned}\sigma_{rr} &= E\epsilon^e_{rr} + 2\nu\sigma_{\theta\theta},\\ \sigma_{rr} &= \frac{-1}{\nu}\Big(E\epsilon^e_{\theta\theta} - (1-\nu)\sigma_{\theta\theta}\Big).\end{aligned} \tag{24}$$

Solving Eq. (24) for the radial stress, we obtain

$$\begin{aligned}\sigma_{\theta\theta} &= \frac{E}{(1-\nu-2\nu^2)}(\nu\epsilon^e_{rr} + \epsilon^e_{\theta\theta}),\\ &= \frac{E}{(1+\nu)(1-2\nu)}(\nu\epsilon^e_{rr} + \epsilon^e_{\theta\theta}).\end{aligned} \tag{25}$$

Subsequently, the radial stress is obtained as follows:

$$\sigma_{rr} = \frac{E}{(1+\nu)(1-2\nu)}\Big((1-\nu)\epsilon^e_{rr} + 2\nu\epsilon^e_{\theta\theta}\Big). \tag{26}$$

Equations (25) and (26) can be expressed in the matrix-vector form:

$$\begin{bmatrix} \sigma_{rr} \\ \sigma_{\theta\theta} \end{bmatrix} = \frac{E}{(1+\nu)(1-2\nu)} \begin{bmatrix} 1-\nu & 2\nu \\ \nu & 1 \end{bmatrix} \begin{bmatrix} \epsilon^e_{rr} \\ \epsilon^e_{\theta\theta} \end{bmatrix}. \tag{27}$$

E. Mechanical equilibrium reformulation

In the absence of body forces, the mechanical equilibrium condition, Eq. (2.27), in the component form, is given by

$$\sigma_{ij,j} = 0. \tag{28}$$

Using Eqs. (5.1), (5.3), and (5.4), we obtain

$$\sigma_{ij} = \frac{E}{1+\nu}\Big[\epsilon_{ij} - \frac{(1+\nu)}{(1-2\nu)}\frac{\Delta C\Omega}{3}\delta_{ij} + \frac{\nu}{1-2\nu}\epsilon_{kk}\delta_{ij}\Big]. \tag{29}$$

Taking the divergence of Eq. (29), and writing the strains in terms of the displacement, $\epsilon_{ij} = \dfrac{u_{i,j}+u_{j,i}}{2}$ and $\epsilon_{kk} = u_{k,k}$, we obtain the displacement formulation of $\sigma_{ij,j}$:

$$\begin{aligned}
\sigma_{ij,j} &= \frac{E}{1+\nu}\Big[\frac{u_{i,jj}+u_{j,ij}}{2} - \frac{C_{,j}\Omega(1+\nu)}{3(1-2\nu)}\delta_{ij} + \frac{\nu}{1-2\nu}u_{k,kj}\delta_{ij}\Big],\\
&= \frac{E}{1+\nu}\Big[\frac{u_{i,jj}+u_{j,ij}}{2} - \frac{C_{,i}\Omega(1+\nu)}{3(1-2\nu)} + \frac{\nu}{1-2\nu}u_{k,ki}\Big],\\
&= \frac{E}{1+\nu}\Big[\frac{u_{i,jj}+u_{j,ij}}{2} - \frac{C_{,i}\Omega(1+\nu)}{3(1-2\nu)} + \frac{\nu}{1-2\nu}u_{k,ik}\Big],\\
&= \frac{E}{1+\nu}\Big[\Big(\frac{1}{2} + \frac{\nu}{1-2\nu}\Big)u_{j,ij} + \frac{1}{2}u_{i,jj} - \frac{(1+\nu)}{(1-2\nu)}\frac{C_{,i}\Omega}{3}\Big],\\
&= \frac{E}{1+\nu}\Big[\frac{u_{j,ij}}{2(1-2\nu)} + \frac{u_{i,jj}}{2} - \frac{(1+\nu)}{(1-2\nu)}\frac{C_{,i}\Omega}{3}\Big],\\
&= \frac{E}{1+\nu}\Big[\frac{u_{j,ji}}{2(1-2\nu)} + \frac{u_{i,jj}}{2} - \frac{(1+\nu)}{(1-2\nu)}\frac{C_{,i}\Omega}{3}\Big],\\
&= \frac{E}{1+\nu}\Big[\frac{e_{,i}}{2(1-2\nu)} + \frac{u_{i,jj}}{2} - \frac{(1+\nu)}{(1-2\nu)}\frac{C_{,i}\Omega}{3}\Big],
\end{aligned} \tag{30}$$

where e is the volumetric strain given by $e = \epsilon_{kk} = u_{k,k}$ [104].

Applying the divergence operator to Eq. (30), and using Eq. (28), we obtain

$$\begin{aligned}
\left[\frac{e_{,i}}{2(1-2\nu)} + \frac{u_{i,jj}}{2} - \frac{(1+\nu)}{(1-2\nu)}\frac{C_{,i}\Omega}{3}\right]_{,i} &= 0,\\
\frac{e_{,ii}}{2(1-2\nu)} + \frac{u_{i,jji}}{2} - \frac{(1+\nu)}{(1-2\nu)}\frac{C_{,ii}\Omega}{3} &= 0,\\
\frac{e_{,ii}}{2(1-2\nu)} + \frac{u_{i,ijj}}{2} - \frac{(1+\nu)}{(1-2\nu)}\frac{C_{,ii}\Omega}{3} &= 0,\\
\frac{e_{,ii}}{2(1-2\nu)} + \frac{e_{,jj}}{2} - \frac{(1+\nu)}{(1-2\nu)}\frac{C_{,ii}\Omega}{3} &= 0,\\
\left(e - \frac{\Omega}{3}\frac{(1+\nu)}{(1-\nu)}C\right)_{,ii} &= 0,\\
\nabla^2\left(e - \frac{\Omega}{3}\frac{(1+\nu)}{(1-\nu)}C\right) &= 0.
\end{aligned} \tag{31}$$

For the state of stresses in our system, e is given by

$$\begin{aligned}
e &= \epsilon_{xx} + \epsilon_{yy} + \epsilon_{zz},\\
&= 2\epsilon_{xx} + \epsilon_{zz}.
\end{aligned} \tag{32}$$

Using Eqs. (5.1), (5.3), and (5.4), we obtain

$$\epsilon_{ij} = \frac{1}{E}\Big[(1+\nu)\sigma_{ij} - \nu\sigma_{kk}\delta_{ij}\Big] + \frac{\Omega}{3}C\delta_{ij}. \tag{33}$$

Subsequently, the non-zero strains are given by

$$\begin{aligned}
\epsilon_{yy} = \epsilon_{xx} &= \frac{\sigma_{xx}}{E} + \frac{C\Omega}{3},\\
\epsilon_{zz} &= -\frac{2\nu\sigma_{xx}}{E} + \frac{C\Omega}{3}.
\end{aligned} \tag{34}$$

As $\sigma_{xx} \approx \overline{\sigma} = \frac{3}{2}\sigma_h$ as per Eq. (5.62), the volumetric deformation simplifies to

$$e = \frac{3(1-2\nu)\sigma_h}{E} + C\Omega. \tag{35}$$

Substituting Eq. (35) in (31), we obtain

$$\nabla^2(\sigma_h + \Gamma C) = 0, \tag{36}$$

where $\Gamma = \frac{2}{9}\overline{E}\Omega$.

In the absence of concentration effects, Eqs. (36) and (31) simplify to equations that are well known in the linear elasticity theory: $\nabla^2 e = 0$, which implies harmonic volumetric deformation and $\nabla^2 \sigma_h = 0$, which implies harmonic mean hydrostatic stress; these correspond to biharmonic stresses in the static problem [105].

F. Helmholtz energy density

The Helmholtz energy density is given by

$$\mathscr{f} = \mathscr{u} - T\mathscr{s}. \tag{37}$$

The total differential of Helmholtz energy density is given by

$$\begin{aligned} d\mathscr{f} &= d\mathscr{u} - Td\mathscr{s} - \mathscr{s}dT, \\ &= \sigma_{ij}d\epsilon_{ij} + \mu dC - \mathscr{s}dT, \end{aligned} \tag{38}$$

where Eq. (3.10) is used to simplify.

At constant temperature, T, and concentration, C, Eq. (38) simplifies to

$$d\mathscr{f} = \sigma_{ij}d\epsilon^{e}_{ij}, \tag{39}$$

where $\epsilon_{ij} = \epsilon^{c}_{ij} + \epsilon^{e}_{ij} = \epsilon^{e}_{ij}$ at constant C.

Integrating at constant T and C from a state of zero stress (zero elastic strain), we obtain

$$\mathscr{f}(C,\sigma) = \mathscr{f}(C,0) - \frac{\nu}{2E}(\sigma_{kk})^2 + \frac{1}{4G}\sigma_{ij}\sigma_{ij}, \tag{40}$$

where $G = \dfrac{E}{2(1+\nu)}$.

For an equibiaxial state of stress, $\sigma_{kk} = \sigma_{xx} + \sigma_{yy} = \sigma$. Subsequently, Eq. (40) simplifies to

$$\begin{aligned} \mathscr{f}(C, \sigma) &= \mathscr{f}(C, 0) + \frac{\sigma^2}{\overline{E}}, \\ \mathscr{f}(C, \sigma) &= \mathscr{f}(C, 0) + \phi. \end{aligned} \tag{41}$$

G. Laplace transformed biaxial modulus

For a Maxwell material, the laplace transformed shear modulus is given by Eq. (7.53):

$$G_V = \frac{Q_m(s)}{P_m(s)} = \frac{s}{\dfrac{s}{G} + \dfrac{1}{\eta}} = \frac{G\eta s}{(G + \eta s)} \tag{42}$$

The linear isotropic elastic moduli are given by

$$\begin{aligned} G &= \frac{E}{2(1+\nu)}, \\ K &= \frac{E}{3(1-\nu)}, \end{aligned} \tag{43}$$

where K is the bulk modulus.

In the elastic equation, G is replaced by G_V for a Maxwell material, while K remains unchanged: $K_V = K$.

Subsequently, using Eq. (42) to replace G in Eq. (43)a, and solving for the *transformed* material parameters, E_V and ν_V, using Eqs. (43), we obtain

$$\begin{aligned} \nu_V &= \frac{3K(G + \eta s) - 2G\eta s}{6K(G + \eta s) + 2G\eta s}, \\ E_V &= \frac{9KG\eta s)}{3K(G + \eta s) + G\eta s}. \end{aligned} \tag{44}$$

Thus, the Laplace transformed biaxial modulus for a Maxwell material is given by

$$\overline{E}_V = \frac{E_V}{(1 - \nu_V)} = \frac{18KG\eta s}{3K(G + \eta s) + 4G\eta s}. \tag{45}$$

H. Transient diffusion analysis

H.1. Discontinuous-weighting function

The eigenfunctions of the series in Eq. (7.42), $f^{\alpha}(z)$ and $f^{\beta}(z)$, are given by Eq. (7.46). These functions are not orthogonal; however, they can be made orthogonal using orthogonality factors[20] [169], which are determined by applying the condition for orthogonality:

$$C_2 \int_0^{z_I} f_n^{\beta}(z) f_m^{\beta}(z) dz + C_1 \int_{z_I}^{z_o} f_n^{\alpha}(z) f_m^{\alpha}(z) dz = 0, \tag{46}$$

where C_1 and C_2 are the orthogonality factors corresponding to $f^{\alpha}(z)$ and $f^{\beta}(z)$ respectively. Setting $C_1 = 1$, we obtain

$$C_2 = -\frac{\int_{z_I}^{z_o} f_n^{\alpha}(z) f_m^{\alpha}(z) dz}{\int_0^{z_I} f_n^{\beta}(z) f_m^{\beta}(z) dz}. \tag{47}$$

This procedure generates the orthogonality factor, which is also known as the discontinuous-weighting function for a composite system.

For our system, $C_2 = \dfrac{C_{eq}^{\alpha}}{C_{eq}^{\beta}}$; the details of the derivation are provided below.

---

[20] Consequently, $f^{\alpha}(z)$ and $f^{\beta}(z)$ are known as *quasi-orthogonal* functions [169].

First, using Eq. (7.28)b in Eq. (7.46), the nonorthogonal eigenfunctions are expressed in terms of λ^{β}:

$$\begin{aligned} f_n^{\alpha}(z) &= \lambda_n \sin(\lambda_n z_I)\cos(\lambda_n \hat{D}(z - z_I)), \\ f_n^{\beta}(z) &= \frac{\lambda_n}{\hat{D}} \sin(\lambda_n \hat{D}(z_I - z_o))\cos(\lambda_n z), \end{aligned} \tag{48}$$

where $\hat{D}^2 \equiv \dfrac{D'^{\beta}}{D'^{\alpha}}$, and the eigenvalue, $\lambda_n = \lambda^{\beta}$. The integrals in Eq. (47) simplify to

$$\begin{aligned} \int_{z_I}^{z_o} f_n^{\alpha}(z) f_m^{\alpha}(z)dz = &-\frac{\lambda_m\lambda_n \sin(\lambda_m z_I)\sin(\lambda_n z_I)}{2\hat{D}(\lambda_n^2 - \lambda_m^2)}\Big[(\lambda_n + \lambda_m)\sin(\hat{D}(\lambda_n - \lambda_m)(z_I - z_o)) \\ &+ (\lambda_n - \lambda_m)\sin(\hat{D}(\lambda_n + \lambda_m)(z_I - z_o))\Big], \\ \int_0^{z_I} f_n^{\beta}(z) f_m^{\beta}(z)dz = &\frac{\lambda_m\lambda_n \sin(\lambda_m \hat{D}(z_I - (z_I))\sin(\lambda_n \hat{D}(z_I - (z_I))}{2\hat{D}^2(\lambda_n^2 - \lambda_m^2)}\Big[(\lambda_n + \lambda_m)\sin((\lambda_n - \lambda_m)z_I) \\ &+ (\lambda_n - \lambda_m)\sin((\lambda_n + \lambda_m)z_I)\Big]. \end{aligned} \tag{49}$$

Subsequently, substituting the integrals of Eq. (49) in Eq. (47) provides the orthogonality factor:

$$C_2 = \hat{D}\frac{\Big(\dfrac{\lambda_n}{\tan(\lambda_m \hat{D}(z_I - z_o))} - \dfrac{\lambda_m}{\tan(\lambda_n \hat{D}(z_I - z_o))}\Big)}{\Big(\dfrac{\lambda_n}{\tan(\lambda_m z_I)} - \dfrac{\lambda_m}{\tan(\lambda_n z_I)}\Big)}. \tag{50}$$

To simplify Eq. (50), we revisit the transcendental Eq. (7.41), which is given by

$$\frac{1}{\tan(\lambda_n \hat{D}(z_I - z_o))} = \frac{\hat{C}}{\hat{D}\tan(\lambda_n z_I)} - \frac{\lambda_n z_o}{\gamma_p \hat{D}}, \tag{51}$$

where $\gamma_p = \dfrac{V_0 z_o}{D'^{\beta}}$.

Equation (51) is used to simplify Eq. (50), which leads to: $C_2 = \hat{C} = \dfrac{C_{eq}^{\alpha}}{C_{eq}^{\beta}}$.

Consequently, the orthogonal eigenfunctions, denoted $g^{\alpha}(z)$ and $g^{\beta}(z)$, are given by

$$\begin{aligned} g^{\alpha}(z) &= C_1 f^{\alpha}(z) = f^{\alpha}(z), \\ g^{\beta}(z) &= C_2 f^{\beta}(z) = \hat{C} f^{\beta}(z). \end{aligned} \tag{52}$$

H.2. Series coefficient F_n

The series coefficient, F_n, appears in the two subproblems of the composite planar system, as seen in Eq. (7.42). To determine F_n, the initial conditions, given by Eq. (7.43), are applied [177, 183].

Applying the initial conditions to each subproblem in Eq. (7.42) leads to

$$\begin{aligned} \sum_{n=1}^{\infty} F_n f_n^{\alpha}(z) &= -w^{\alpha}(z), \\ \sum_{n=1}^{\infty} F_n f_n^{\beta}(z) &= -w^{\beta}(z). \end{aligned} \tag{53}$$

Next, we multiply Eq. (53)a by $g_m^{\alpha}(z)$ and integrate it within the α-phase; repeating the same step for the series corresponding to the β-phase, and adding the two subproblems together, we obtain

$$\begin{aligned} \sum_{n=1}^{\infty} F_n \Big[\int_{z_I}^{z_o} f_n^{\alpha}(z) g_m^{\alpha}(z) dz + \int_{0}^{z_I} f_n^{\beta}(z) g_m^{\beta}(z) dz \Big] = \\ -\Big[\int_{z_I}^{z_o} w^{\alpha}(z) g_m^{\alpha}(z) dz + \int_{0}^{z_I} w^{\beta}(z) g_m^{\beta}(z) dz \Big]. \end{aligned} \tag{54}$$

Using Eq. (52) in Eq. (54), we obtain

$$\begin{aligned} \sum_{n=1}^{\infty} F_n \Big[\int_{z_I}^{z_o} f_n^{\alpha}(z) f_m^{\alpha}(z) dz + \hat{C} \int_{0}^{z_I} f_n^{\beta}(z) f_m^{\beta}(z) dz \Big] = \\ -\Big[\int_{z_I}^{z_o} w^{\alpha}(z) f_m^{\alpha}(z) dz + \hat{C} \int_{0}^{z_I} w^{\beta}(z) f_m^{\beta}(z) dz \Big]. \end{aligned} \tag{55}$$

The sum of the two integrals on the LHS of Eq. (55) is 0 as per Eq. (46), unless $m = n$. Subsequently, the sum in Eq. (55) reduces to one term, $m = n$, and we obtain an expression for the series coefficient, F_n:

$$F_n = -\frac{\int_{z_I}^{z_o} w^{\alpha}(z) f_n^{\alpha}(z) dz + \hat{C} \int_0^{z_I} w^{\beta}(z) f_n^{\beta}(z) dz}{\int_{z_I}^{z_o} w^{\alpha}(z) (f_n^{\alpha}(z))^2 dz + \hat{C} \int_0^{z_I} w^{\beta}(z) (f_n^{\beta}(z))^2 dz}. \tag{56}$$